X-751-72-208
PREPRINT

NASA TM X- 65990

EARTH-SATELLITE PROPAGATION ABOVE 10 GHz

PAPERS FROM THE 1972 SPRING URSI SESSION ON EXPERIMENTS UTILIZING THE ATS-5 SATELLITE

Compiled By
LOUIS J. IPPOLITO

MAY 1972

GSFC — GODDARD SPACE FLIGHT CENTER —
GREENBELT, MARYLAND

X-751-72-208

EARTH-SATELLITE PROPAGATION ABOVE 10 GHz

PAPERS FROM THE 1972 SPRING URSI SESSION

ON EXPERIMENTS UTILIZING THE ATS-5 SATELLITE

Compiled By

Louis J. Ippolito

Principal Investigator
ATS Millimeter Wave Experiments

May 1972

GODDARD SPACE FLIGHT CENTER
Greenbelt, Maryland

PREFACE

This document presents a collection of papers from the Special Session on Earth-Satellite Propagation Above 10 GHz, presented at The 1972 Spring Meeting of the United States National Committee, International Union of Radio Science (USNC-URSI), April 1972, Washington, D.C.

This Special Session was devoted to propagation measurements associated with the Applications Technology Satellite (ATS-5), which provided the first operational earth-space links at frequencies above 15 GHz. The papers present a comprehensive summary of the major results of the ATS-5 experiment measurements and related radiometric, radar and meteorological studies.

The papers for the Session were organized around seven selected areas of interest, with the results of the various investigators combined into a single paper presented by a Principal Author for that area. This format was adopted to provide a comprehensive report on the results of the ATS-5 satellite to earth transmissions and to avoid redundancy in the presentations.

A complete list of published reports and presentations related to the ATS-5 Millimeter Wave Experiment is included at the end of this document.

Archie W. Straiton
The University of Texas
Austin, Texas
(Session Chairman)

Louis J. Ippolito
NASA Goddard Spaceflight Center
Greenbelt, Maryland
(Principal Investigator, ATS-5 Experiment)

CONTENTS

Section		Page
1.	ATS-5 MILLIMETER WAVE EXPERIMENT FLIGHT HARDWARE HISTORY: J. L. King, Goddard Space Flight Center, National Aeronautics and Space Administration, Greenbelt, Md.	1-1
2.	ATTENUATION PROBABILITIES OF 15 GHz RADIO WAVES OVER EARTH-SATELLITE PATHS: A. W. Straiton, The University of Texas at Austin, Texas	2-1
3.	RELATIONSHIP BETWEEN THE ATMOSPHERIC ATTENUATION OF SATELLITE PATH SIGNALS AND GROUND RAIN RATE: E. A. Robertson, COMSAT Laboratories, Clarksburg, Md.; and D. E. Sukhia, Martin Marietta, Orlando, Florida	3-1
4.	THE RELATIONSHIP BETWEEN SATELLITE SIGNAL ATTENUATIONS AND SKY TEMPERATURE MEASUREMENTS IN THE RAIN ENVIRONMENT: D. A. Gray, Bell Telephone Laboratories, Crawford Hill Laboratory, Holmdel, N.J.	4-1
5.	SIMULTANEOUS DIRECT, RADIOMETRIC, AND RADAR MEASUREMENTS OF PRECIPITATION ATTENUATION AT 15.3 GHz: J. I. Strickland, Communications Research Centre, Ottawa, Canada	5-1
6.	THE USE OF SPACE DIVERSITY IN THE RECEPTION OF MILLIMETER WAVELENGTH SATELLITE SIGNALS: D. B. Hodge, Department of Electrical Engineering, Ohio State University, Columbus, Ohio	6-1
7.	THE ESTIMATION OF ATTENUATION STATISTICS FOR EARTH-SPACE MILLIMETER WAVELENGTH PROPAGATION: L. R. Zintsmaster, Department of Electrical Engineering, Ohio State University, Columbus, Ohio	7-1

CONTENTS (Continued)

Section		Page
8.	SUMMARY AND EVALUATION OF RESULTS FROM THE ATS MILLIMETER WAVE EXPERIMENT: L. J. Ippolito, Goddard Space Flight Center, National Aeronautics and Space Administration, Greenbelt, Md.	8-1
APPENDIX 1 —	PUBLISHED REPORTS ON THE ATS-5 MILLIMETER WAVE EXPERIMENT	A-1

SECTION 1

ATS-5 MILLIMETER WAVE EXPERIMENT

FLIGHT HARDWARE HISTORY

J. L. King
NASA Goddard Space Flight Center
Greenbelt, Maryland

ABSTRACT

The fifth Applications Technology Satellite (ATS-5) was launched August 12, 1969 marking the start of the first NASA Goddard Space Flight Center millimeter wave experiment. The experiment was designed to determine both short- and long-term propagation characteristics for operational millimeter wavelength earth-space links as a function of defined meteorological conditions. Data were collected at sites scattered throughout North America (U.S. and Canada) utilizing 15.3-GHz spacecraft transmitters with an earth-coverage antenna pattern. The experiment also included a 31.65-GHz spacecraft receiver to make on-board attenuation measurements of the signal from a 1-kw transmitter located at Rosman, N.C. This paper will emphasize the hardware implementation and operational constraints that have confronted this experiment. The satellite was planned to be 3-axis gravity-gradient-stabilized. However, control problems during the transfer orbit injection caused the satellite to become spin-stabilized, rotating at approximately 75 rpm. This condition caused the experiment antenna pattern to sweep across the earth yielding a pulsed signal resulting in reduced measurement dynamic range. The spinning also resulted in loss of the short-term data (< 2 Hz) and meaningful phase measurements. The spin-stabilized ATS-5 was placed in a geosynchronous orbit located at 104°W longitude. However, this orbit had a 2° inclination with the equator which resulted in a 2.5 dB diurnal signal variation. This variation depends on the site's latitude, and in order to maintain the desired 1-dB measurement accuracy, this variation had to be removed from the attenuation data during processing. The orbit and spin conditions were aggravated by spacecraft hardware problems. The primary 15.3-GHz transmitter suffered a 6-dB, and then an additional 3 dB, loss of power early in the program which limited the dynamic measurement range. The second 15.3-GHz backup transmitter had thermal problems which limited its operating time to about 2.5 hours per day. Near the end of the experiment in the summer of 1971, the primary transmitter failed completely which also resulted in the

loss of the local oscillator for the 31-GHz receiver. Even with these problems the various sites had adequate measurement ranges to acquire a significant data base on the long-term propagation characteristics at 15.3 and 31.65 GHz. The satellite data were supplemented by radiometric and rain-gauge data to fill in voids when the satellite was not available.

INTRODUCTION

Radio communications over the past few decades have been characterized by a continued extension to higher and higher frequencies to support the increased demands on available spectrum. To date, the common carrier bands in the microwave region below 10 GHz have supported the bulk of the high bandwidth requirements for video and data transmissions. However, these bands are rapidly approaching saturation because of the sharing required between many satellites and terrestrial links on a global basis. To satisfy the increasing demands for communications bandwidth, the communications system designers are planning to utilize the frequencies above 10 GHz more extensively within the next decade as evidenced by the recent frequency assignments in the 10-100 GHz band by the WARC.

The ATS-5 Millimeter Wave Experiment was designed in 1965 to investigate propagation in the earth space path at 15.3 GHz and 31.65 GHz. The primary objective included measuring carrier attenuation at these frequencies to statistically determine fade margins required for various outage times at several locations in the U.S. and Canada. The secondary experiment objectives also included measuring channel coherence over a 100 MHz maximum bandwidth and conducting a narrowband (40 MHz bandwidth) communications transponder test using the 31.65 GHz uplink and the ATS-5 L-band downlink. Unfortunately the ATS-5 spin condition and primary transmitter power degradations which will be discussed in later sections resulted in the loss of the data which could have been used to meet the secondary objectives.

The experiment system consisted of two 15.3 GHz transmitters and a 31.65 GHz receiver on the satellite. This configuration (see Figure 1-1) allowed many ground receiving stations located in various parts of North America to measure 15.3 GHz downlink data simultaneously. The more limited 31.65 GHz uplink receiver was selected as part of the system because of the limited availability of high efficiency 31 GHz satellite transmitters in 1966 and because of the power and weight limitations placed on the satellite experiment package.

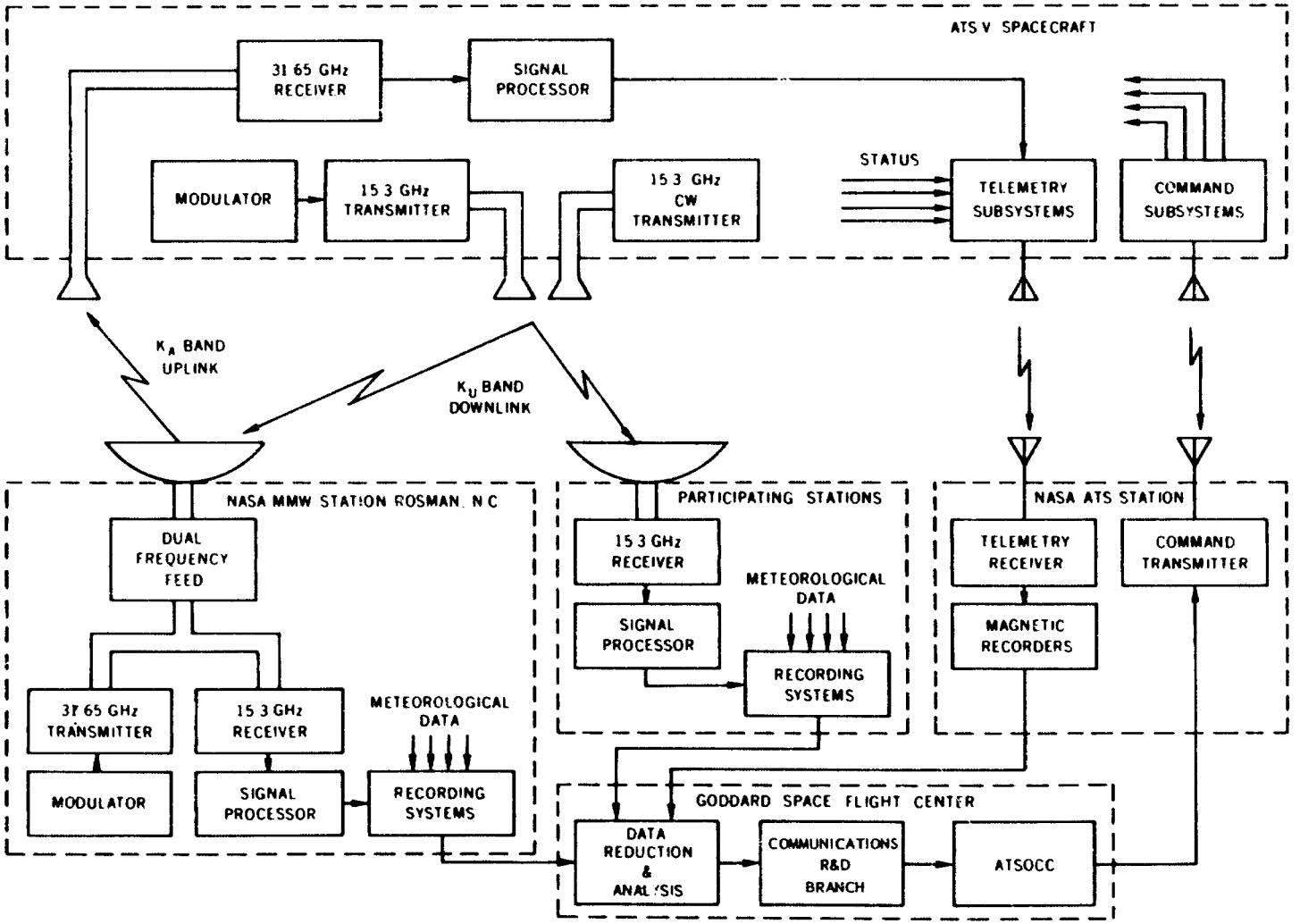

Figure 1-1. The ATS-V Millimeter Wave Propagation Experiment

THE ATS-5 LAUNCH

The ATS-5 was launched in August 1969, but stabilization problems caused by fluid moving in the spacecraft heat pipe thermal control system caused the satellite to tumble about the wrong axis at the conclusion of the transfer orbit. The separation of the apogee motor from the satellite was delayed at that point because of the possibility of damaging the ATS-5. (Figure 1-2 shows the ATS-5 with apogee motor attached.) As it turned out, there was a collision of the apogee motor and satellite when the separation occurred, but this resulted in only minor damage to a few strings of solar cells, the major impact was that the satellite began to spin in the wrong direction after separation. The tumble was corrected, but the unfortunate clockwise rotation would not allow the satellite despin mechanism to reduce the spin rate so that the gravity gradient system could be deployed. Consequently, the ATS-5 became a spin stabilized satellite instead of a gravity gradient three axis stabilized spacecraft as originally planned.

The satellite was able to be positioned with spin axis nearly parallel to the North South axis of the earth and the spin rate was approximately 76 rpm. In this orientation, the 17° beamwidth millimeter wave antennas swept across the earth once every 789 milliseconds producing a pulsed signal. The pulsed signal produced by the 17° antenna pattern has a duration of about 40 milliseconds (3 db points) followed by about 740 milliseconds period without a signal (see Figure 1-3). This represents a 5% duty cycle which reduces the average received power by 14 db. This resulted in a loss of dynamic measurement range which will be discussed in detail in the section on the ground receivers.

The orbit also had a 2° inclination at launch which resulted in a diurnal (24 hour) variation of the signal levels. Figure 1-4 shows the results of a 35 hour test in which five stations participated. The attenuation in db below a reference versus GMT in hours for July 6 and 7, 1970 is plotted for each station. Also shown at the bottom on this figure is a plot of the A-A angle versus GMT for the same period. This A-A angle is the angle between the line of sight from Rosman to the ATS-5 and the ATS-5 angular momentum vector. This geometry is shown in Figure 1-5. The A-A angle varies from 92 to 99 degrees, the maximum angle occurring some 2 hours and 40 minutes before the minimum elevation angle. When the A-A angle is maximum, the satellite beam will intersect Rosman at 9 degrees from the beam center. This corresponds approximately to the 3 db point on the spacecraft transmitter pattern, and at this point in the spacecraft orbit, Rosman will receive the minimum signal. The maximum signal will occur when the A-A angle is 92°. At this angle the antenna beam is within 2 degrees of Rosman on the pattern which is within one db of maximum signal. The angle between the spacecraft geometric axis and the spin axis is less than

ATS-V
SPACECRAFT

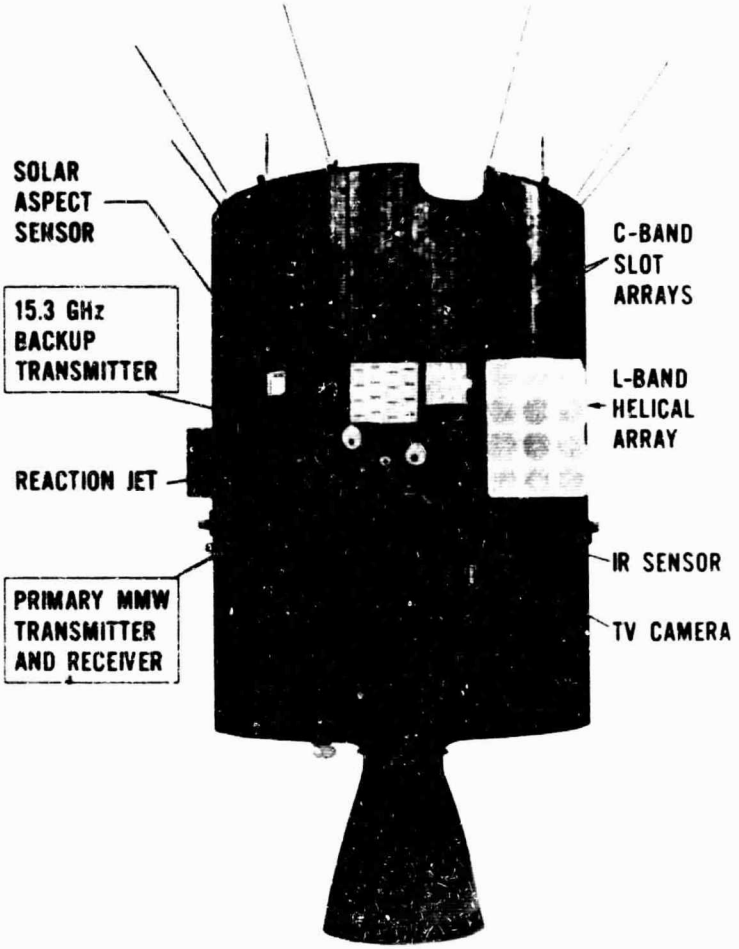

Figure 1-2. ATS-V Spacecraft

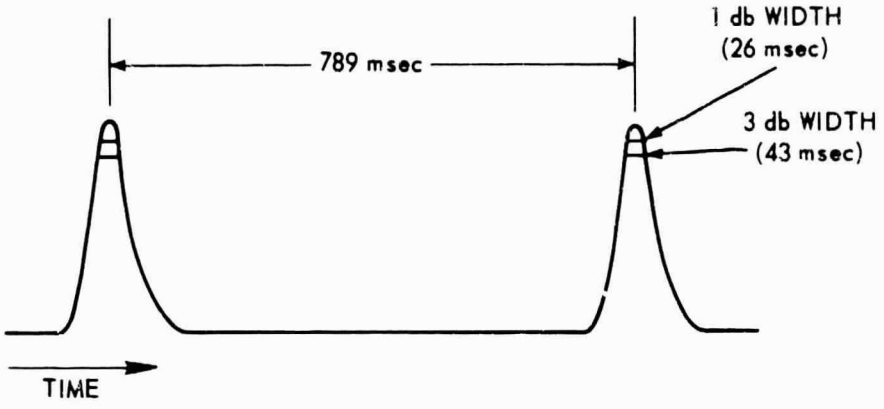

(A) CHARACTERISTICS OF SPIN-MODULATED AMPLITUDE DATA

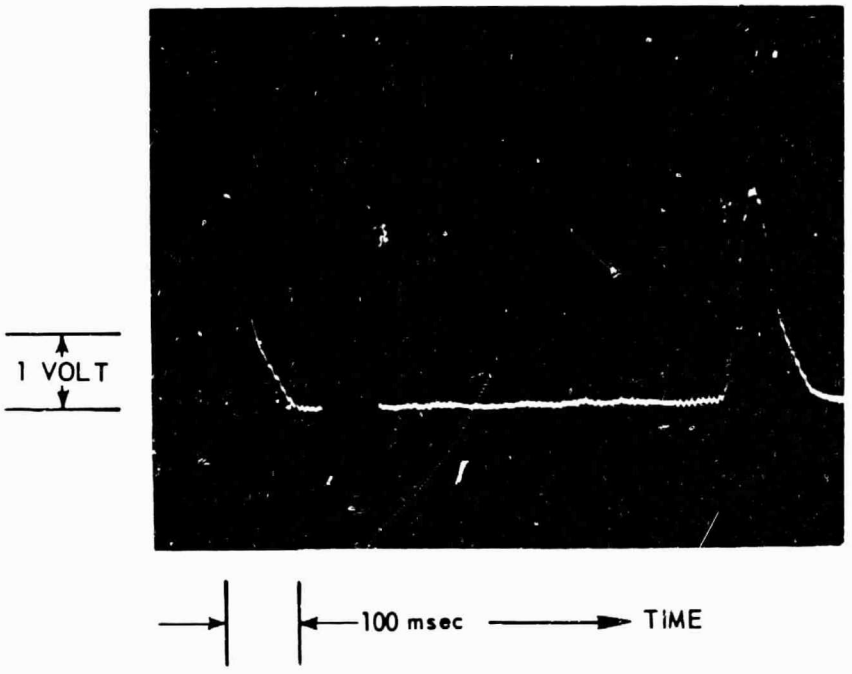

(B) PHOTO OF 15.3 GHz DOWNLINK CARRIER AMPLITUDE RECEIVED AT ROSMAN, N.C., SEPT. 29, 1969.

Figure 1-3

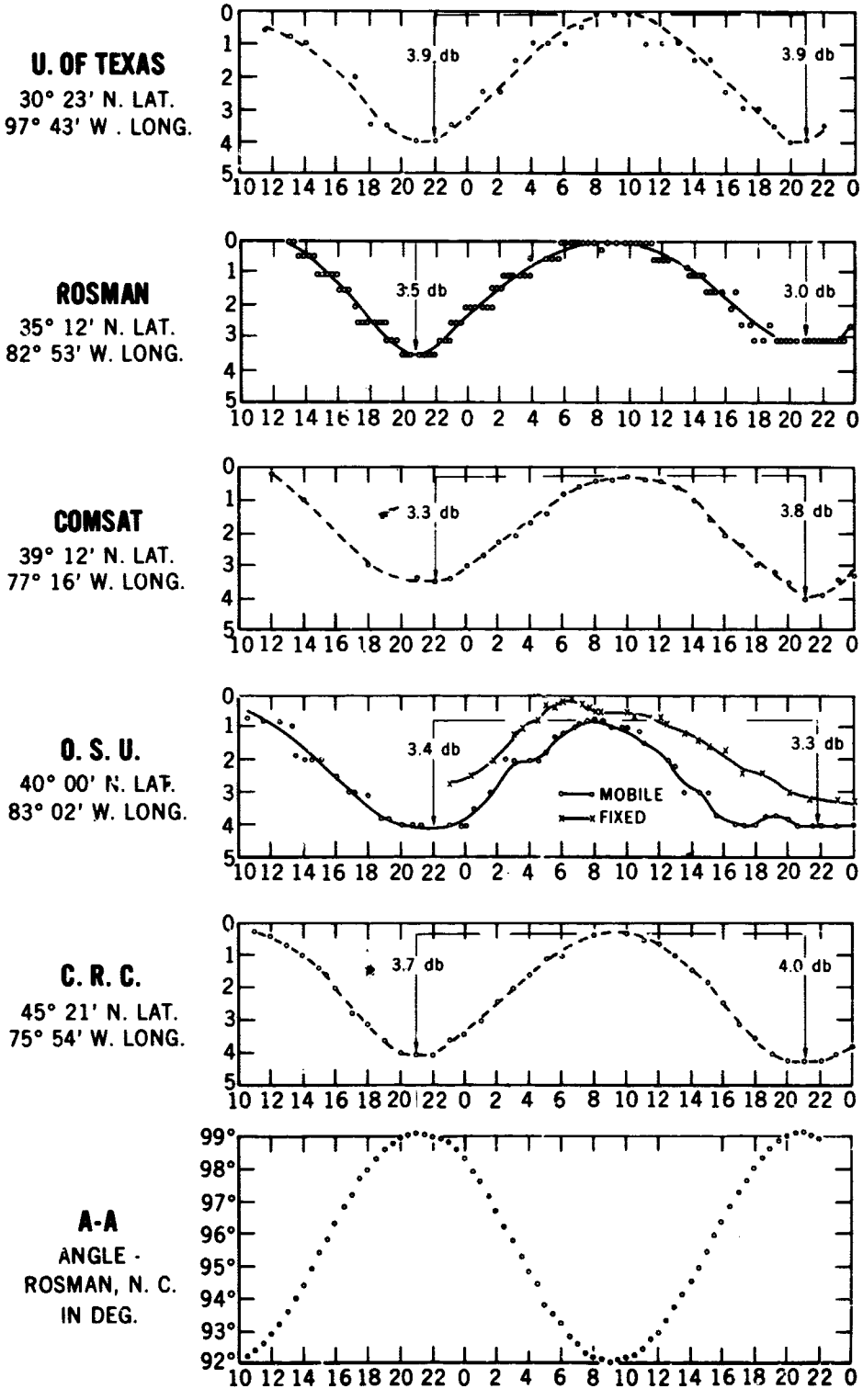

Figure 1-4. ATS-5 Long Term Data Run July 6-7, 1970

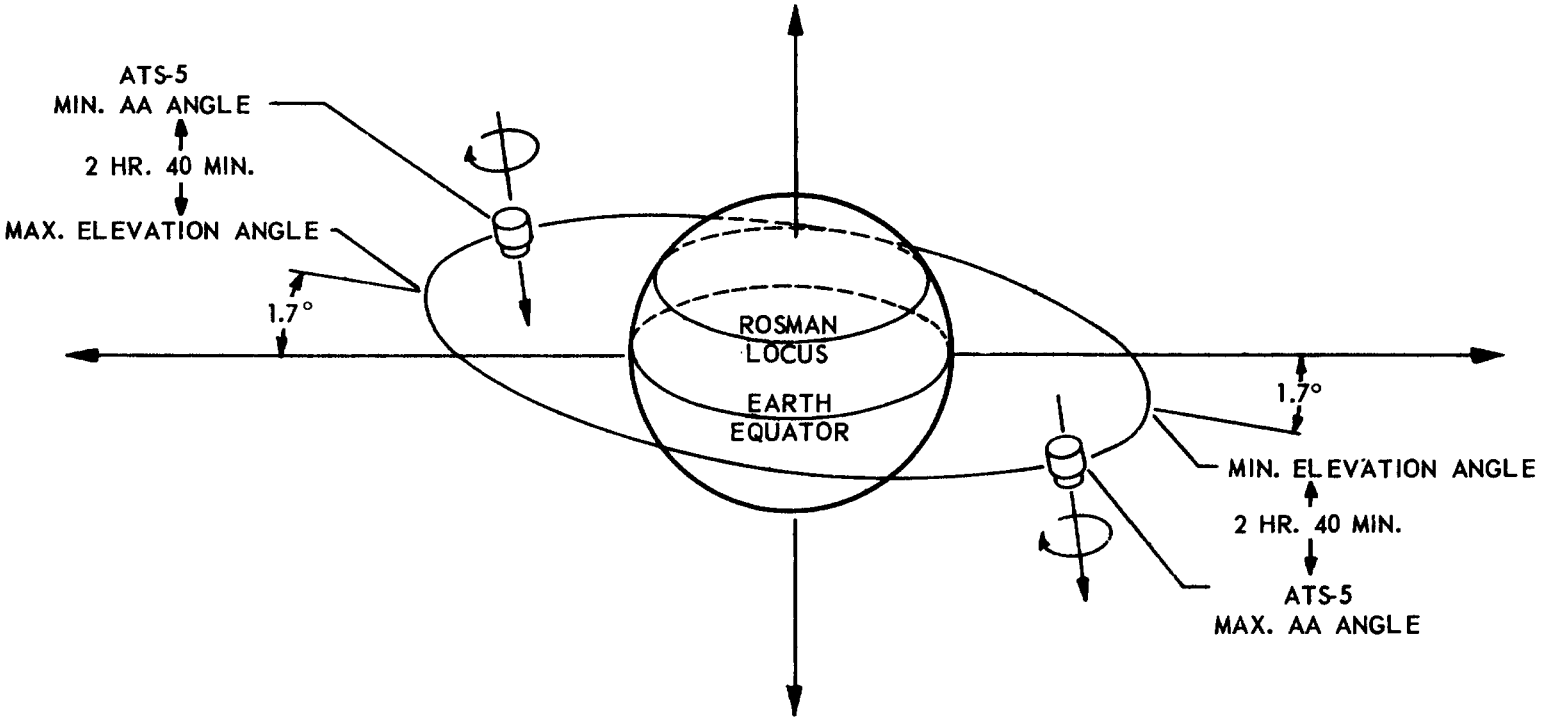

Figure 1-5. ATS-5 Orbit and Attitude Geometry

one degree, so that little error results in assuming the two axis are coincident. The inclination and ellipticity of the orbit resulted in an elliptical pattern being traced in the sky with a 24 hour period and this required the ground stations to track the satellite with their antennas.

SPACECRAFT HARDWARE

The millimeter wave experiment spacecraft package consisted of 15.3 GHz solid state transmitter and a 31.65 GHz phase lock receiver. This primary spacecraft experiment package weighed about 40 lbs. The backup transmitter which was a separate package with its own antenna weighed about 10 lbs. The primary transmitter and receiver required about 40 watts of DC power and the backup 15.3 GHz transmitter used 24 watts.

The 15.3 GHz transmitter was designed to provide the local oscillator for the 31 GHz phase lock receiver as can be seen in Figure 1-7. The 15.3 and 30.6 GHz multiplier chains were separated at the common L-band output coupler to eliminate some of the series components which lower the inherent reliability of the transmitter. This separation proved to be an important factor during the experiment when the primary transmitter lost 9 db of the 250 milliwatt 15.3 GHz output without affecting the 30.6 GHz local oscillator power. Eventually, the 30.6 GHz local oscillator did fail due to a loss in the L-band stages, but 1 1/2 years of additional Ku data were possible because of this design.

The history of the 15.3 GHz primary transmitter performance is not a very bright picture. The full 250 milliwatt 15.3 GHz output lasted only three months and then two abrupt losses of power in November and December 1969 reduced the power to about 30 milliwatts. This 30 milliwatt level remained stable for about a year until February 1971 at which time further losses of power rendered this transmitter useless. The 30.6 GHz output was not affected until July 1971 when problems in the multiplier or amplifier stages below 1.7 GHz caused the local oscillator to fall below a useable level. Until this failure of the local oscillator, the 31 GHz receiver was used along with the 15.3 GHz backup transmitter to take useful simultaneous 15.3 and 31.65 GHz measurements.

The 15.3 GHz backup transmitter which was used a great deal in the second year of the experiment was identical to the primary transmitter except it could not be modulated. It suffered from temporary power losses during the second and third month after launch. These losses were traced to a thermal condition related to an inadequate heat sink surface. To compensate for this, the operational time of this transmitter was limited to three 45 minute on periods, separated by 1-5 minute off periods. This cycle was permitted to be repeated after

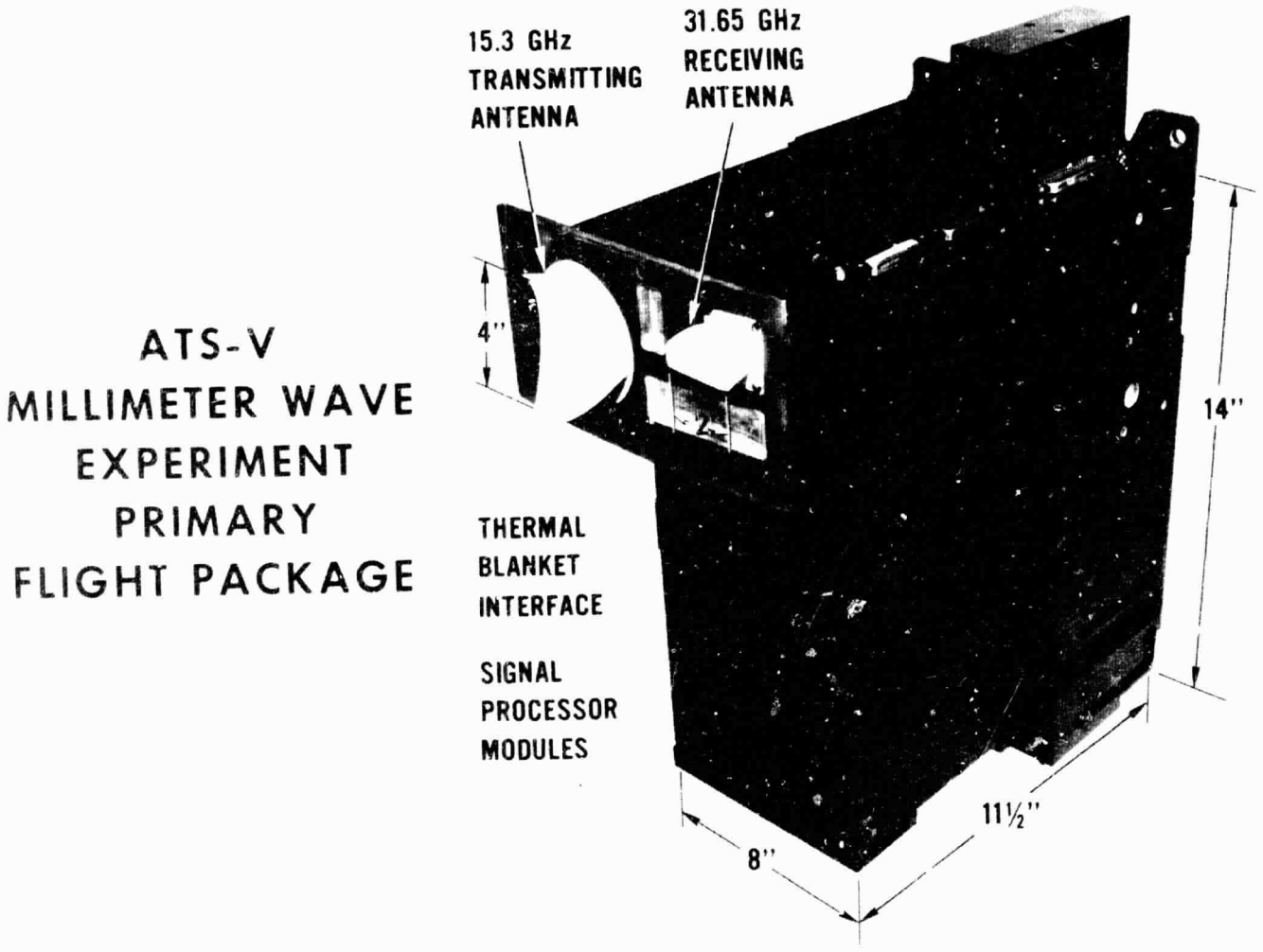

Figure 1-6. ATS-V Millimeter Wave Experiment Primary Flight Package

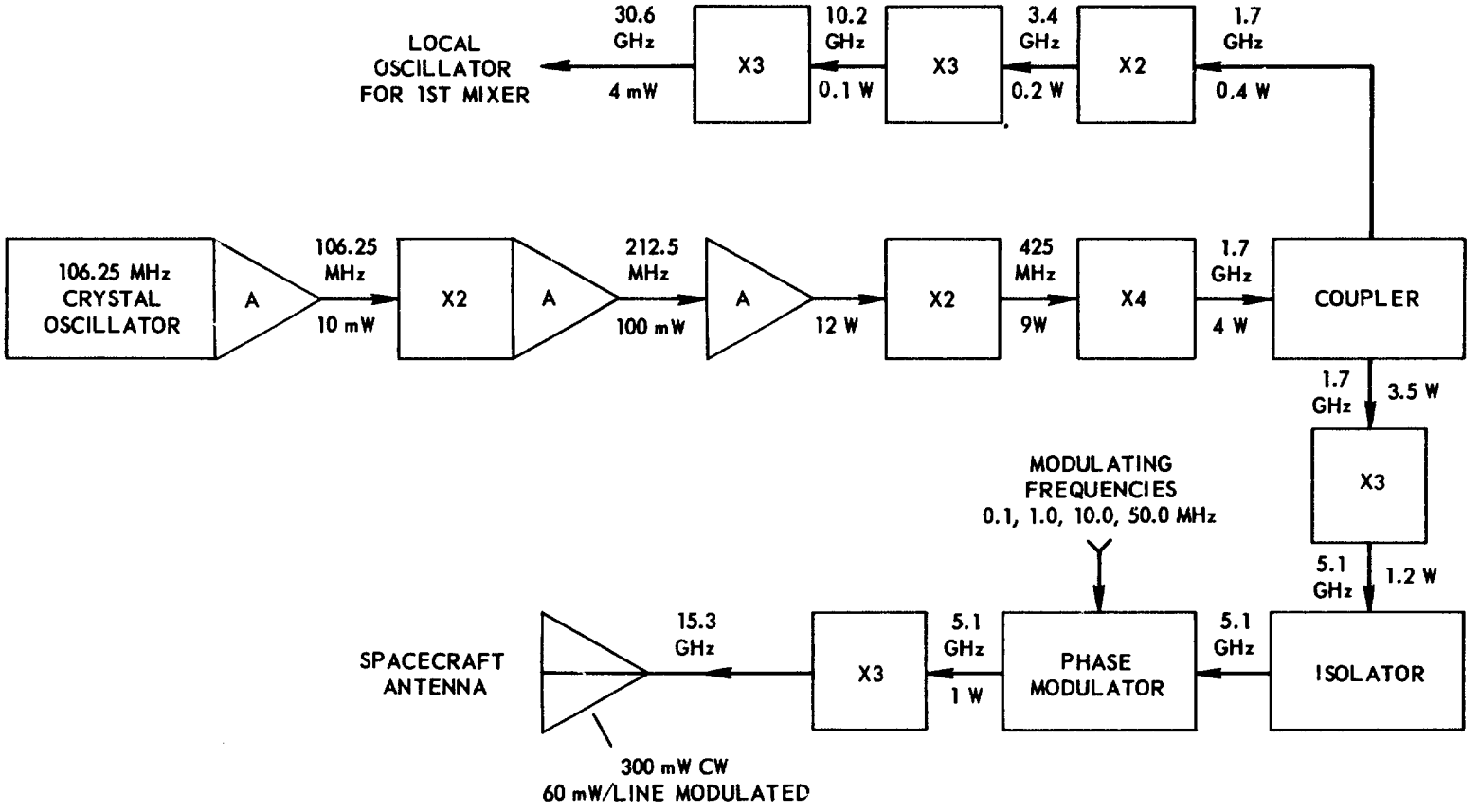

Figure 1-7. 15.3 GHz Transmitter/30.6 GHz Local Oscillator Block Diagram

3 hours off. This procedure resulted in a number of conflicts when several parts of the country were experiencing rainy weather the same day, but a decision was made to limit the power roll off to one db or less before shut down. This conservative procedure has resulted in the 15.3 GHz backup transmitter being able to maintain the same 250 milliwatt performance over the past two years.

The 15.3 GHz solid state transmitter used a 5.1 GHz phase modulator to produce three approximately equal 60 milliwatt signals spaced at either .1, 1.0, 10.0, or 50 MHz from the carrier. Some coherence bandwidth data was taken using the modulated sidebands, but after the power losses in the primary transmitter and the unfortunate spin conditions, a CW mode was required to provide adequate attenuation measurement range.

The 31.65 GHz spacecraft receiver is the second major experiment subsystem included as part of the ATS-5 spacecraft hardware. The receiver utilizes a balanced mixer front end with a 17 db maximum noise figure and a 1.05 GHz first intermediate frequency. The receiver is designed to phase lock onto a 31.65 GHz carrier and measure the received power in the carrier and also the power in either 1, 10, or 50 MHz sidebands if the carrier is modulated. (See Figure 1-8.) The receiver can also measure differential phase between the modulated sidebands using the carrier as a reference.

The signal paths in the receiver can be traced in Figure 1-8 through the 1.05 GHz wideband first intermediate frequency amplifier and the second 60 MHz IF conversion stage including the phase lock loop. The carrier and sidebands are then separated in a bank of band pass filters. The three channels are then converted to 10 MHz in separate mixers. The 1050 MHz to 60 MHz carrier mixer closes the phase lock loop in which the phase comparison is made at 10 MHz. The bandwidth of the phase lock loop was set around 100 Hz to maximize to hold in range without making the frequency acquisition problem too difficult. This resulted in a dynamic range of -85 dbm to approximately -120 dbm. The phase lock loop had an automatic sweep acquisition circuit to acquire the carrier but the satellite spin condition rendered the system useless. A command to stop the sweep was used along with manual tuning of the ground transmitter to acquire the signal.

The receiver data included the amplitudes of the carrier and sidebands along with the differential phase outputs and these processor outputs were used to frequency modulate subcarrier VCO's. These VCO frequencies were then mixed and the sum FM modulated the C-band wideband link for transmission to the ground.

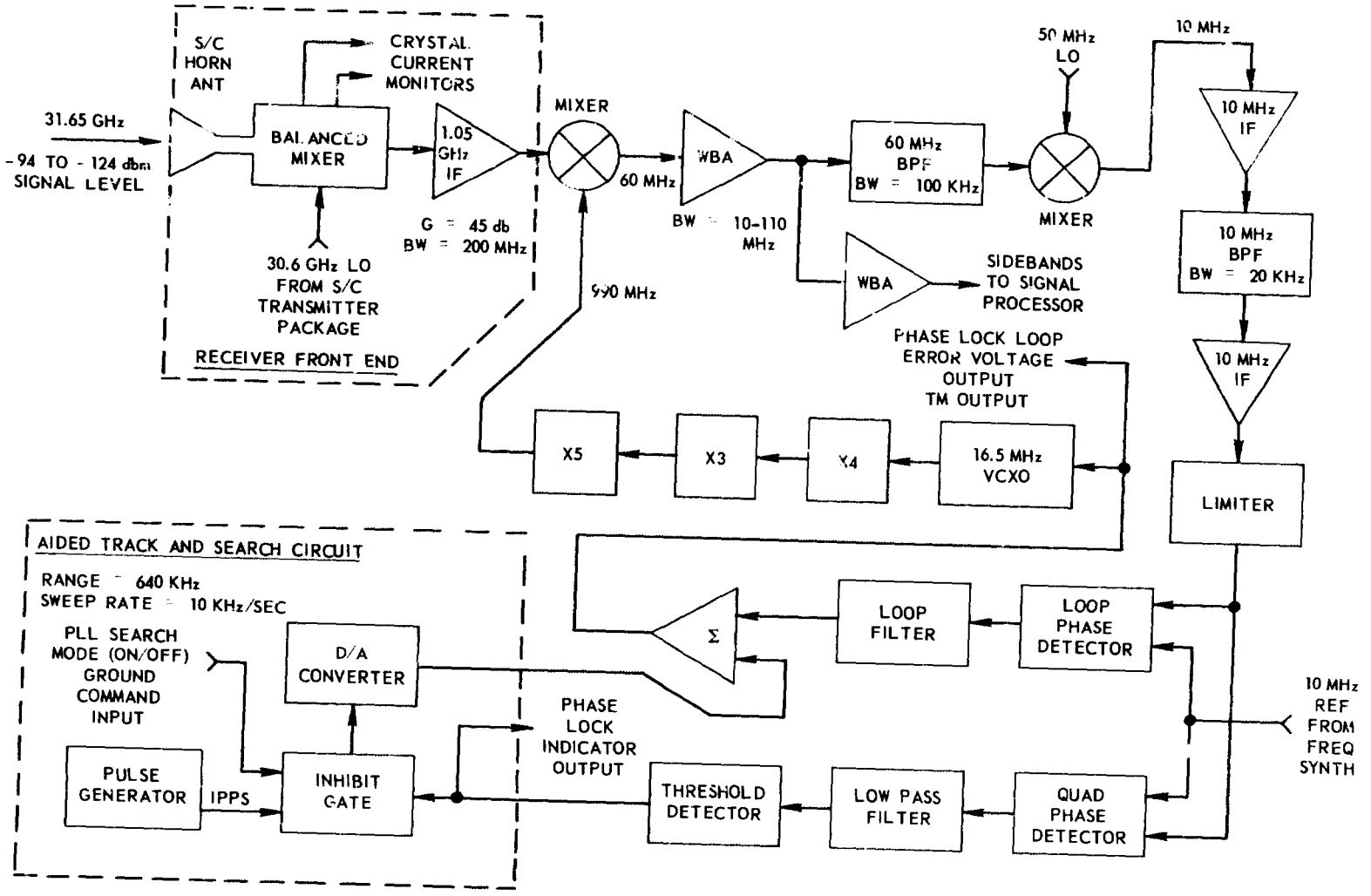

Figure 1-8. Receiver Front End and Phase Lock Loop Block Diagram

The spacecraft antenna were conical horns designed to produce 17° beams which provided full earth coverage at synchronous altitude. These horns had peak gains of approximately 19.5 db.

ATS-5 MILLIMETER WAVE EXPERIMENT GROUND STATIONS

The ground stations which participated in the ATS-5 Millimeter Wave Experiment might best be characterized by saying that they varied from a simple 10 foot manually pointed antenna to 60 foot antennas with computer controlled tracking facilities costing millions of dollars. The stations which have participated had geographical locations ranging from San Diego, California to Ottawa, Canada to Orlando, Florida and they are listed in Table 1-1 along with the antenna sizes and special areas of interest.

Most of the participants used NASA supplied receivers to take the 15.3 GHz data, with the exception of BTL, Comsat, and CRC. The BTL receiver used narrowband (approximately 50 kHz) predetection filters at the output of one of their radiometers to measure the pulse amplitude. Comsat used a phase lock receiver which was similar to the NASA design, and CRC used a phase lock telemetry receiver at the output of a 15.3 GHz converter to make the measurements. The rest of the sites used either NASA supplied Martin sideband receivers or Martin CW/radiometer receivers.

The Martin sideband receivers had the capability of making both amplitude and differential phase measurements. The receivers employed a phase lock loop with a minimum bandwidth of about 50 Hz to provide a continuous signal dynamic range of approximately -112 dbm to -145 dbm. Unfortunately, the satellite spin condition caused the phase lock loop to loose lock on each revolution and the 40 millisecond pulsed single condition reduced the minimum detectable signal to about -136 dbm. This resulted in a 24 db dynamic range at Rosman using a 15 foot antenna with a 250 milliwatt 15.3 GHz transmitter. The receiver used a tunnel diode amplifier front-end with a noise temperature of about 1000°K. The 1.05 GHz first IF frequency and the subsequent mixing stages (Figure 1-9) converted all of the signal (carrier and sidebands) to 10 MHz where the differential phase measurements were made using the carrier as a reference. The 10 MHz signals were then converted to 2.5 kHz where they were processed in linear amplitude detectors. The receivers also included a calibration signal and attenuators to make daily checks of the receiver's performance.

The Martin CW/Radiometer receivers used similar front ends and conversion stages with the addition of a ferrite modulator, a 1.05 GHz detector, calibration loads, and a synchronous detector. These additional components along

Table 1-1

ATS-5 Millimeter Wave Experiment Participating Stations

	Stations	Antenna Sizes	Nominal Elevation Angle	Primary Areas of Interest
Primary Data Stations	Communications Research Centre Ottawa, Canada	30'	30°	Radar and radiometer satellite data correlation
	Bell Telephone Laboratories Holmdel, N.J.	20'	34°	Radiometer and satellite data correlation
	Comsat Laboratories Clarksburg, Md.	16'	36°	Radiometer, radar and rain rate correlations with satellite data
	Goddard Transportable Rosman, N.C. (Only 31.65 GHz XTR Site)	15'	42°	Radiometer, radar and rain rate correlations, 15.3 GHz and 31.65 GHz satellite statistical data
	Ohio State University Columbus, Ohio (2 Sites)	30' 15'	39°	Site diversity data, radar, radiometer and rain rate correlations with satellite data
	Naval Electronics Laboratory San Diego, Calif.	60'	50°	Satellite data
	Naval Research Laboratories Waldorf, Md.	60'	36°	Radiometer and satellite data correlations
	University of Texas Austin, Texas	2-10'	51°	Radiometer, ground link measurements, rain rate correlations with satellite data
	Martin Marietta Corp. Orlando, Fla.	12'	48°	Rain rate and satellite data correlations
Active Stations	AFCRL Bedford, Mass.	28'	30°	
	Dept. of Transportation Cambridge, Mass.	10'	30°	
	Rome Air Development Center Rome, N.Y.	15'	32°	
	ESSA Wave Prop. Lab Boulder, Colo.	10'	44°	
	Westinghouse Georesearch Lab Boulder, Colo.	10'	44°	
	USASCA Lakehurst, N.J.	30'	34°	

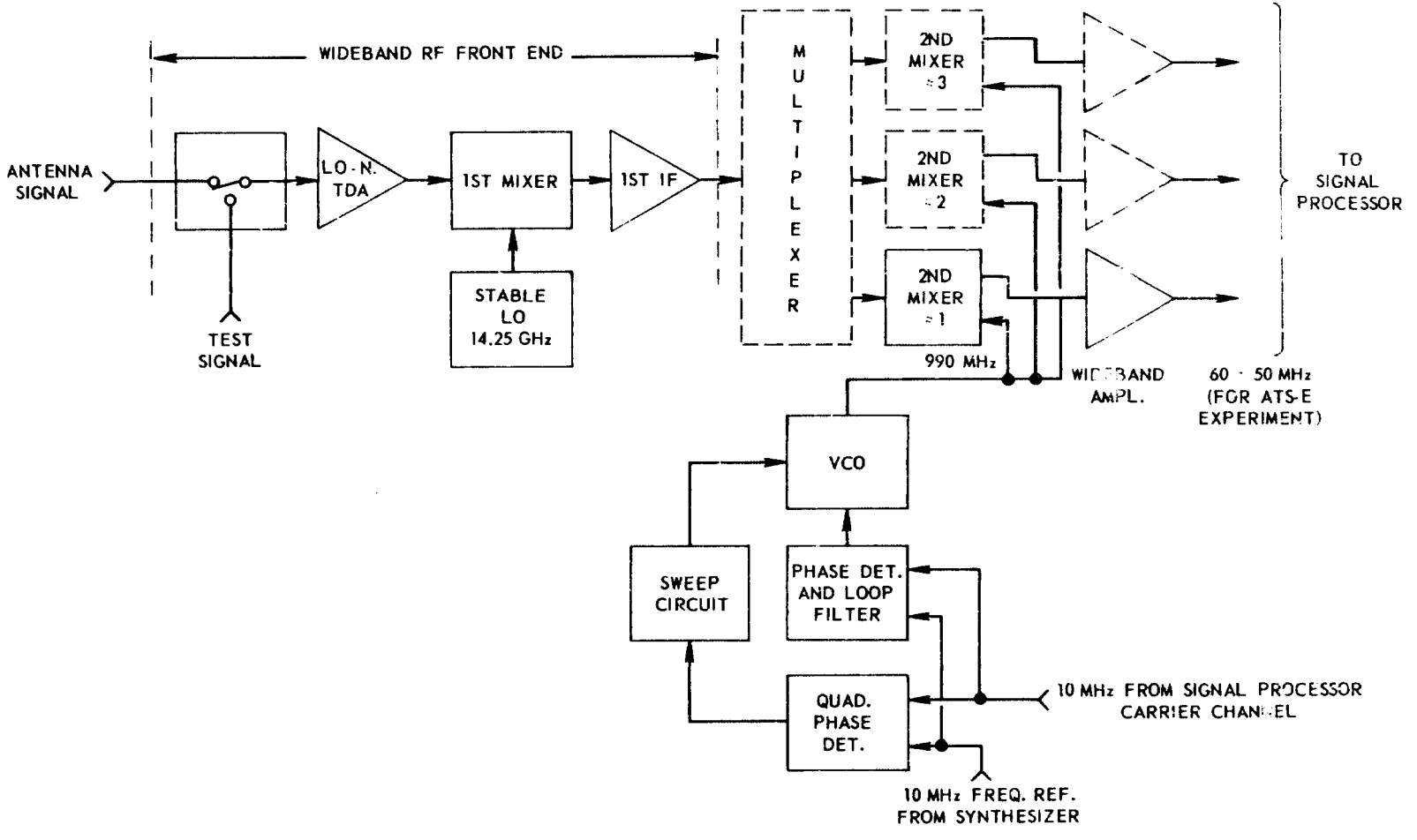

Figure 1-9. Front End Multiplexing for Wideband Operation

with filters and hybrid couplers shown in Figure 1-10 enabled the receiver to make sky temperature measurements while receiving the satellite carrier signal. The radiometer modulator did cause an additional 6 db loss of dynamic range, however, and most sites turned off the radiometer when making satellite attenuation measurements. Only NRL with a 60 foot antenna was able to make useful simultaneous measurements. These receivers used temperature controlled loads and noise sources for calibration of the radiometers, and 15.3 GHz CW signals with attenuators were also provided to calibrate the amplitude dynamic range.

The NASA station located at Rosman, North Carolina consisted of a trailer, a 15 foot computer tracking antenna system, radiometers, radar systems, and a 31.65 transmitter. (See Figure 1-11.) This was the only station equipped to transmit at 31.65 GHz. Plans to install a second transmitter at the NELC site were abandoned because of the satellite problems and because the weather conditions at the site were not favorable for gathering rain data. The Rosman 31.65 GHz transmitter was a 1 kw TWTA built by Hughes Aircraft Company (see Figure 1-12). The 1 kw power amplifier was driven by a 31.75 GHz phase locked klystron. The transmitter could be AM modulated by upconverting 1, 10, or 50 MHz sidebands onto the 31.65 GHz carrier.

Some bandwidth data was taken using the sidebands early in the program, but difficulties in maintaining phase lock in the satellite receiver caused by the ATS-5 spinning limited this data. After the first 3-4 months more emphasis was placed on trying to measure simultaneous 15.3 downlink and 31.65 GHz CW uplink attenuation during rain to establish a statistical plot of the ratio between the losses at the two frequencies. Unfortunately the 31 GHz uplink data was limited during most of the experiment because it required the use of the C-band downlink and the 85 foot C-band receiving system at Rosman to collect the 31 GHz satellite receiver data.

The Rosman site had 16 and 35 GHz radiometers and a 2 mile rain gauge system (10 gauges placed under the path to the satellite) which were used to derive correlation functions with the satellite data. These supporting data were also used to fill in voids when the satellite was not available for direct measurements. The RDR-100 15.6 GHz weather avoidance radars were also used at Rosman during the experiment. These radars were used to provide photographs of vertical cuts through the atmosphere and also to measure gross integrated backscatter signals looking along the satellite path which were recorded during precipitation.

The 15 foot diameter cassegrain antenna system at Rosman used a dual frequency feed which allowed simultaneous 1 KW transmissions at 31 GHz while

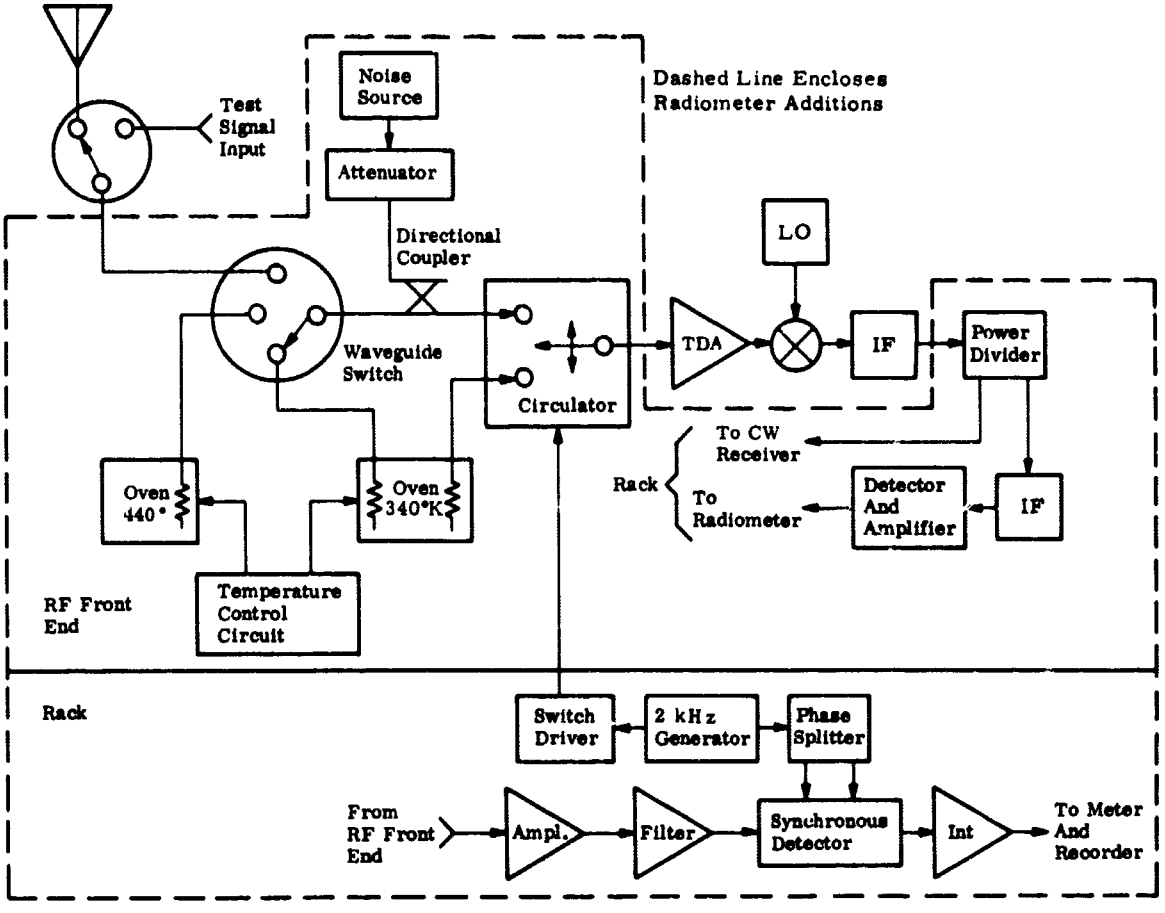

Figure 1-10. Radiometer System Block Diagram

NASA ROSMAN, NORTH CAROLINA STATION

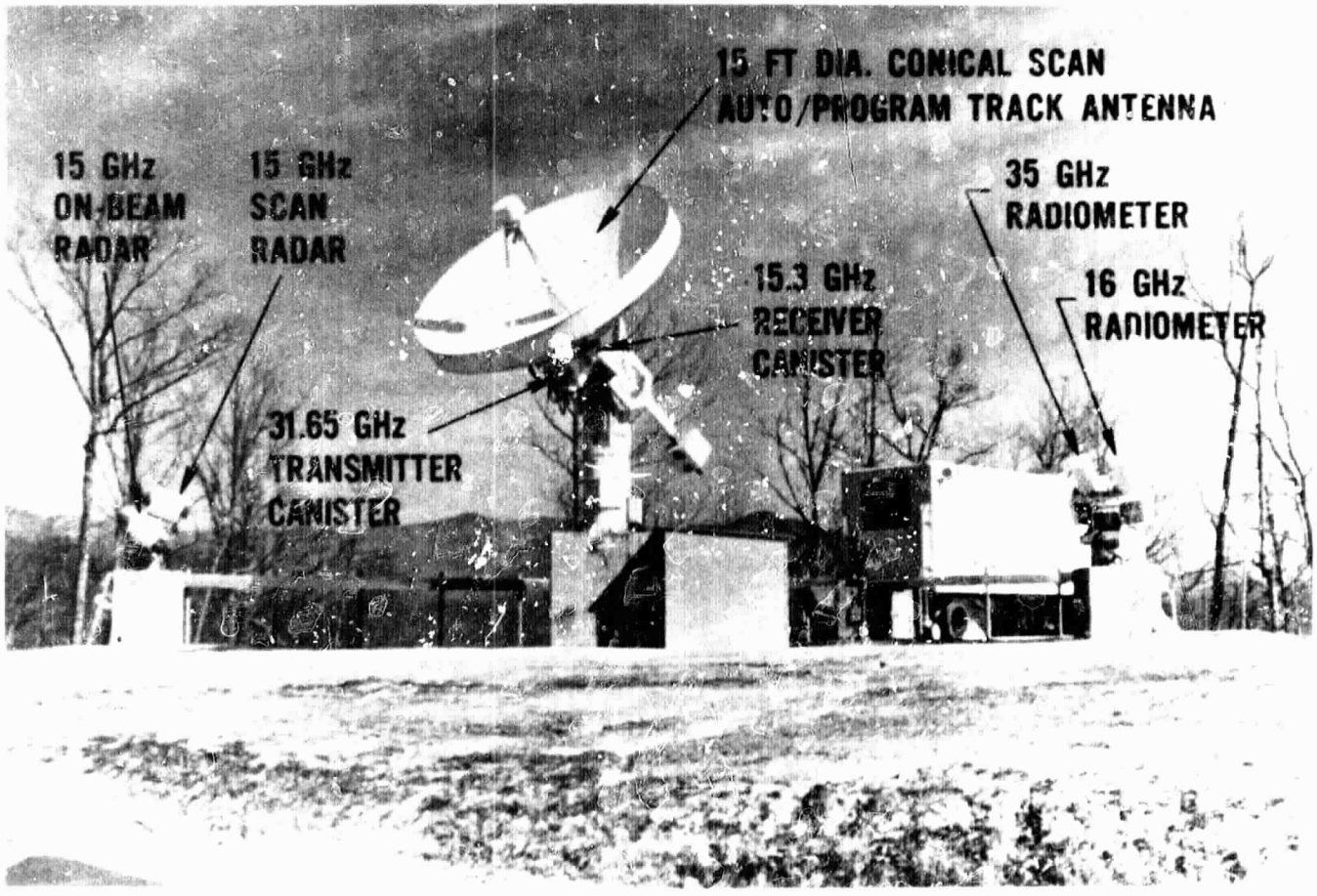

Figure 1-11. NASA Rosman, North Carolina Station

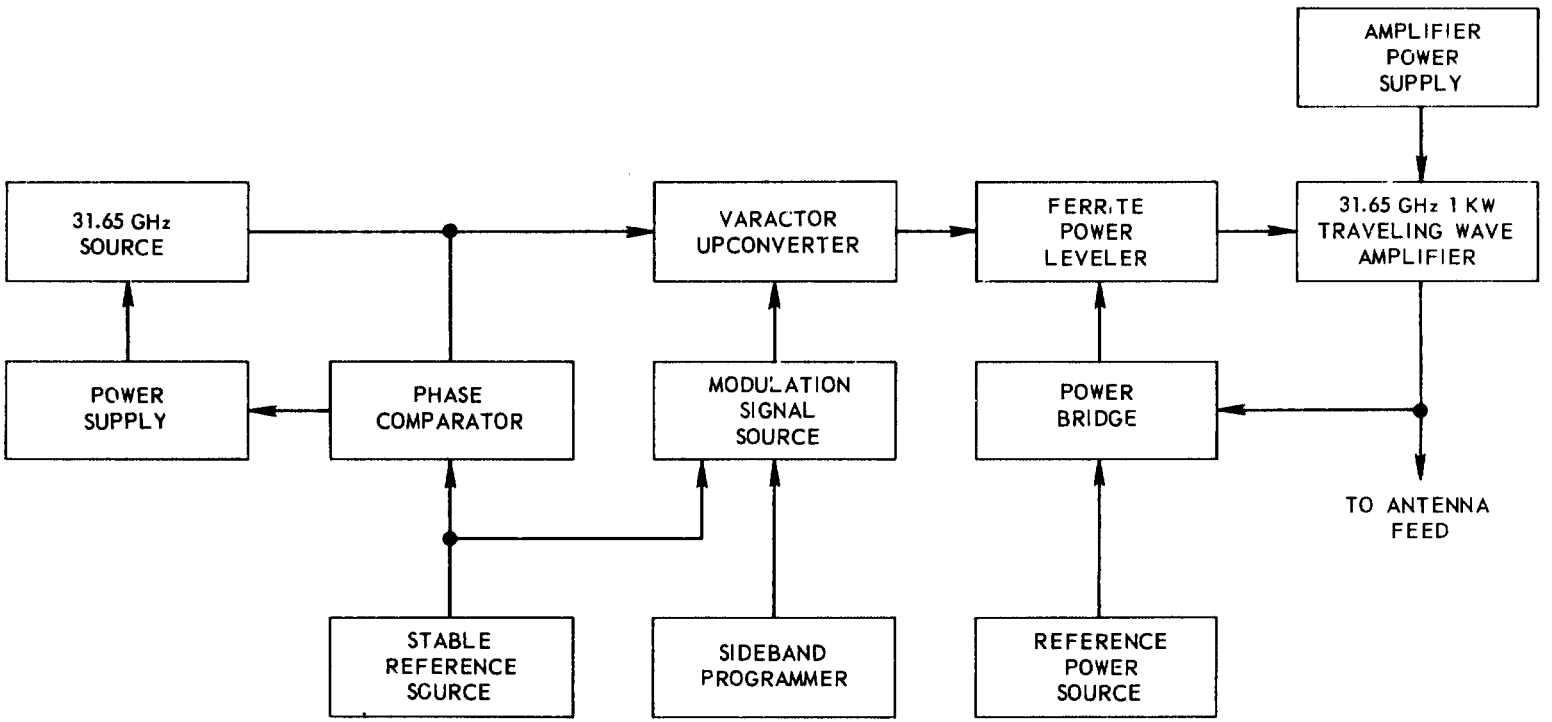

Figure 1-12. 31.65 GHz Transmitter System Block Diagram

receiving at 15.3 GHz. The Rosman antenna tracking system uses a PDP8 computer to calculate pointing angles and position the antenna to follow the satellite's slow elliptical pattern it traces in the sky.

Several of the other sites had areas of particular interest on which they concentrated during the two years of data collection (see Table 1-1). Ohio State University, for instance, concentrated on investigating site diversity by using two stations spaced at several separations; BTL took particular interest in the correlation of the attenuation predicted using radiometric data and the direct satellite attenuation measurements; and most of the sites, including Rosman, Texas, Ohio State, Comsat, and CRC also collected radiometric data. The Communications Research Center in Ottawa, Canada gave more priority to the correlation of radar backscatter and satellite attenuation data. Comsat and Rosman collected a great deal of rain rate data to show correlations with these statistics and the University of Texas used ground link measurements as a means of determining rain rates for analysis with the satellite data. The complete scope of the propagation work being done at these stations is too extensive to be present here and these special areas of interest apply only to their contributions to the experiment.

EXPERIMENT OPERATIONS

The ATS-5 satellite was controlled by the ATS Operations Control Center (ATSOCC) at GSFC which was available 24 hours a day during the first two years of the experiment. Each of the participants could call ATSOCC and request that either the primary or backup millimeter transmitters be turned on. These requests were usually accommodated early in the program before the transmitter problems occurred, but there were some conflicts because only one command transmitter was available during part of the day and ATSOCC had three satellites to control and interrogate. After the power degradations problems with the transmitters more conflicts occurred because of the limited three 45 minute operating periods allowed when using the backup transmitter. When several areas were experiencing rain on the same day, Murphy's Law usually prevailed, and some of the sites could not complete their data runs before the transmitter had to be turned off. This did not become a significant problem until the second year of operation (after February 1971) when the primary transmitter power losses rendered that transmitter useless. During the first year, the primary transmitter was used more extensively even with the 9 db power degradation because no time limitations were imposed.

The limited availability of the backup transmitter and a ATSOCC schedule caused some loss of satellite data, but most of the sites had ratiometers, radars,

or rain gauges that were used to predict attenuation on a statistical basis during most of these times when the satellite was not available. These instruments allowed the participants to generate meaningful statistical propagation data at 15.3 and 31.65 GHz which can be used by communications system designers to plan new communication systems in these new band to alleviate the spectrum crowding which is now taking place below 10 GHz.

REFERENCES

1. Binkley, Ippolito, King, and Ratliff, The ATS-E Millimeter Wave Propagation Experiment, April 1968, NASA/GSFC Report X733-68-196.

2. Ippolito, Louis J., ATS-V Millimeter Wave Experimert Data Report, October-December 1969, March 20, 1970, NASA/GSFC Report X-733-70-123.

3. Ippolito, Louis J., Millimeter Wave Propagation Measurements from the Applications Technology Satellite (ATS-V), IEEE Trans. on Antennas and Propagation, July 1970, pg. 525-552.

4. ATS Technical Data Report, Section 7.3 — The ATS-5 Millimeter Wave Experiment; ATS Program GSFC.

SECTION 2

ATTENUATION PROBABILITIES OF 15 GHz RADIO WAVES OVER EARTH-SATELLITE PATHS

A. W. Straiton
The University of Texas at Austin

ABSTRACT

This paper surveys the probability of occurrence of various attenuation levels of 15 GHz radio signals over earth-satellite paths at seven locations in the United States and one in England.

Three methods of measurements provided the data used for this paper. One of these was the observation of the coherent signal from the ATS-5 satellite. The second was the measurement of the solar radiation received and the third was by use of sky temperature observations. The attenuations experienced at the various stations are interpreted in terms of the number and intensity of thunderstorms occurring at these stations. It is shown that this thunderstorm activity is a good index of the amount of the attenuation at the various stations. The probability of occurrence of losses in excess of 10 dB was found to vary between stations from .008% to .13% of time while the probability of occurrence of attenuation as great as 5 dB was found to vary from .015% to .45%.

INTRODUCTION

The use of radio waves at frequencies greater than 10 GHz for earth-satellite communication in the near future seems to be needed and probable. It is essential that information be obtained on the reliability of receiving these signals at a given site so that the receiver requirements and antenna sizes may be determined.

This paper surveys the probability of occurrence of various attenuation levels of 15 GHz radio signals over earth-satellite paths as reported for seven locations in the United States and one in England. The participating organizations, their locations, the techniques used and the references from which the attenuation data was obtained are shown in Table 2-1. Details of the individual experiments are presented in these references.

Table 2-1

Observation Stations

Location	Organization	Techniques Used	Reference
Clarksburg, Maryland	Communication Satellite Corporation	ATS-5 Sun Tracker Sky Temperature	(1)
Slough, Bucks, England	Solar Research Observatory	Sun Tracker (19 GHz)	(2)
Holmdel, New Jersey	Bell Telephone Laboratories	Sun Tracker (16 GHz) Sky Temperature (16 GHz)	(3)
Point Reyes, California	Bell Telephone Laboratories	Sun Tracker (16 GHz) Sky Temperature (16 GHz)	(4)
Orlando, Florida	Martin Marietta Corporation	ATS-5	(5)
Rosman, North Carolina	Goddard Space Flight Center NASA	ATS-5	(6)
Austin, Texas	The University of Texas	ATS-5 Sky Temperature (35 GHz)	(7)
Mt. Locke, Texas	The University of Texas	ATS-5	(8)

The results are admittedly somewhat crude because of the variety of methods of measurement and the limited amount of data on which the results were based. In spite of these limitations, the general trends of the probability curves are believed to be quite useful. The probability of occurrence of high attenuation levels is quite small and will depend on the very severe storms which occur infrequently. Accordingly the amount of data available for the higher attenuation levels is very limited and its interpretation is difficult because of the variability of the worst weather conditions from year to year.

The atmosphere is very transparent to 15 GHz radio waves except when rain or rain clouds occur along the path. The most severe attenuation occurs when the rain is associated with thunderstorms. Although many of the observations were made only during periods when the rain was occurring, the signals for clear weather may be assumed to be unattenuated.

TYPES OF MEASUREMENT

Observation of ATS-5 Satellite Transmissions

The ATS-5 satellite provided a signal at 15.3 GHz which was observed by a number of stations in the United States and Canada. The spinning of the satellite as described elsewhere resulted in a reduction of the average power received of approximately 14 dB and power problems on the satellite further reduced the available signal levels. As a result the signal-to-noise ratio at the receiving stations was limited to 12 to 25 dB. In order to conserve power the satellite was turned on only on request so that sufficient lead time was necessary to have the satellite transmitting during a rain storm. A number of rain storms were missed because of insufficient lead time or from the commitment of the satellite to other experiments.

The satellite was observed at essentially constant elevation angle from each station with variations from approximately 30 to 60 degrees between stations. The ATS-5 signal provided the only coherent source used for these studies and was the basis to which the other techniques were compared.

Sun-tracking Data

A good source of data on attenuation through the atmosphere is provided by tracking the sun as it moves across the sky. In particular, Bell Telephone Laboratories obtained data taken in this fashion over an extended period of time. The sun-tracking data gives a high signal-to-noise ratio but is limited to daylight hours and requires a variable elevation angle. This makes it somewhat

difficult to compare these data with those obtained at constant elevation angles. Meteorological experience, however, has indicated that in many instances the thunderstorm shapes are such that their horizontal and vertical extents are comparable and thus the pathlength through the storm may be essentially independent of angle of elevation. For this reason the comparison of the sun-tracker data with other types of data is felt to be justified. For sun tracker data taken at frequencies other than 15.3 GHz adjustment was made in accordance with the frequency dependence of rain loss as given by Setzer[10].

Sky Temperature Data

The third method by which data were obtained was the measurement of the radiation from the sky. It has been shown that the equivalent sky temperature can be converted to total attenuation through the atmosphere for attenuations of approximately 12 dB or less. The conversion depends on neglecting scattering from the raindrops and on knowing the temperature of the rain. Although the effects of these assumptions are not fully understood, the resulting losses determined from sky temperature measurements have been found to agree quite well with those obtained by the use of sun-tracking or ATS-5 observations. The main limitation of the use of the sky temperature data is that as saturation approaches the accuracy of the measurements decreases, thus providing the 12 dB limit previously mentioned. Losses determined at frequencies other than 15.3 GHz were adjusted to this frequency by the same method used for the sun tracker results.

RELATION TO THUNDERSTORMS

A single meteorological parameter was sought as a frame work for comparing the site variations and as a possible means of extrapolating the result to other locations. A parameter proposed for this purpose is the thunderstorm activity at each observation site. The annual distribution of thunderstorms in the United States is shown in Figure 2-1 as taken from a Weather Bureau publication.[9] The average number of thunderstorms experienced annually at each of the eight locations is shown in Table 2-2.

The relationship between the maximum attenuation experience during a particular thunderstorm to the height of the clouds was studied. The results of this study are shown in Figure 2-2 with the locations of the storms shown in the figure legend. It is noted that there is a consistent increase of the attenuation level with an increase in height of the storms. There is no assurance that the transmission path follows the route of maximum attenuation for each case. Thus some of the plotted points may indicate less attenuation than would have

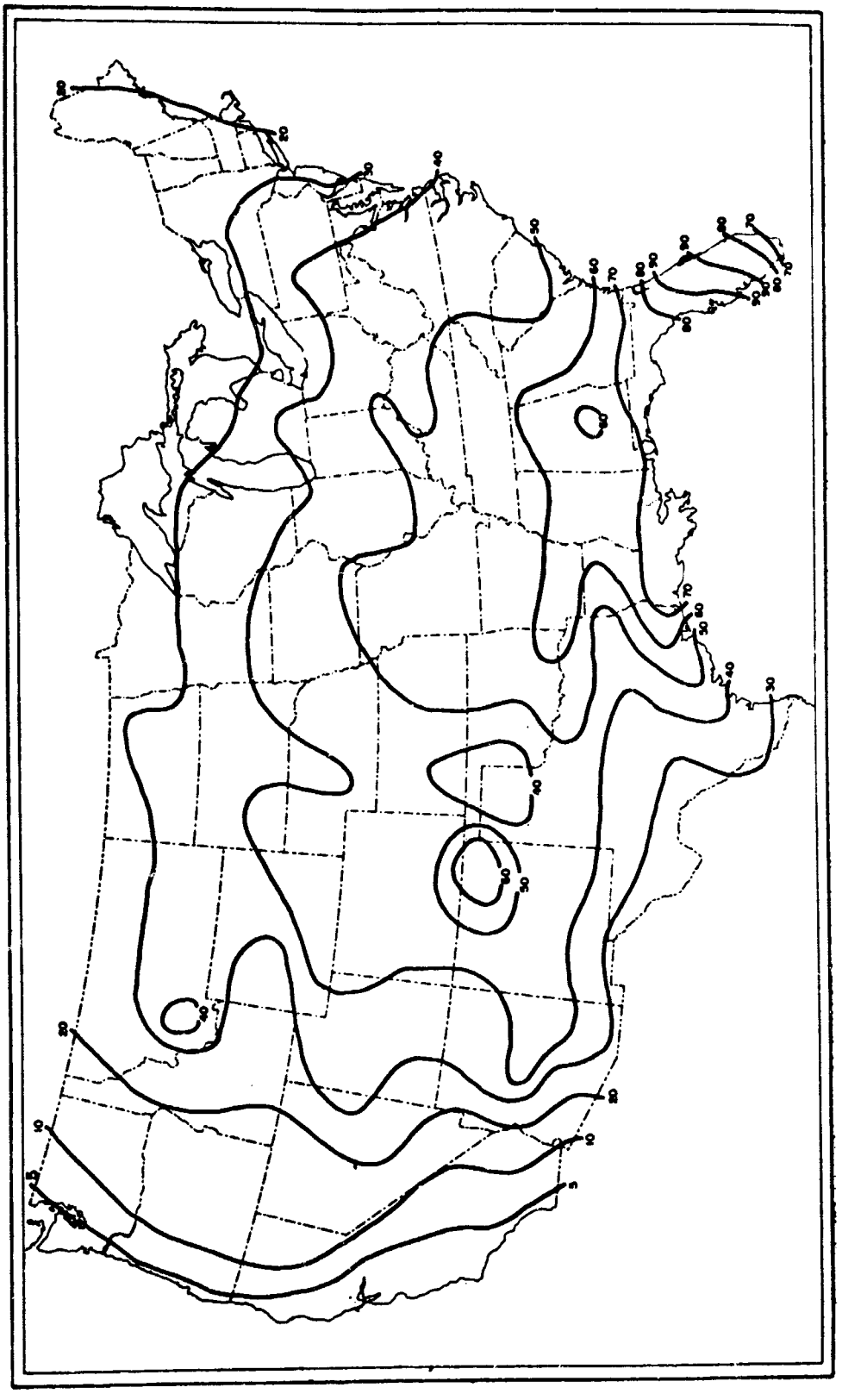

Figure 2-1. Annual Mean Number of Thunderstorms

Table 2-2

5 and 10 dB Probabilities and Number of Thunderstorms

Location	Observation Interval	Probability of Losses		Annual Number of Thunderstorms
		>5 dB	>10 dB	
Orlando, Florida	Feb 71-Sept 71	0.13%	0.07%	90
Rosman, North Carolina	Jan 70-Dec 70	0.4%	0.015%	45
Austin, Texas	Jan 70-Jun 71	0.3%	0.013%	40
Clarksburg, Maryland	Jul 70-Dec 71	0.12%	0.05%	35
Holmdel, New Jersey	Dec 67-Dec 68	0.12%	0.05%	30
Mt. Locke, Texas	Sept 71-Oct 71	0.00%	0.00%	30
Slough, Bucks, England	Jun 68-Aug 70	0.02%	Not available	15
Point Reyes, California	Dec 70-Aug 71	0.015%*	0.008%*	5

*Daytime Only

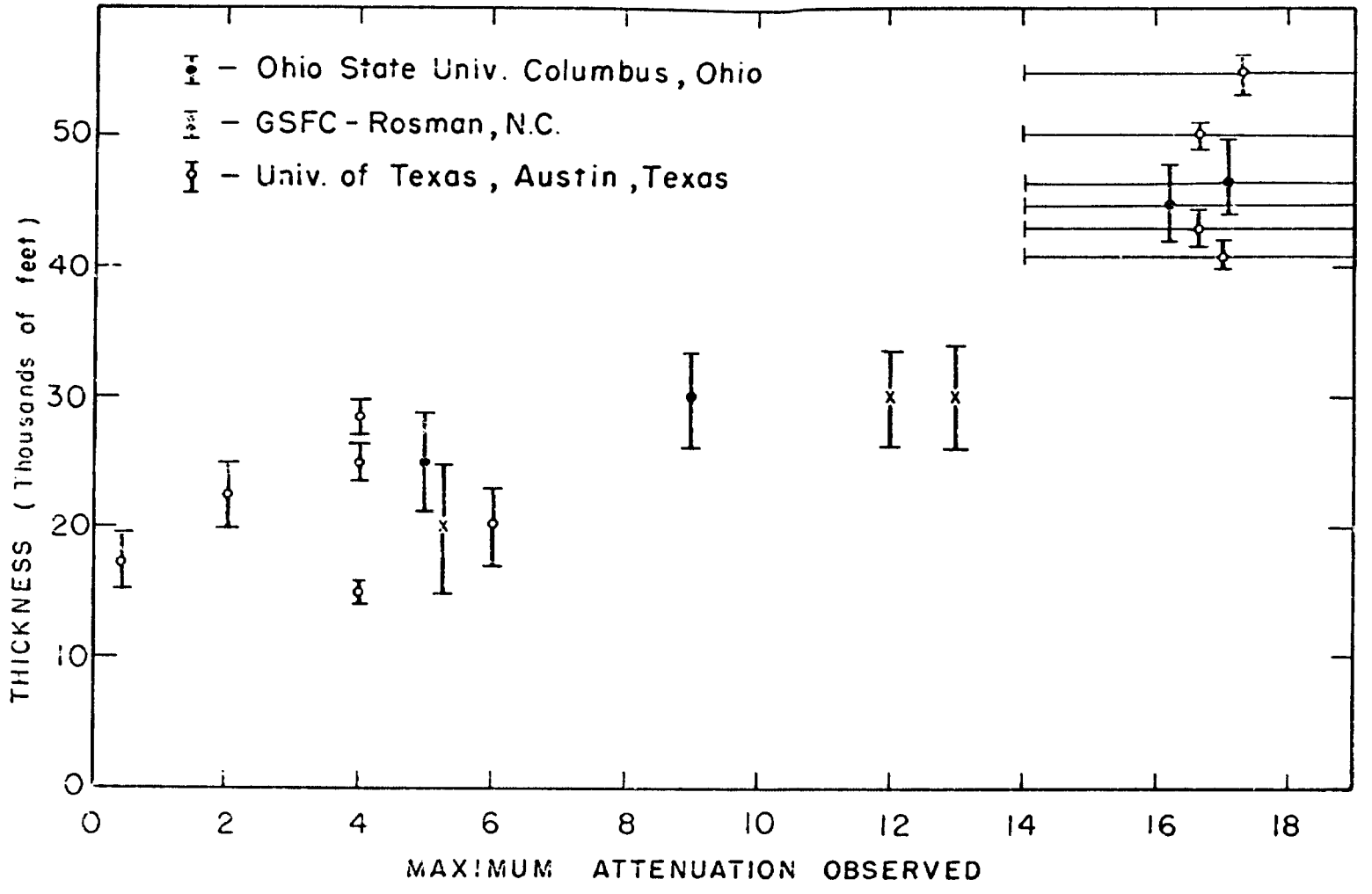

Figure 2-2. Thunderstorm Thickness Vs. Attenuation

occurred on a maximum loss path. This is believed to be the case for some of the low attenuations with the higher thunderstorm heights.

All of the storms which exceeded 40,000 feet in elevation were such as to cause the signal level to be lost in the noise. The resulting attenuation for these cases is shown by the lines extending above the 12 dB level. In spite of these limitations, the trend in the curve is well enough defined to indicate that the thunderstorm height is a good index for the occurrence of various levels of attenuation.

COMPARISON OF ATTENUATION STATISTICS AT VARIOUS STATIONS

In order to study the relationship between the attenuation statistics at various stations, the available data have been grouped together according to several criteria. In Figure 2-3, three sets of loss data are presented each of which was based on sun-tracker data only. The locations were (1) Holmdel, New Jersey, (2) Point Reyes, California, and (3) Slough, Bucks, England. It is noted that there is a sharp contrast between the attenuation levels at Holmdel and at the other two locations. This is in general agreement with the average number of thunderstorms expected in these areas. The attenuation levels differ by a factor of ten or more in their probabilities of occurrence between Holmdel and the other sites for losses greater than 6 dB. Since the curves are based on sun-tracker data they are for daylight hours.

Figure 2-4 shows a comparison of the statistics from Clarksburg, Maryland, and Holmdel, New Jersey on a 24-hour basis with the same Point Reyes sun-tracker results. Data taken by the different methods have been combined to give these 24-hour statistics. It is noted that the curves for Clarksburg, Maryland and Holmdel, New Jersey essentially coincide. This is in agreement with the fact that these two sites have very similar meteorological conditions. The curve for California again is very much lower than those for the Eastern Coast but the difference is not as much as in the case of the daytime comparisons. These curves on a 24-hour basis show a lower probability of occurrence of various loss levels than do the sun-tracker data. When the daytime and nighttime data are compared, it is found that probability of occurrence of a given attenuation level is three or four times higher during the day than at night. This again corresponds to the greater number of thunderstorms during the day than at night.

Figure 2-5 shows the seasonal trend at Clarksburg, Maryland. These curves are based on minutes of observing time rather than a percent of total time. These results emphasize the fact that the intervals during which thunderstorms were more frequent are also those when the attenuation probability is larger.

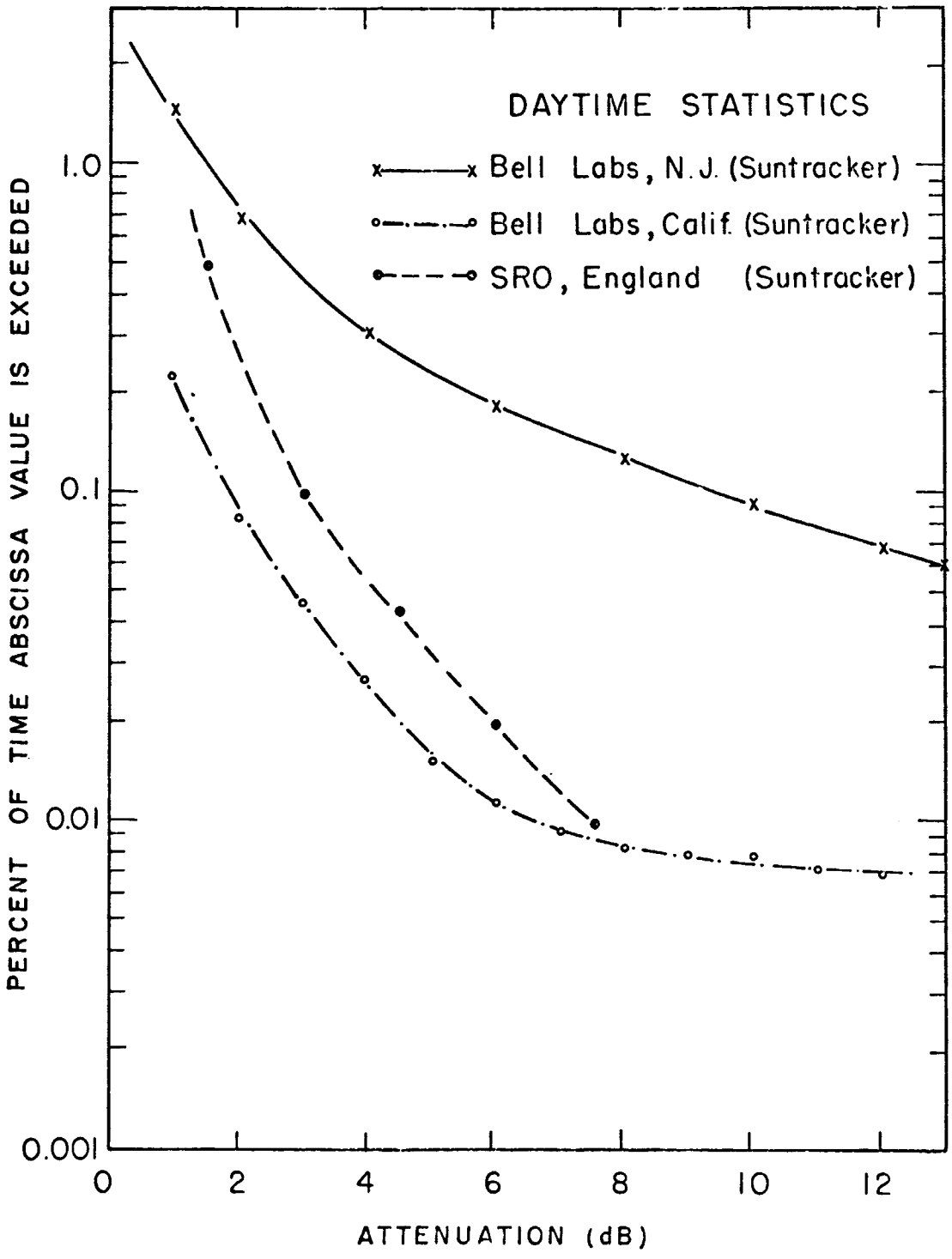

Figure 2-3. Sun Tracker Comparisons

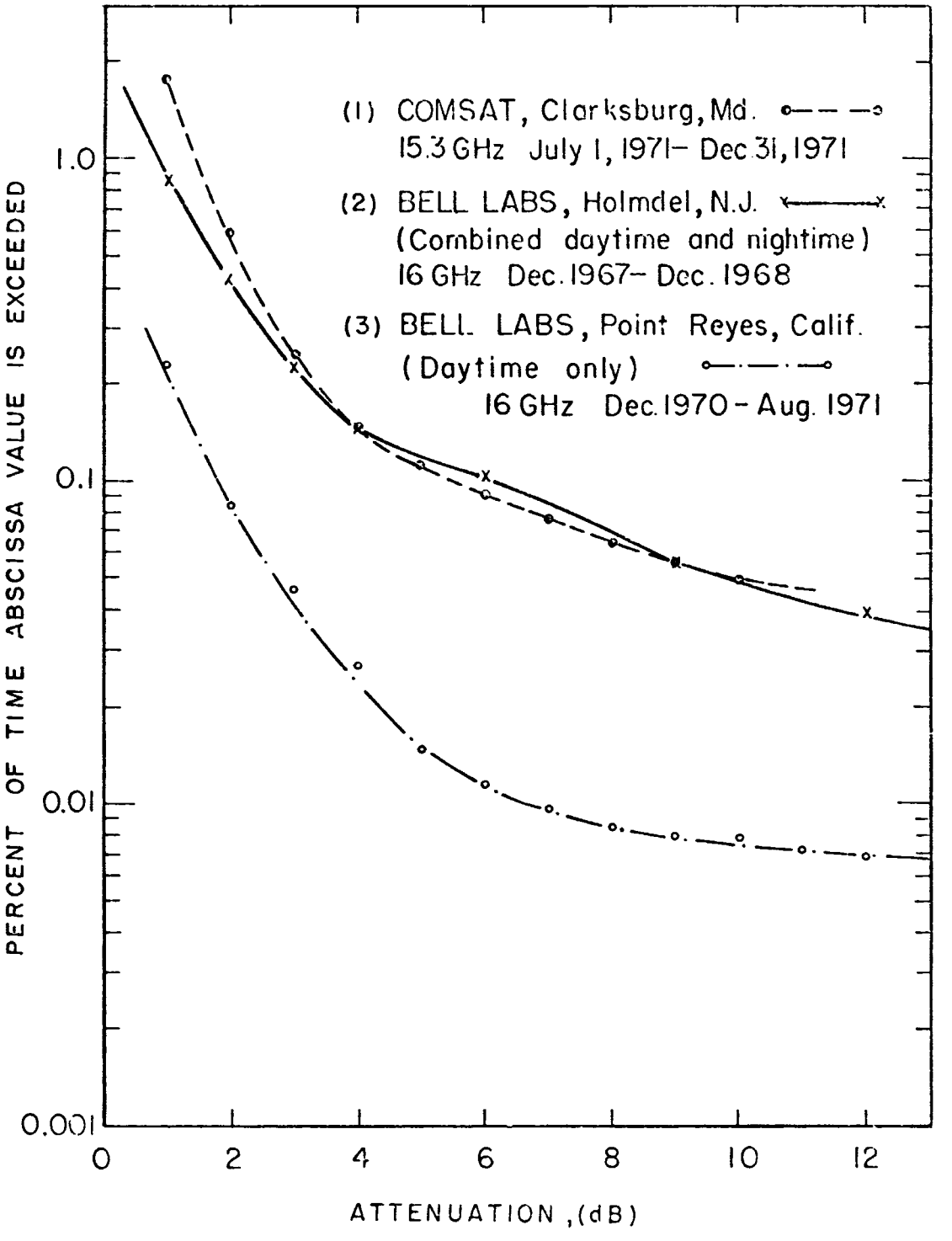

Figure 2-4. Composite Comparisons

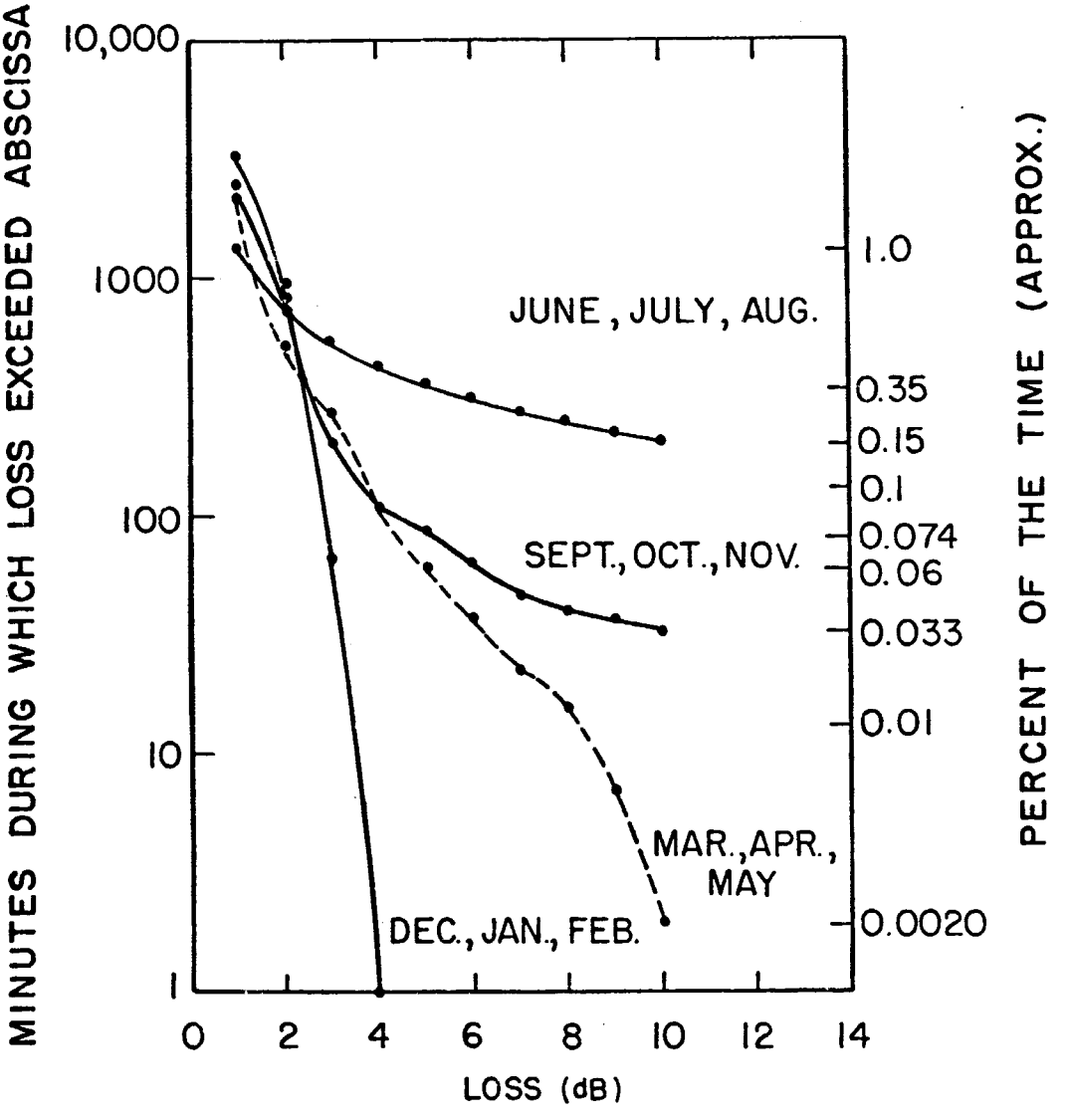

Figure 2-5. Seasonal Attenuation Statistics for Clarksburg, Md.

The period of December, January, and February at Clarksburg shows very small attenuations while those in June, July and August are quite high.

Figure 2-6 shows a comparison of the data taken at Rosman, North Carolina with that taken at Orlando, Florida. Two different observation intervals are shown in each case but their general features are the same when only the one site is considered. There is somewhat of an anomaly in that the losses at Rosman are greater for the lower attenuation levels than those in Florida, even though the thunderstorm activity in Florida is much greater. However, the total rainfall in North Carolina during the interval of these measurements was high and resulted in the high probabilities of the lower attenuations. It is believed that if these curves were extended to the higher loss levels, the Orlando data would consistently show higher probability of attenuation than the data at Rosman. The seasonal trend mentioned earlier was quite evident in the Orlando data for two time intervals as shown in Figure 2-7. A loss of 10 dB is shown to be 100 times more likely to occur during June, July and August than during February through May. This again is in agreement with the expected occurrence of thunderstorms.

Figure 2-8 compares two sets of observations made by The University of Texas in Texas. One of these was made in Austin, Texas and the other was made at Mt. Locke in West Texas approximately 400 miles west of Austin. The Austin data is based on ATS-5 observations and 35 GHz sky temperature measurements adjusted to 15 GHz over a period of 18 months and is considered to be a reliable picture for the time interval considered. The Mt. Locke data were taken from ATS-5 observations over a two-month interval. Although this is a short measurement period, it covered most of the rainy season for West Texas and included seven intervals during which rain showers occurred. There is a very significant contrast between the attenuation in Austin and that at Mt. Locke. In spite of the fact that the total annual rainfall in the two places is roughly the same, the Mt. Locke results showed very low probabilities of occurrence of significant loss. The only attenuation over one dB experienced at Mt. Locke was during one rain storm and the maximum attenuation during that storm was only slightly over 4 dB. The site at Mt. Locke was the only one of those considered which was on a mountain. The elevation at Mt. Locke was 6600 feet. The number of thunderstorms in the area is rather large but because of the high elevation and the fact that the thunderstorms usually appear in somewhat isolated rain showers the attenuation was quite low.

CONCLUSION

This paper has presented a comparison of the attenuation statistics obtained at seven locations by three different techniques. Although the amount of data

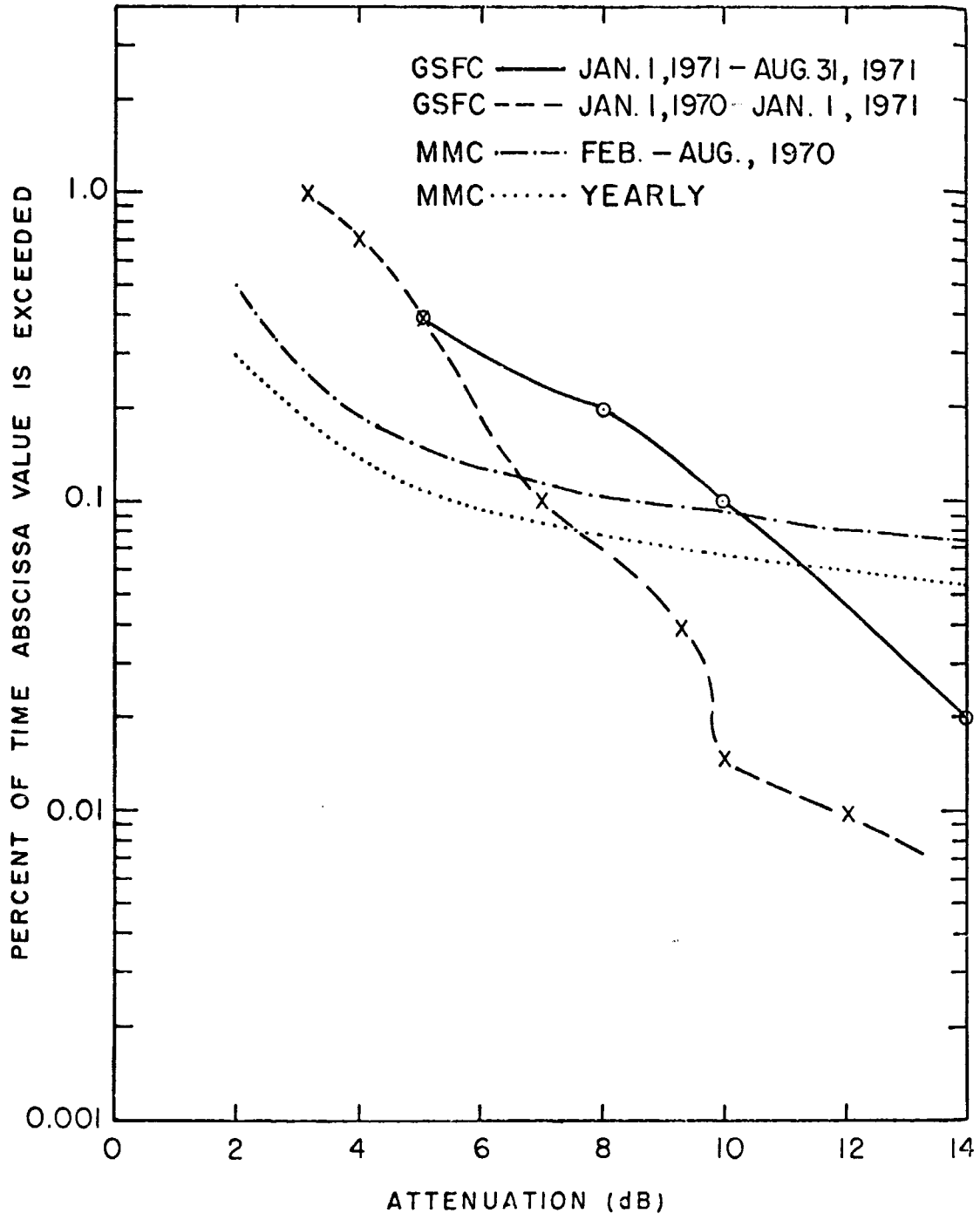

Figure 2-6. Comparison of North Carolina and Florida Data

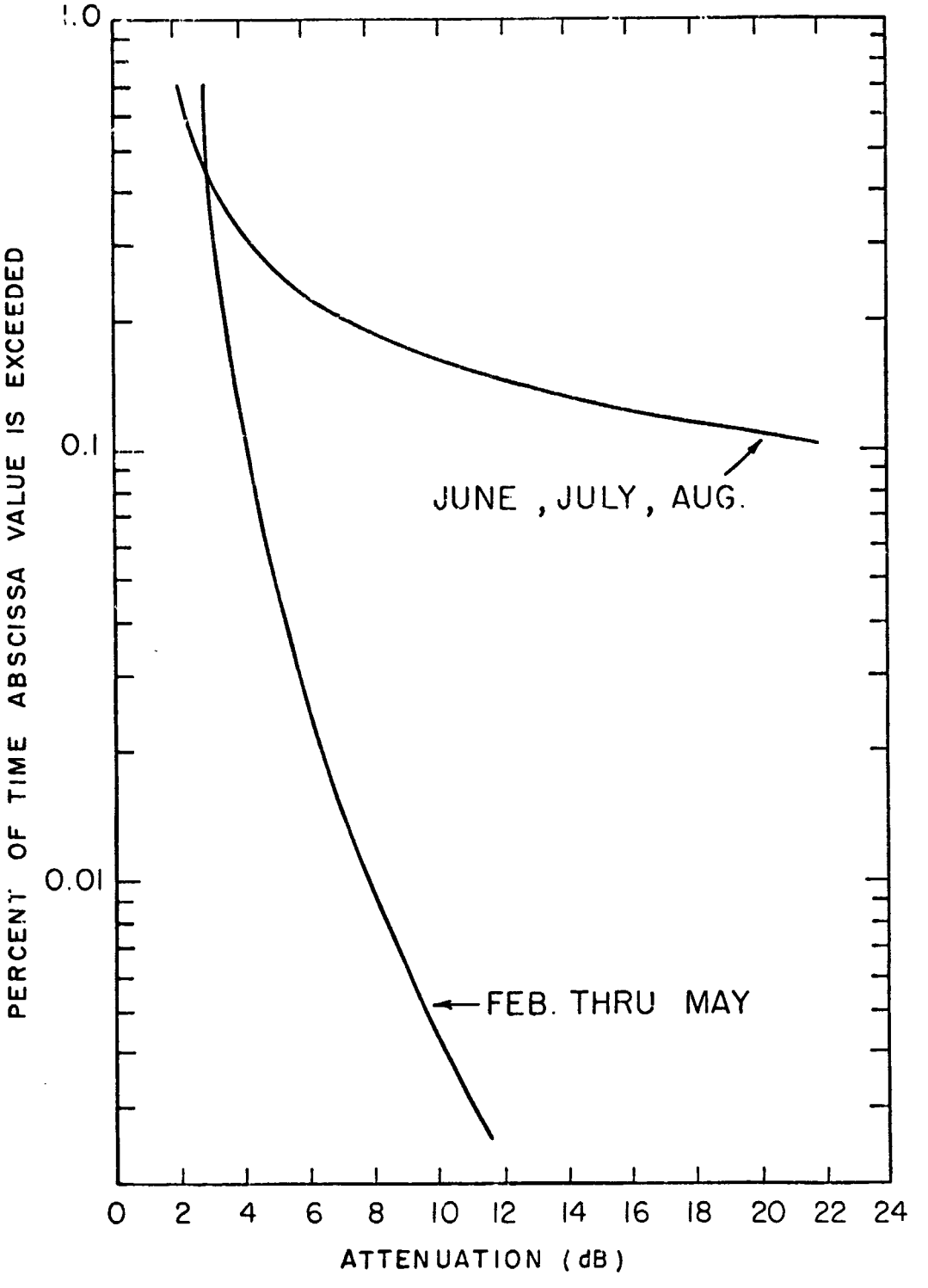

Figure 2-7. Season Distributions at Orlando, Florida

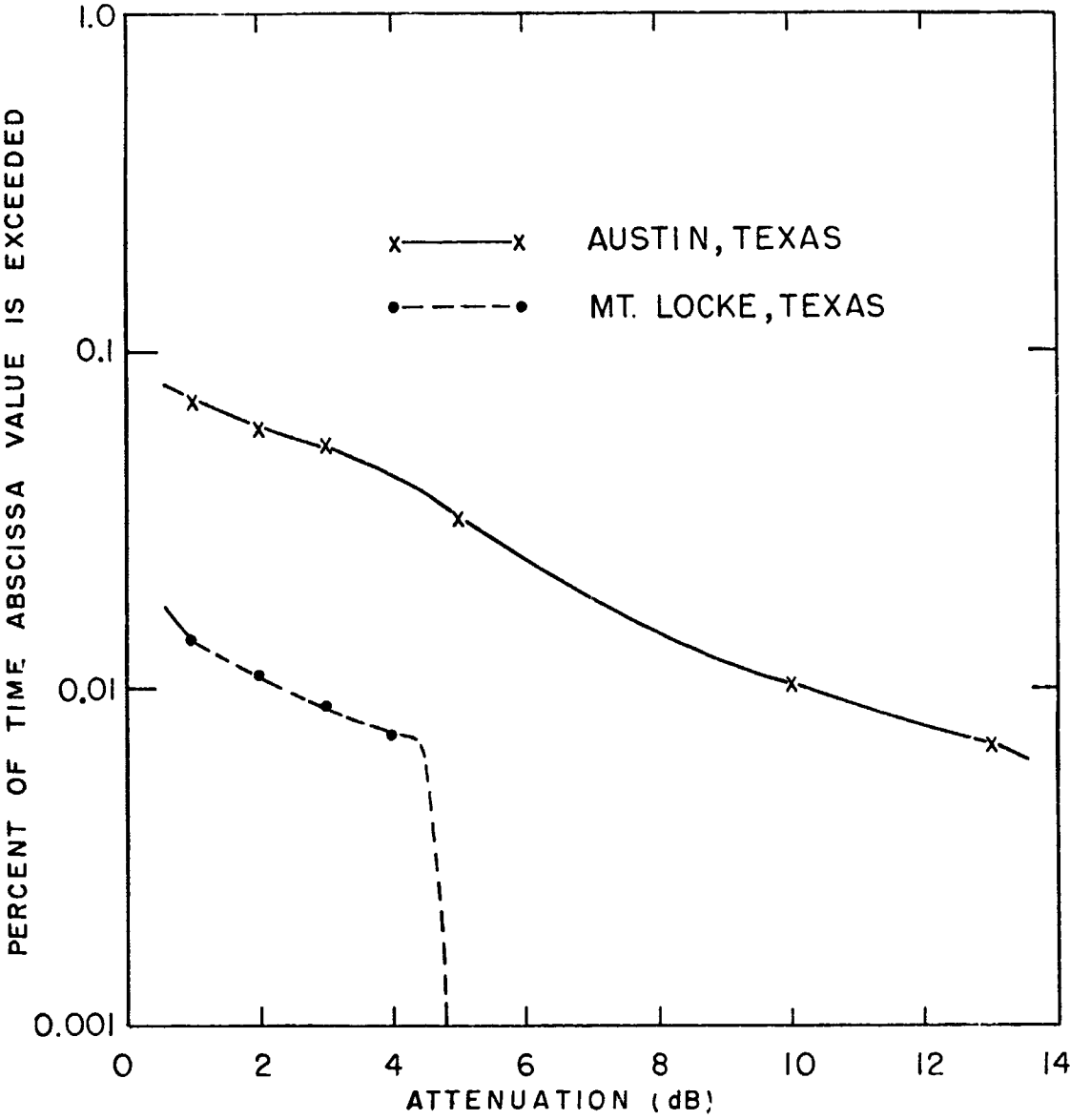

Figure 2-8. Estimated Attenuation Statistics for the University of Texas

taken at some of the sites was somewhat limited and the techniques used varied widely, the results have provided valuable information on the probability of occurrence of various attenuation levels up to 12 dB for a variety of meteorological conditions. A survey of the attenuations experienced at each of the stations for losses in excess of 5 and 10 dB and information on the periods of observation are given in Table 2-2.

REFERENCES

1. Craft, H. D., Jr., "Attenuation Statistics at 15.3 GHz for Clarksburg, Maryland," COMSAT Technical Review, 1 (1971), pp. 221-224.

2. Davies, P. G., "Radiometer Studies of Atmospheric Attenuation of Solar Emission at 19 GHz," Proc. IEEE, 118 (1971), pp. 737-741.

3. Wilson, R. W., "Measurements of Attenuation by Rain at 16 and 30 GHz with a Sun Tracker," BSTJ 48, p. 1383.

4. O'Brien, K. S., "16 GHz Earth-Space Attenuation Measurement in Central Coastal California," 1971 Fall URSI Meeting, Los Angeles, Calif., September, 1971, p. 12.

5. Sukhia, Darvis E., ATS-V Satellite Propagation Measurements at Orlando, Florida, Martin Marietta Corporation Report OR11, Orlando, Florida, December 1971.

6. Ippolito, Louis J., "Attenuation Statistics at 15.3 GHz for Earth-Space Propagation at Rosman, North Carolina," 1972 Spring URSI Meeting, Washington, D.C., April, 1972.

7. Progress Report March 1, 1971 - August 31, 1971, NASA Contract NAS5-10387, Millimeter Wave Group, The University of Texas at Austin.

8. Progress Report 1 September 1971 - 30 November 1971, NASA Contract NAS5-10387, Millimeter Wave Group, The University of Texas at Austin.

9. "Mean Number of Thunderstorm Days in the United States," Technical Paper #19, U.S. Department of Commerce, The Weather Bureau, U.S. Government Printing Office, Washington, D.C., December 1952.

10. Setzer, David E., "Computed Transmission Through Rain at Microwave and Visible Frequencies," BSTJ, Vol. 49, October 1970, pp. 1873-1892.

SECTION 3

RELATIONSHIP BETWEEN THE ATMOSPHERIC ATTENUATION OF SATELLITE PATH SIGNALS AND GROUND RAIN RATE

E. A. Robertson
COMSAT Laboratories
Clarksburg, Maryland

and

D. E. Sukhia
Martin Marietta Corp.
Orlando, Florida

ABSTRACT

Measurements of atmospheric attenuation at 15.3 GHz using the ATS-5 satellite transmissions and/or radiometric techniques have been in progress since the launch of ATS-5 in August 1969. In conjunction with these measurements several experimenters have also made simultaneous measurements of ground rain rate using a variety of rain-gauge types. The objective has been to determine the nature of the relationships between elevated path attenuation and ground rain rate if any, and to determine if elevated path attenuation can be predicted from ground rain-rate measurements. The paper reviews the attenuation-rain-gauge measurements obtained by several participants in the ATS-5 program. Conclusions obtained from comparing the several measurements are presented.

INTRODUCTION

In connection with the 15.3-GHz attenuation measurements several of the participants in the ATS-5 program also made simultaneous measurements of point ground rainfall rate. These measurements employed one or more tipping bucket rain gauges located near the receiving antenna that was used for the attenuation measurements or located out under the propagation path to the satellite.

The objective was to determine if a useful relationship between the ground rain rate measurements and the attenuation measurements could be found. If such a relationship could be determined, then attenuation statistics could be estimated for locations where only ground rainfall rate data were available.

Figure 3-1 provides a scatter plot of simultaneous and essentially instantaneous measurements of attenuation of the 15.3 GHz signal from the ATS-5 satellite and point rainfall rate. The measurements were taken at the Martin Marietta facility in Orlando, Florida. Shown on the figure are simultaneous 20-second averages of attenuation and ground rainfall rate. The Martin experimental set-up includes four rain gauges, one located near the 15.3 GHz receiving antenna and the remaining three located about 0.8 km, 2.7 km and 7.1 km from the antenna and approximately under the propagation path from the satellite.

Figure 3-1 illustrates the large scatter that results when simultaneous measurements of attenuation and ground rain rate are compared. The figure shows many cases of large attenuation with low ground rain rate. This results when a heavy rain cell intercepts the antenna beam but little rain falls on the gauge. However, all cases of heavy rainfall on the ground are accompanied by large attenuation. The figure does not indicate a preference of one gauge location over another with respect to the correlation with attenuation. Curves B, C and D drawn on the figure represent the theoretical relationships between attenuation and rainfall rate for three path lengths derived using the Mie theory with Laws and Parsons drop size distribution.[1] Curve A represents an average relationship derived by Medhurst[2] from measurements comparing attenuation on terrestrial links with path average rainfall rate measured along the link.

Figure 3-2 provides a similar picture as Figure 3-1 from the data obtained by NASA at the Rosman, North Carolina, facility. The figure shows measured 15.3 GHz attenuation distributions parametric in four rain rate intervals. The curves were obtained from 422.3 minutes of measurements taken over several storm periods, totaling 19 hours at Rosman. Each distribution is with respect to the appropriate duration of the measurement, as given on the figure. The distributions show the expected trend toward increasing attenuation with increasing rain rate. However, each distribution is quite wide, indicating that a wide range of path average rain rates can exist for each rate measured at the ground rain gauge.

The above data indicate the futility of attempting to compare simultaneous instantaneous measurements of satellite path attenuation and ground rain rate. However, when looking at a complete storm event, one often observes high attenuation and high rain rates, although they may be separated in time by tens of seconds to several minutes. This suggests alternative methods for comparing the attenuation with ground rain rate. One technique time-shifts the attenuation history with respect to the rain-rate history so as to maximize the covariance coefficient between the two. The attenuation and rain rate are then compared for that time shift which maximizes the covariance coefficient. A second method is to construct an attenuation distribution curve (giving the percent of time the

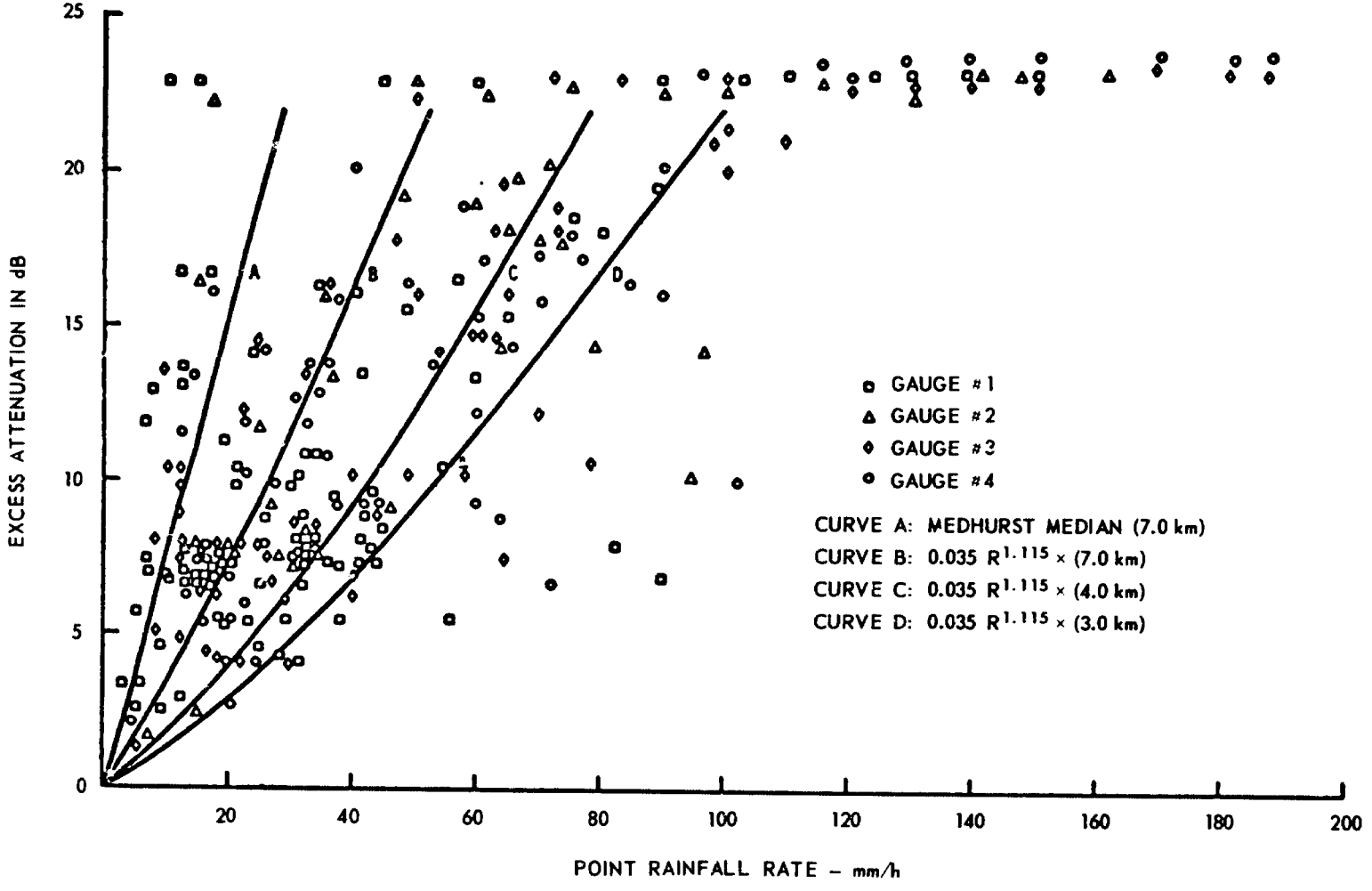

Figure 3-1. Comparison of Measured and Theoretical Attenuation with Point Rainfall Rate (20 Second Averages)

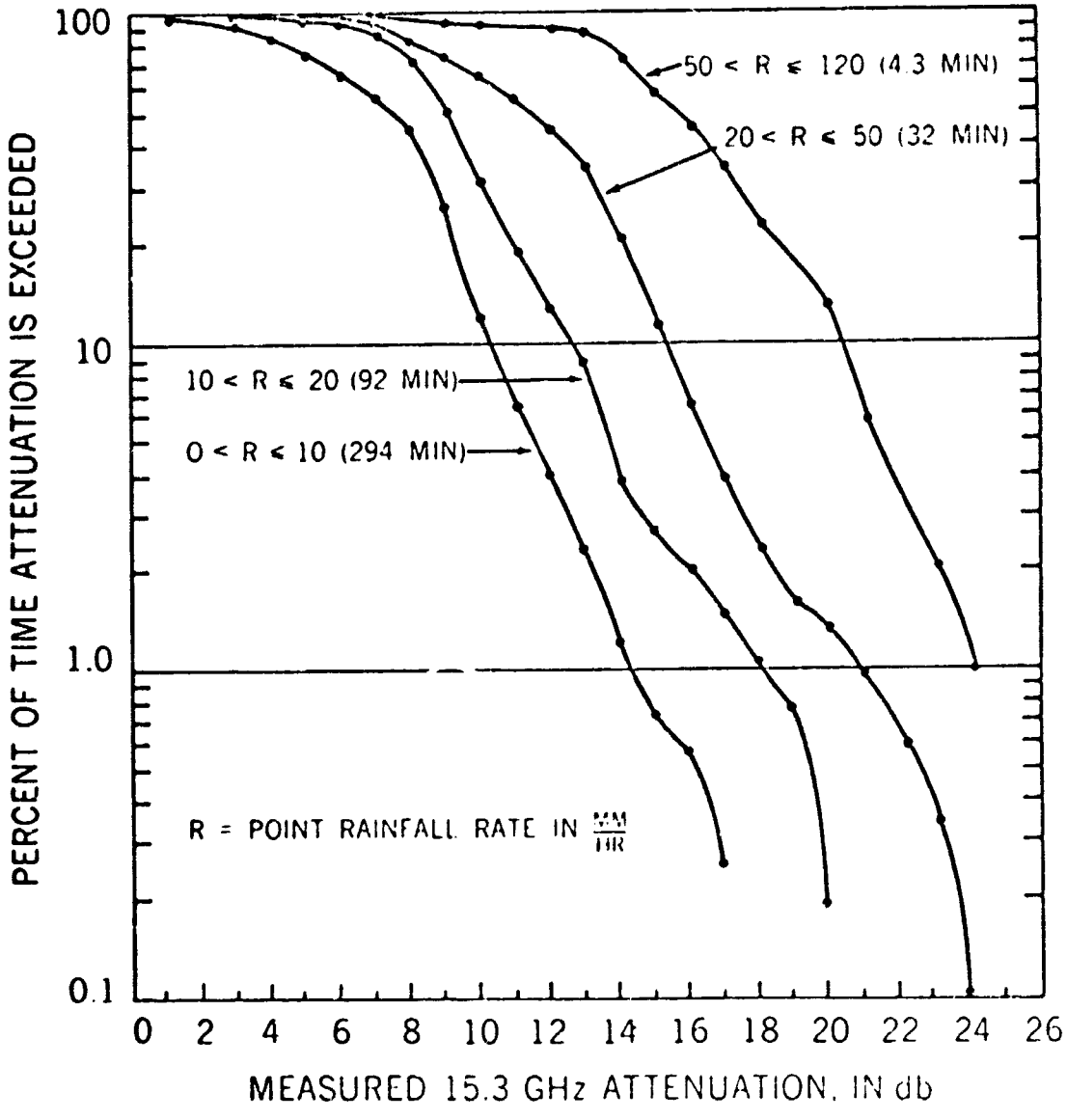

Figure 3-2. Distribution of 15.3 GHz Attenuation, for Various Rainfall Rate Intervals, Rosman, North Carolina, 1971

attenuation exceeds given values) and a ground rain rate distribution curve. By eliminating the percent of time between the two curves a relation between attenuation and ground rain rate is obtained.

The above-described procedures have been followed to generate the curves in Figure 3-3. Curves 1, 2, 3 and 4 were generated by the time-shift method applied to NASA data for four storms in 1971. The curve labeled CY 1970 was obtained by NASA from the distributions for the data taken for all of 1970. The remaining three curves were obtained by comparing attenuation and ground rain rate distributions supplied by Ohio State University, University of Texas, and COMSAT Laboratories.

The data from the four locations are quire different, perhaps illustrating the differing climatic conditions obtaining. It should be noted that the curves of Figure 3-3 are derived from rather meager amounts of data, as can be seen from Table 3-1 below, which gives the number of observing hours and the time for which the observed rain rate exceeded 10 mm/hr.

Table 3-1

	Observing Hours	Time > 10 mm/hr.
Ohio	3-1/2	40 min.
Texas	6-1/2	3-1/2 hrs.
NASA CY 1970	196	20 hrs.
COMSAT	6600	33 hrs.

Also shown on Figure 3-3 are the theoretical relationships between attenuation and path average rain rate for path lengths from 1 to 20 km. Using these curves, equivalent path lengths for given rain rates can be determined as shown in Figure 3-4.

Figure 3-4 shows the general relationship of decreasing path length with increasing rain rate in keeping with the generally accepted model of thunderstorms with intense rain cells of limited extent. Some of the data indicate rather large path lengths for low rain rates. A 12 km path length at 10 mm/hr at an elevation angle of 35° would require a minimum altitude of about 20,000 feet,

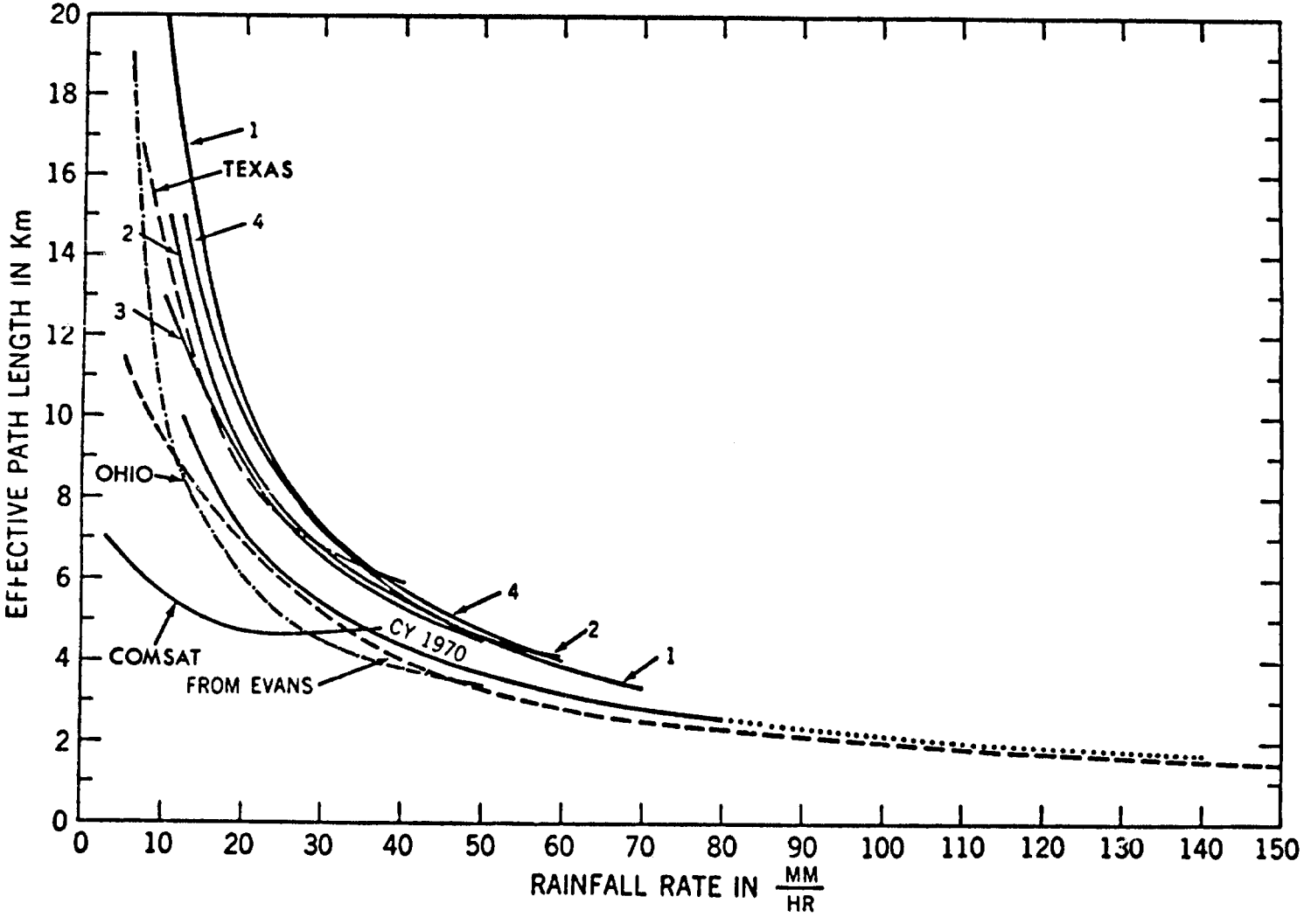

Figure 3-3. Effective Path Length Required for a Given Rainfall Rate from 15.3 GHz Measurements at Rosman, North Carolina

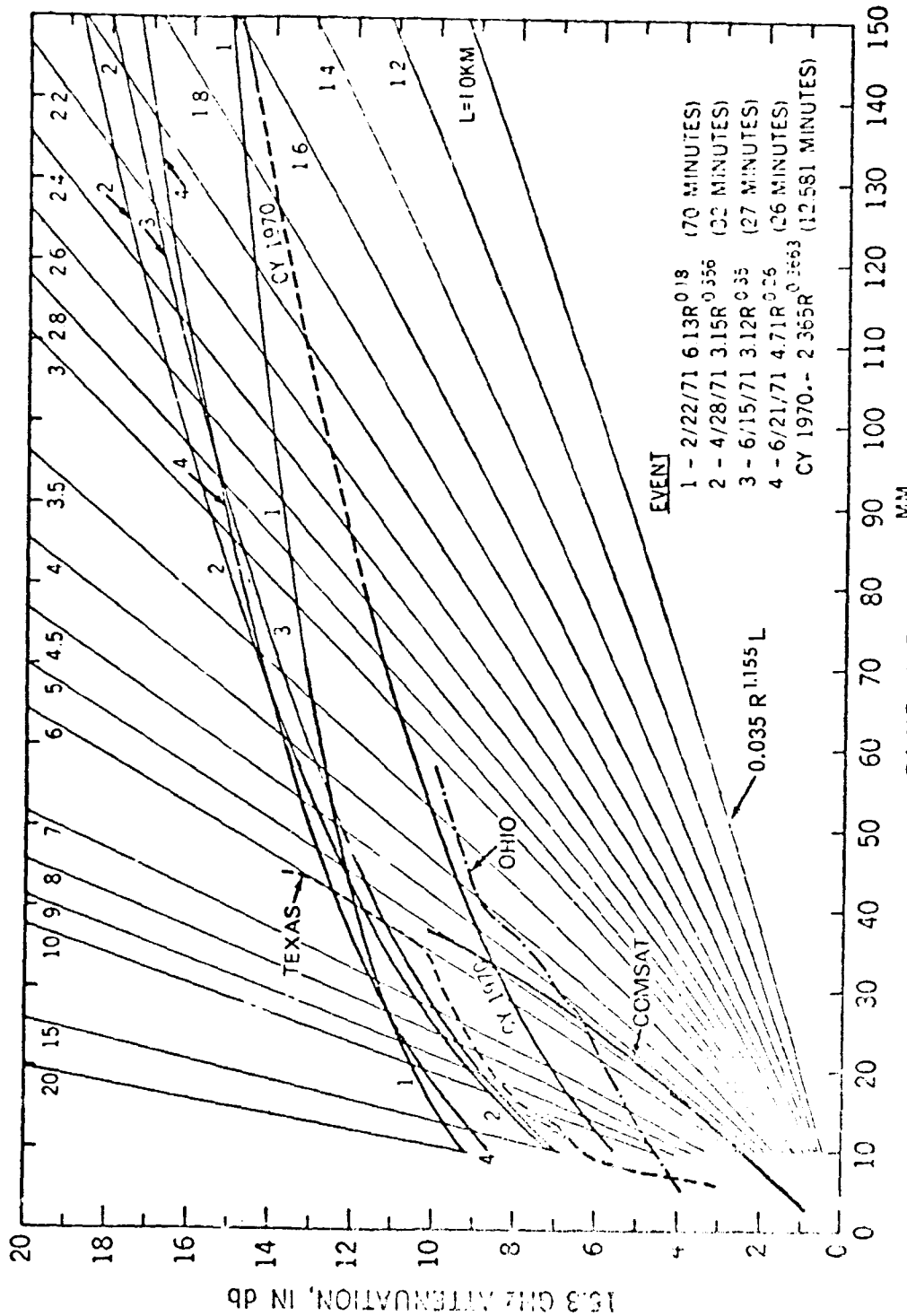

Figure 3-4. Measured 15.3 GHz Attenuation vs. Rainfall Rate Compared with Laws and Parsons Prediction

which can occur in heavy thunderstorms, but may not be typical of lighter rains. Also shown on the figure is the result given by Evans[3] obtained by comparing suntracker measurements at 16 and 30 GHz.

A large quantity of ground rain gauge data is available from the Weather Bureau. From this data, hourly rain rate distributions can be obtained. However, there can be large differences between the rain rate distributions obtained from hourly data and from those obtained from rain gauges with shorter time resolutions. An example of this is shown in Figure 3-5, where the data from the COMSAT tipping bucket gauge has been processed with one-minute, five-minute, and one-hour resolutions. Also shown is a one-hour distribution obtained from the Weather Bureau gauge at Washington airport. The large differences between the one-hour and one-minute gauge illustrated the difficulty in using the Weather Bureau data to predict attenuation statistics.

In summary, the ATS-5 experiment showed that the correlation between instantaneous measurements of satellite path attenuation and ground rain rate is poor. By comparing attenuation and ground rainfall rate distributions, the effective path length was found to decrease with increasing rain rate. However, there were large differences between the path length to be associated with a given rate as derived from the data provided by the various experimenters. These differences may be a result of the differing climates in various locations at which the measurements were performed. Additional uncertainty is also introduced by the limited amount of data acquired.

ACKNOWLEDGEMENT

The data upon which this paper is based were provided by Dr. A. Straiton of the University of Texas, Dr. D. Hodge of Ohio State University, Mr. L. Ippolito of NASA/Goddard Space Flight Center, Mr. D. Sukhia of Martin Marietta, and Mr. E. Robertson of COMSAT Laboratories.

REFERENCES

1. Gunn, L. S. and East, T. W. R., "The Microwave Properties of Precipitation Particles," Journal of the Royal Meteorological Society, Vol. 80, 1954.

2. Medhurst, R. G., "Rainfall Attenuation of Centimeter Waves: Comparison of Theory and Measurement," IEEE Transactions on Antennas and Propagation, AP-13, July 1965, pp. 550-564.

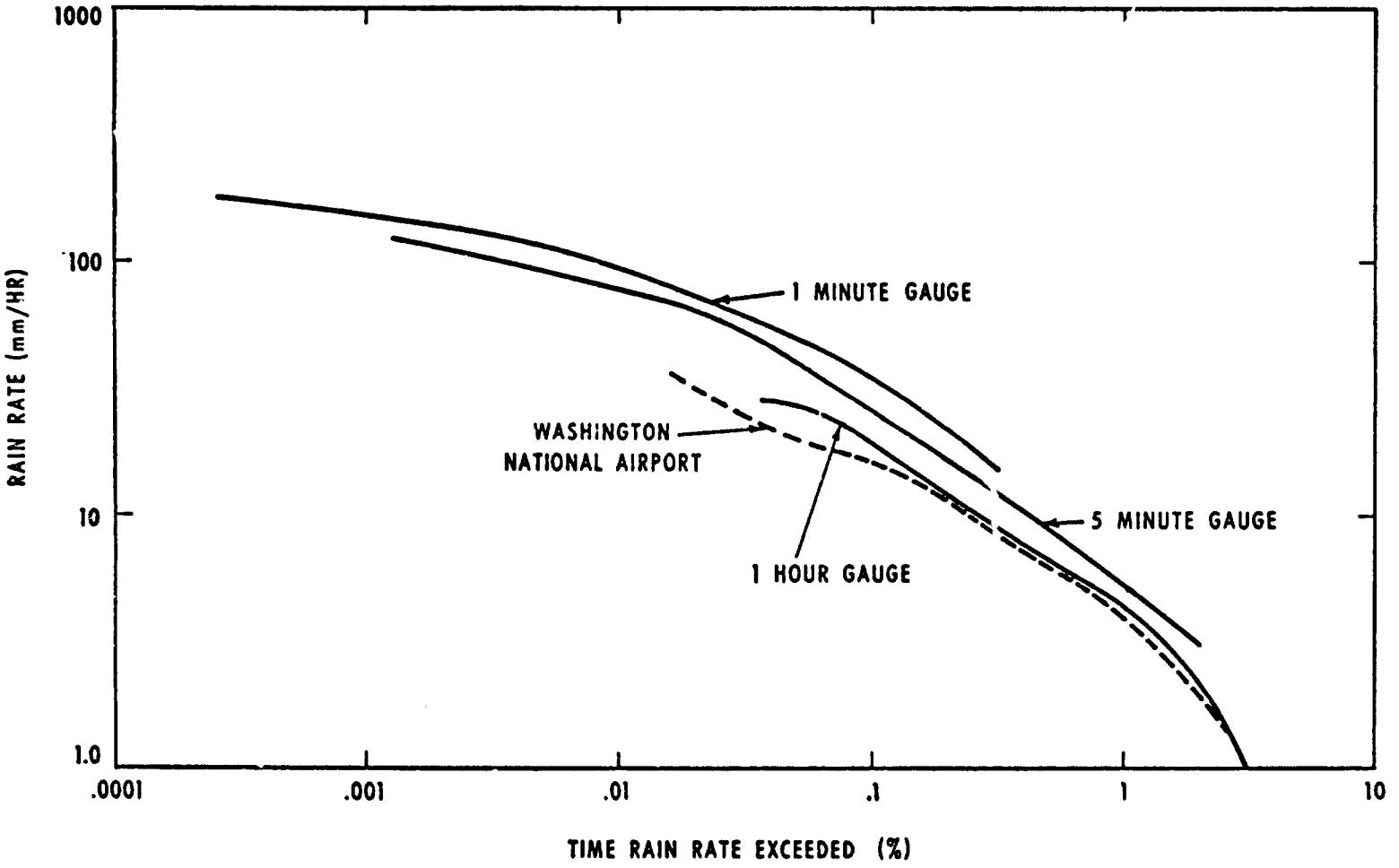

Figure 3-5. Rain Rate Distribution COMSAT Tipping Bucket Rain Gauge April 1, 1971-December 31, 1971

3. Evans, H. W., "Attenuation on Earth-Space Paths at Frequencies up to 30 GHz," International Conference on Communications, June 1971, Montreal, Canada, pp. 27-1 to 27-5.

SECTION 4

THE RELATIONSHIP BETWEEN SATELLITE SIGNAL ATTENUATIONS AND SKY TEMPERATURE MEASUREMENTS IN THE RAIN ENVIRONMENT

D. A. Gray
Bell Telephone Laboratories
Holmdel, New Jersey

ABSTRACT

The ATS-5 satellite and sun-trackers have afforded an evaluation of the ability to obtain earth-to-space path attenuation statistics through radiometric measurements of the sky temperature. Experiments using the satellite show that directly measured attenuations of the ATS-5 signals (15.3 and 31.65 GHz) and attenuations derived from concurrent sky temperature measurements compare favorably. In computing attenuations from sky temperature measurements on the basis that rain is a pure absorber, best agreement with directly measured attenuations is achieved when the value taken for the kinetic temperature of the rain is colder than one would expect, in some cases below freezing. This experimental result agrees with theoretical computations of the effects of scatter by rain. At 15.3 GHz, for example, an assumed kinetic temperature of 273 K gives good agreement for many storms. The comparison experiments have shown that radiometers are a viable, alternate means for obtaining attenuation statistics on earth-space paths when the effect of scatter is taken into account.

(PAPER NOT AVAILABLE FOR PRINTING)

SECTION 5

SIMULTANEOUS DIRECT, RADIOMETRIC, AND RADAR MEASUREMENTS OF PRECIPITATION ATTENUATION AT 15.3 GHz

J. I. Strickland
Communications Research Centre
Ottawa, Canada

ABSTRACT

During 1970, the signal strength received at 15.3 GHz from the ATS-5 satellite was measured using a 9-m antenna. The receiving antenna, with a beamwidth of 0.15°, was also connected as a total-power radiometer providing simultaneous measurements of the sky noise temperature at 15.3 GHz. Attenuations, calculated from the measured sky noise temperature, show very good agreement with the directly measured attenuations. Also during the occurrence of rain, the 3-m antenna of an S-band radar located nearby was directed at the satellite. The output of the logarithmic radar receiver was sampled at accurately determined intervals to provide digital A-scans with a range resolution of 100 m. Three-dimensional plots of successive digital A-scans show the temporal variation in evolution of the spatial distribution of precipitation along the propagation path. For many attenuation events, there was evidence of a bright band. The mean reflectivity at each range is calculated, and path attenuations at 15.3 GHz derived. Generally good agreement between measured and calculated attenuation is obtained for most meteorological conditions. The effects on the calculated attenuati of radar returns from the bright band and snow aloft will be discussed.

INTRODUCTION

Precipitation attenuation along slant paths can be determined from direct measurements of received signal strength, calculated from sky noise temperature measurements, or calculated from radar measurements of the power backscattered from precipitation. As part of a continuing study of microwave propagation, the Communications Research Centre participated as an independent experimenter in the NASA ATS-5 Millimetre Wave Experiment. From September 1969 to July 1971, the ATS-5 satellite was used as a source of coherent

radiation at 15.3 GHz. Simultaneously, the sky noise temperature at 15.3 GHz and the power at 2.9 GHz backscattered fr precipitation along the propagation path were measured. This paper compares attenuations measured directly with those calculated from sky noise temperature and from radar backscattered power measurements.

EXPERIMENTAL ARRANGEMENT

A block diagram of the experimental system is shown in Figure 5-1. Signals at 15.3 GHz from the ATS-5 satellite were received at Ottawa, using a precision 9.1 metre antenna[1] at an elevation angle of approximately 30 degrees. The pulsed output from the logarithmic phase-lock receiver was measured by a peak-riding detector with an overall resolution of better than 0.2 dB. In the absence of rain, the received signal showed a diurnal variation of ±2 dB. A margin for attenuation measurements of approximately 15 dB was available.

The receiving antenna, with a beamwidth of 0.15 degrees, was also connected as a total-power radiometer at 15.3 GHz to provide simultaneous measurements of the sky noise temperature along the propagation path.

Radar has the advantage of providing information on the spatial distribution of precipitation along the propagation path. An S-band weather radar operating at 2.86 GHz was used to measure the backscatter from precipitation. A 3 metre antenna provided a conical beam of 2.3 degrees width. The radar operated with a peak output power between 150 and 200 KW, a pulse width of 0.67 μsec (spatial resolution of 100 m), and a pulse repetition period of 682.7 μsec, resulting in a maximum range of 102.4 km. The overall dynamic range, including the logarithmic IF amplifier, was greater than 70 dB.

Digital A-scans were obtained by sampling the radar video output at accurately determined intervals following each transmitter pulse.[2],[3] Successive complete digital A-scans were acquired every 50 milliseconds. An estimate of the backscattered power was obtained for each 100 metre range interval from 14 such A-scans. An additional 0.3 second was required for data manipulation and recording on digital magnetic tape. Thus, radar data specifying the power backscattered from precipitation as a function of range could be acquired every second.

THEORY

For a purely absorbing medium, the attenuation is given by

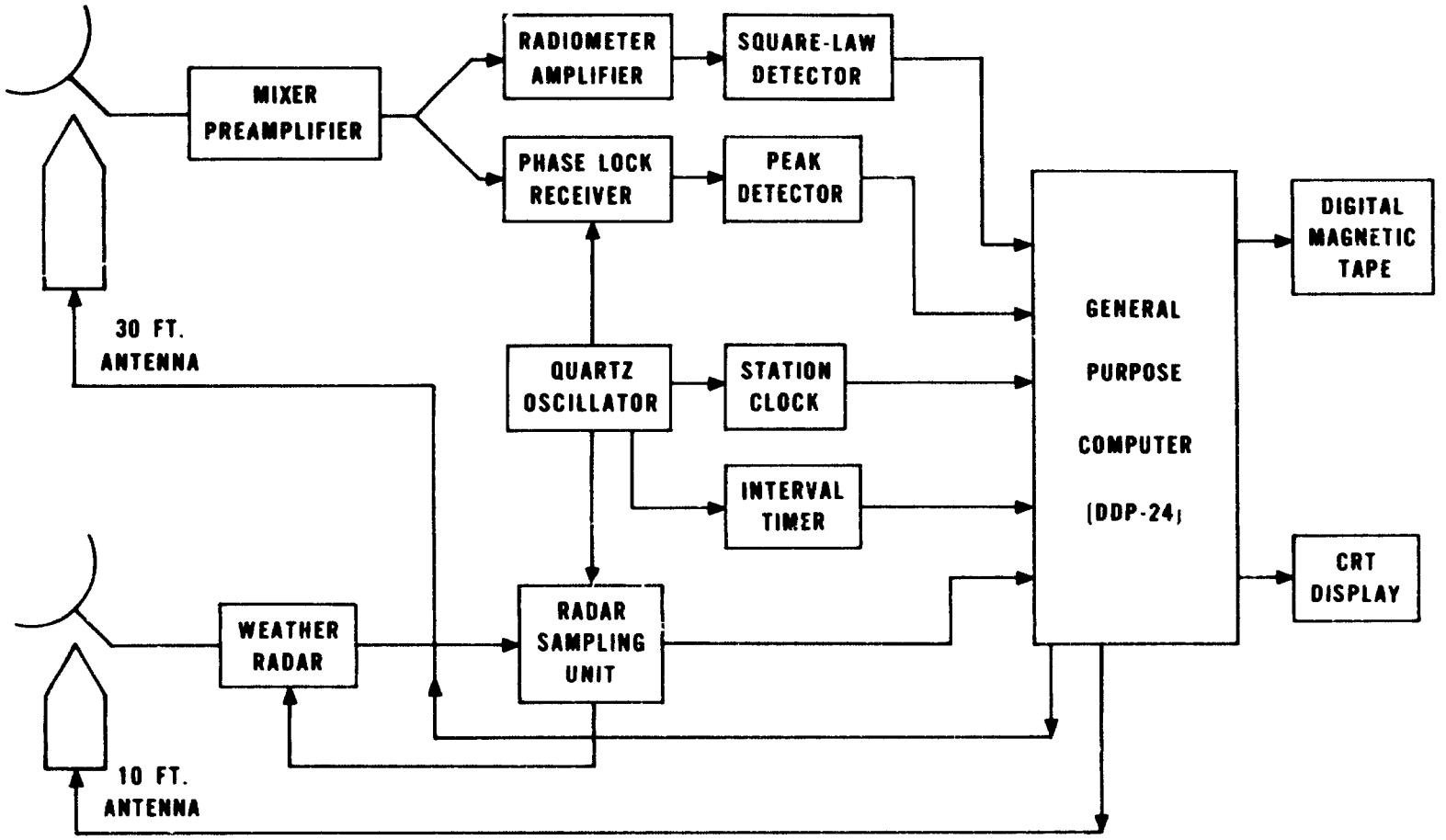

Figure 5-1. Block Diagram of the Experimental System

$$A = 10 \log \frac{T_m}{T_m - T_a} \text{ dB},$$

where T_a is the measured sky noise temperature and T_m is the kinetic temperature of the medium. Although the rain medium is not a pure absorber, at 15.3 GHz the single scattering albedo is less than 0.3 for all but the heaviest rains.[4] Thus, attenuation can be calculated from the above formula by assuming an effective medium temperature T_m approximately equal to the kinetic temperature of the rain. This relation has been empirically verified for more than 60 attenuation events.[5] It was found that 273°K is a suitable effective medium temperature, and that the standard deviation of the difference between the measured and calculated attenuations increased with attenuation, reaching a value of 1.2 dB at 8 dB attenuation.

For a pulse volume uniformly filled with precipitation[6]

$$Z = c_R r^2 \bar{P}_r,$$

where Z is the radar reflectivity factor of the precipitation, $\bar{P}_r$ is the average received power, and r is the distance from the radar to the pulse volume. The constant c_R includes not only the characteristics of the radar, but also the dielectric constant of the precipitation, i.e., snow or rain. It is assumed that the drop diameters are much less than a wavelength, and that the radar signal is unattenuated by rain. Because of the fluctuating nature of the power backscattered from an ensemble of randomly distributed scatterers, such as snow or rain, several independent samples of the received power are required to estimate the average received power.[7] Smith[8] has shown that an estimate of $\bar{P}_r$ can be obtained from the maximum received power in a set of n measured values of the received power, by applying a correction which depends on the value of n. This procedure was employed in this work.

Empirically, it is found that the radar reflectivity factor Z is related to the rainfall rate R by $Z = aR^b$. Much work has been devoted to studying the Z-R relation at the ground. As might be expected, the variation in the constants of the Z-R relationship is reduced if the data are grouped according to the type of rain. Probably the simplest division is into continuous rain, showers, and thundershowers. Johnson[9] has shown that further subdivision provides only a slight reduction in the variation of a and b. Using drop size distributions measured by Andrews at London, and forcing the exponent b to equal 1.6, it is found[10] that the Z-R relations become

$$Z = 200\ R^{1.6} \quad \text{for continuous rain}$$

$$Z = 280\ R^{1.6} \quad \text{for showers, and}$$

$$A = 350\ R^{1.6} \quad \text{for thundershowers,}$$

where Z is expressed in units of mm^6/m^3 and R in mm/hr.

For frequencies which are attenuated, the specific attenuation varies with rainfall rate as $A = kR^{\gamma}$, where k and γ depend on frequency. Combining these equations, the path attenuation A' is given by

$$A' = c \sum_i Z_i^{\beta} \Delta r_i \ dB$$

where c and β depend on frequency and synoptic type, and the summation is over all intervals of path length Δr_i from which significant echoes are received. Values of 7.15×10^{-4} and 0.75 are assumed for c and β respectively.

It is not possible to use a radar operating at the frequency of interest for attenuation, since the radar beam itself suffers two-way attenuation, and serious errors in estimates of precipitation intensities result. Even at a wavelength of 5.7 cm, this attenuation can be serious for widespread heavy rains.[10]

In frontal rains, the radar beam may intersect snow at heights above the zero degree isotherm. This snow, generated approximately uniformly over a relatively large area, falls with a velocity of 2 to 3 m/sec. Below the zero degree isotherm level, the snow melts, forming a mixture of large wet flakes and raindrops at 0°C which produce a bright band of enhanced radar reflectivity. The reflectivities both above and below the bright band are nearly the same, while within it, the peak reflectivity can be 10 to 30 times higher. Finally, the rain falls with velocities of 5-15 m/sec. The height of the zero degree isotherm varies during the year from ground level to somewhat less than 5 km, at least for temperate zones.

Within convective rain, the zero-degree isotherm is not at a well-defined height, and in updrafts, raindrops are carried above the zero degree level and can sometimes remain as water drops supercooled to as low as -20°C. In decaying convective cells, however, updrafts are weak, and a bright band is often present. Therefore, when convective cells are imbedded within a front, a bright band may be observed except within the active portion of convective cells.

RESULTS

From many attenuation events, two have been selected. In both cases, the measured attenuation at times exceeded 15 dB, the margin available for measurements. The attenuation event shown in Figure 5-2 occurred during a 5-day period characterized by cool temperatures, cloud, some drizzle, and a thunderstorm. The plot in the upper left shows the variation of measured attenuation with time using the ATS-5 transmitter as source. The three spikes between 1715 and 1720 are due to momentary loss of phase lock. The attenuations calculated from measurements of sky noise temperature, assuming an effective medium temperature of 273°K, are shown in the lower left. The scatter plot in the upper right corner shows the calculated attenuation as a function of the measured attenuation. The centre line, of unit slope, represents exact correspondence between measured and calculated values of attenuation. The curved lines show the errors in calculated attenuation as a function of measured attenuation for errors in the assumed effective medium temperature of ±10 and ±20 degrees. In addition, these limits are adjusted to allow for fluctuations of ±0.5 dB in the received signal strength in the absence of rain attenuation. A few points fall outside the limit lines. Some of these are associated with the periods of loss of receiver phase lock.

Attenuations calculated from measurements of backscattered power obtained with the S-band radar are shown in the lower right corner. These somewhat exceed the corresponding measured attenuations. The excess is within uncertainties in the radar calibration and the expected variation of the A-Z constants from storm to storm and within a storm.

Each digital A-scan is converted to a plot of reflectivity factor versus slant range. If successive plots are stacked along a time axis, a three-dimensional plot results with slant range as the x-axis, time as the y-axis, and reflectivity factor in dBZ (dB above Z = 1 mm^6/m^3) as the z-axis. The peak reflectivities in dBZ are shown to the right of each plot. Such a plot shows the variation in time and space as the precipitation passes through the radar beam. Such passage is due to two motions of the precipitation:

(i) horizontal translation of a cell or precipitation at some angle to the propagation path, and

(ii) descent of precipitation from a high altitude to the ground.

In the first plot of Figure 5-3, features of the cells appear to be moving toward the radar with a velocity of approximately 40 km/hr. Since the azimuth to ATS-5 is approximately 220° and storms tend to come from the west or southwest, such an approach velocity is reasonable.

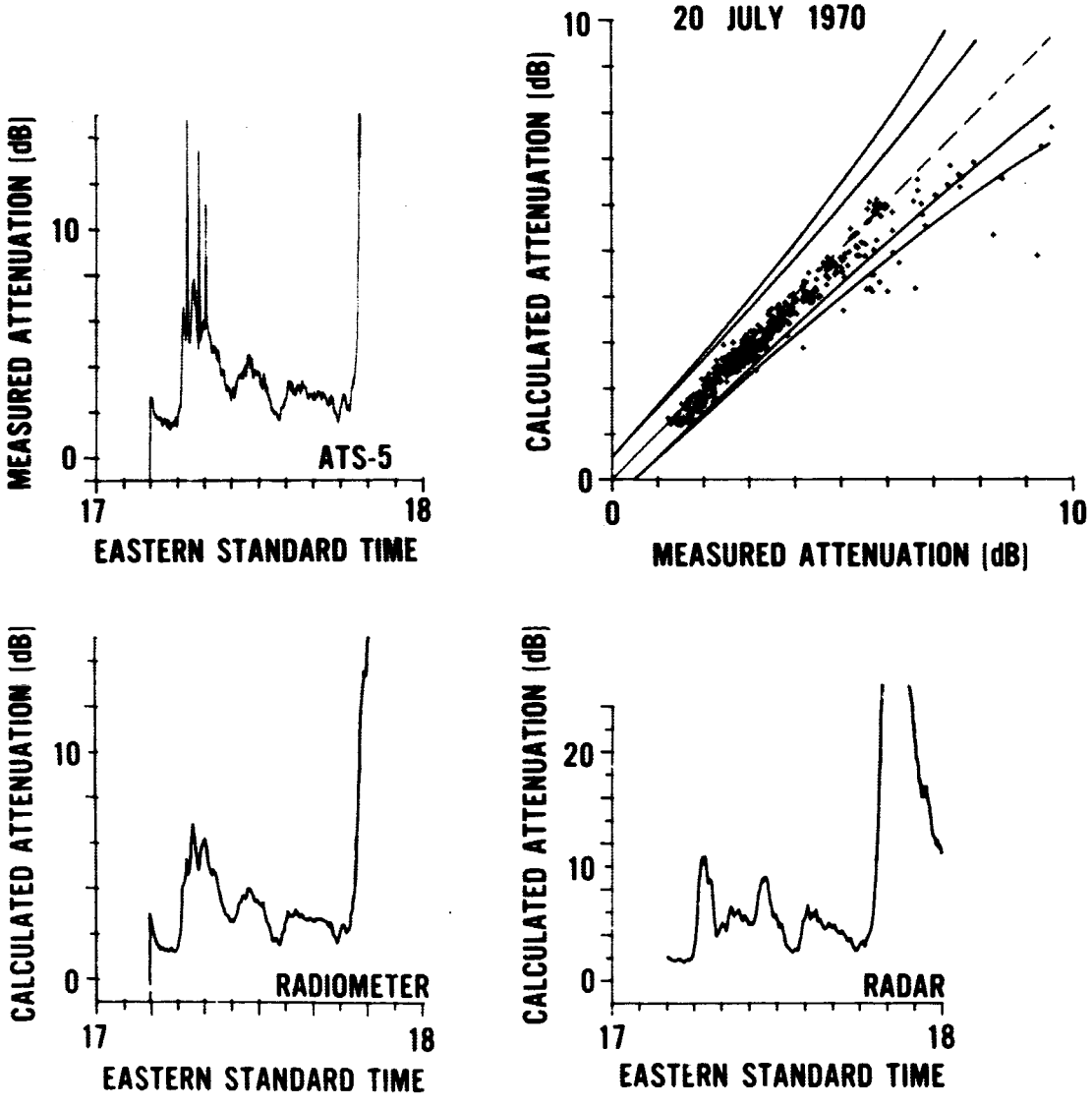

Figure 5-2. Direct and Calculated Attenuations at 15.3 GHz (20 July 1970)

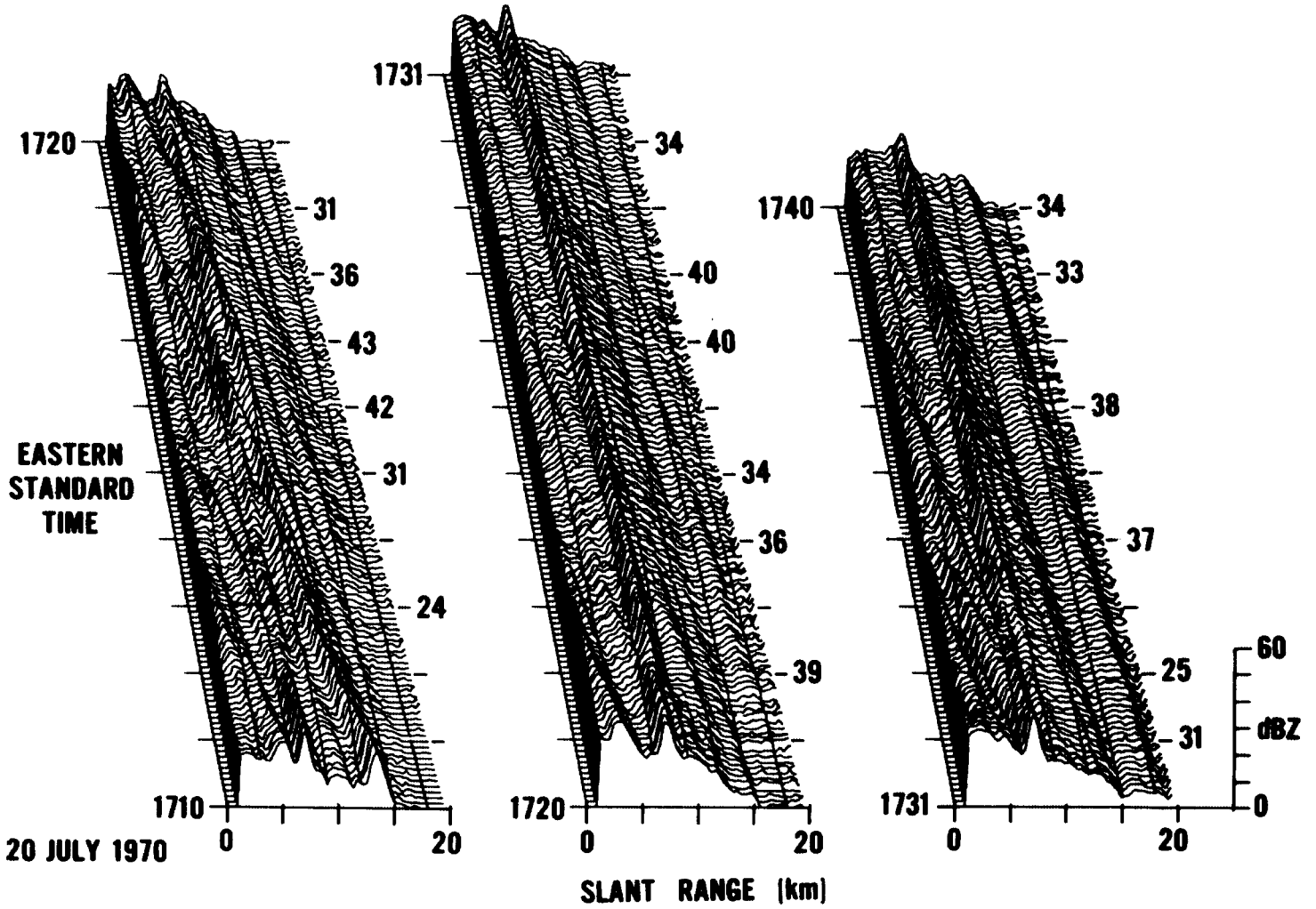

Figure 5-3. Variation of reflectivity with Slant Range and Time (1710-1740 EST, 20 July 1970)

Both the second and third plots of Figure 5-3 show the obvious presence of a bright band; i.e., enhanced reflectivity at a constant altitude for a relatively long period of time. The lines running over the hills and valleys of the plots are separated by 3 km. Thus, the melting layer starts at somewhat less than 8 km slant range and extends to perhaps 6.5 km slant range. Since the elevation angle is approximately 30°, the zero-degree isotherm is at a height of approximately 4 km and the melting layer has a thickness of less than 700 m. This is in good agreement with the measured height of the zero-degree isotherm, which was 3.7 km at the closest radiosonde station 100 km north of Ottawa.

In addition, there is an apparent motion toward the radar. Assume, for the moment, that the precipitation structure at any given time is relatively uniform over any horizontal plane, and there is an increase in the generation of snow aloft. As this snow descends, it will appear to move toward the radar, and the resulting rain below the melting layer will also appear to approach. From the apparent rates of approach, the fall velocity of the snow is approximately 2.5 m/second, and of the rain, 8-10 m/sec. These values agree with those measured by Doppler radars.

It is also clear from the variation in the rate of approach in the third plot that horizontal structure does exist and has a velocity component toward the radar.

In the two plots of Figure 5-4, which include the time during which the measured attenuation exceeded 15 dB, the melting layer has vanished altogether after 1744 EST, and the peak reflectivity is beginning to rise. Indeed, from the reflectivity plot at 1750 EST, it is apparent that a reflectivity exceeding 30 dBZ exists over more than 10 km slant range. The apparent motion is most likely due primarily to translation of the convective cell across the propagation path. Although not shown here, the melting layer does indeed reappear shortly after 1800 EST.

An attenuation event which occurred on 20 August 1970 is shown in Figure 5-5. The weather was cloudy and warm with scattered thundershowers during the early morning. Both the directly measured attenuation and the radiometrically calculated attenuation exceed 10 dB.

Radar-calculated attenuations exceed both the measured and radiometrically calculated attenuations, at least during the central portion of the event. It is important to note that the same radar constant was employed as in the previous event. Although some of the increase in attenuation may be due to errors in radar calibration, it is more likely that the constants in the Z-R relation are different.

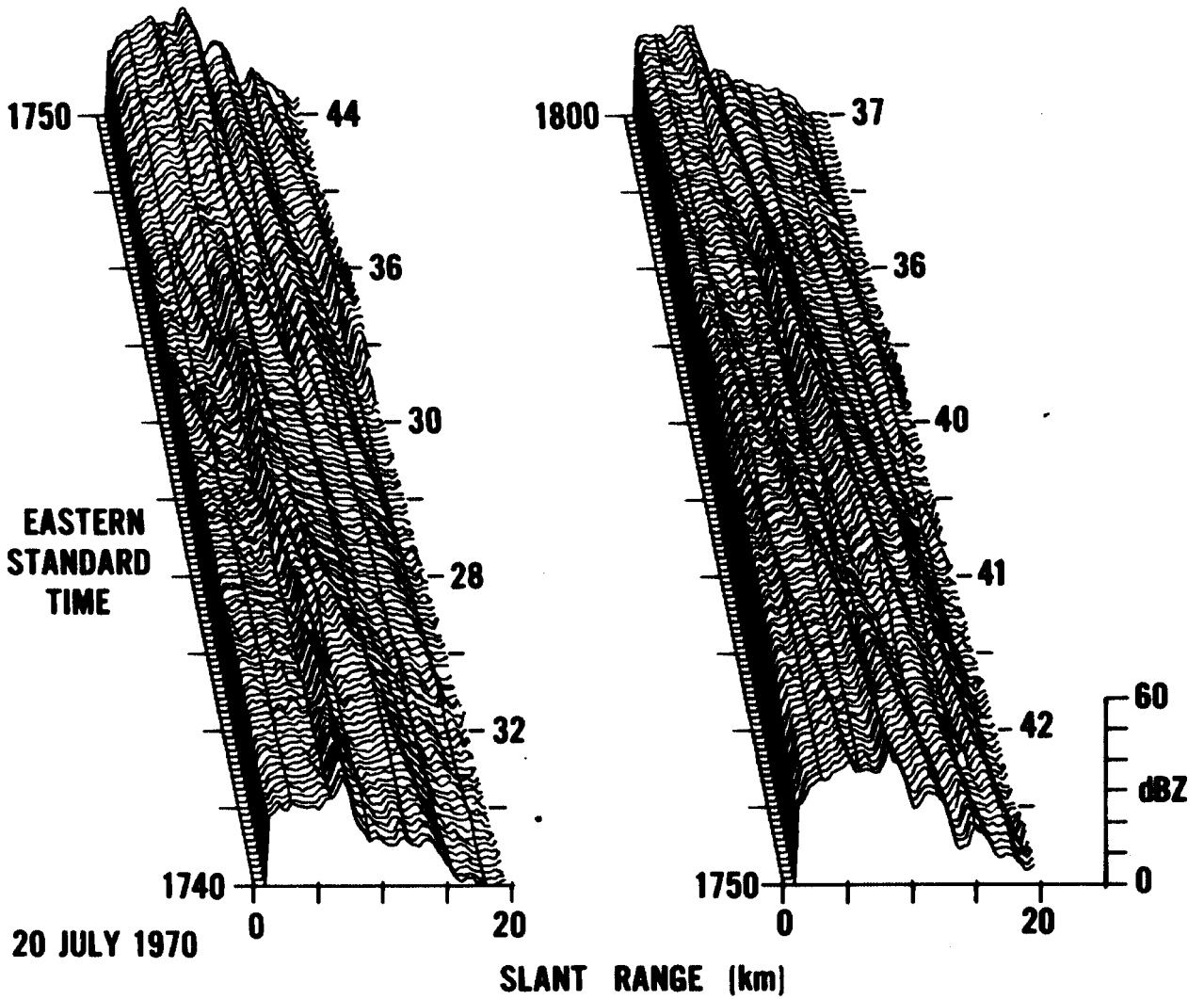

Figure 5-4. Variation of Reflectivity with Slant Range and Time (1740-1800 EST, 20 July 1970)

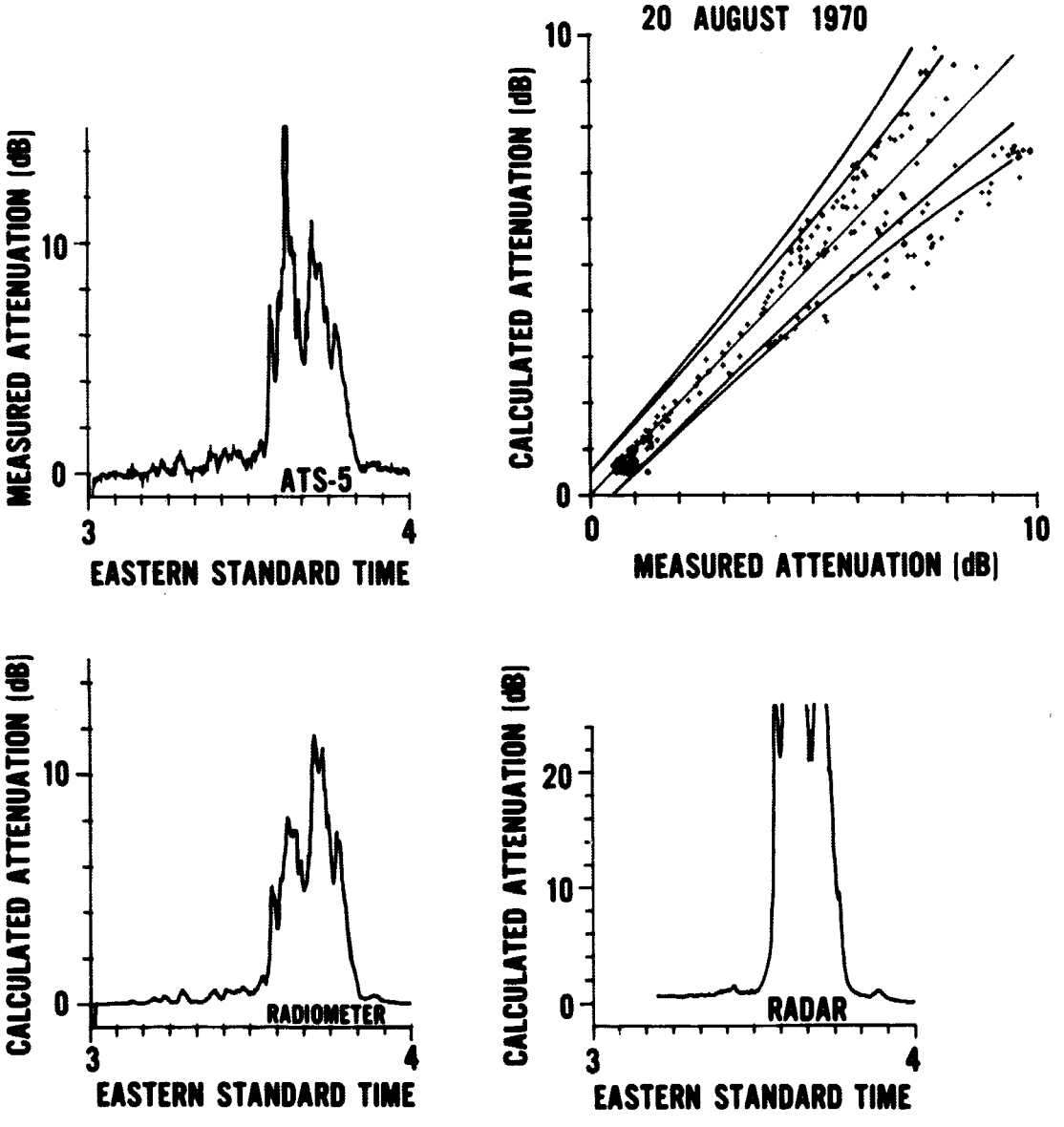

Figure 5-5. Direct and Calculated Attenuations at 15.3 GHz (20 August 1970)

The three dimensional plots of Figure 5-6 show that the storm is characterized by steep gradients in reflectivity. The initial portion of the event at 0335 EST is due to a ridge of precipitation at a slant range of approximately 12 km, with further maxima closer to the radar. At 0340 EST, the peak reflectivity is at a slant range of 8 km, and the maximum reflectivity drops sharply after 0345 EST. If the storm cell were moving across the propagation path with an assumed velocity of 40 km/hr, the transverse extent of the cell would be approximately 7 km, in agreement with other measurements of the size of strong convective cells.

CONCLUSIONS

From these and similar measurements, it is concluded that the radiometer is a simple and accurate device for obtaining measurements of rain attenuations not exceeding values of about 10 dB. Radar, although less accurate in predicting attenuation and more cumbersome to operate, provides detailed information on the spatial and temporal distribution of precipitation which cannot be obtained by other methods.

REFERENCES

1. Cogdell, J. R., et al, "High Resolution Millimeter Reflector Antennas", IEEE Transactions on Antennas and Propagation, AP-18, pp. 515-529, July, 1970

2. Pawziuk, W. J., K. S. McCormick and N. K. Hansen, "A Digital System For Recording Radar A-Scans", Proc. Thirteenth Radar Meteorology Conference, Am. Meteor. Soc., Boston, pp. 336-338, 1968

3. Strickland, J. I. and J. W. B. Day, "Microwave Attenuation Measurements Using the ATS-5 Satellite", AGARD Conference Proceedings No. 70, Technical Symposium on "Tropospheric Wave Propagation", 1971

4. Crane, R. K., "Propagation Phenomena Affecting Satellite Communication Systems Operating in the Centimeter and Millimeter Wavelength Bands", Proc. IEEE, Vol. 59, February, 1971

5. Strickland, J. I., "Comparison of Direct and Radiometric Measurements of Rain Attenuation at 15.3 GHz", To be published

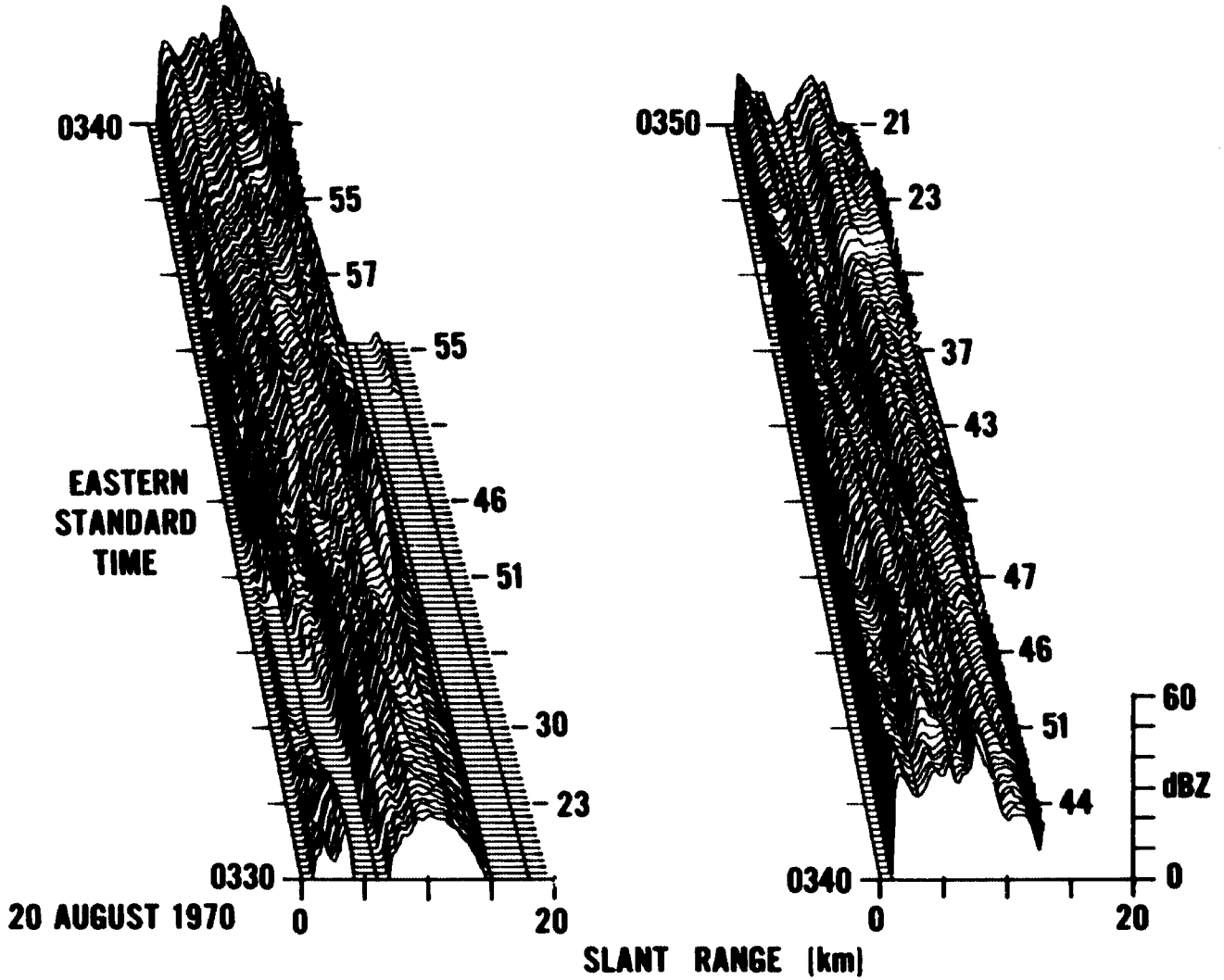

Figure 5-6. Variation of Reflectivity with Slant Range and Time (0330-0350 EST, 20 August 1970)

6. McCormick, K. S., "Simultaneous Measurements of Precipitation Attenuation and Radar Reflectivity at Centimeter Wavelengths", Preprints of the 14th Radar Meteorology Conference, Am. Meteor Soc., Boston, pp. 19-24, 1970

7. Marshall, J. S. and W. Hitschfeld, "Interpretation of the Fluctuating Echo from Randomly Distributed Scatterers — Part 1", Can. J. Physics, 31, pp. 962-994, 1953

8. Smith, P. L., Jr., "Interpretation of the Fluctuating Echo from Randomly Distributed Scatterers — Part 3", Stormy Weather Group Report MW-39, McGill University, Montreal, December 1964

9. Johnson, R. M., "The Effects of Stability on Drop-size Distributions", Proc. 9th Weather Radar Conference, Kansas City, Missouri, 1961, p. 286

10. Harrold, T. W., "Estimation of Rainfall using Radar — a Critical Review", Meteorological Office, Scientific Paper No. 21, London, 1965.

SECTION 6

THE USE OF SPACE DIVERSITY IN THE RECEPTION OF MILLIMETER WAVELENGTH SATELLITE SIGNALS

D. B. Hodge
Ohio State University
Columbus, Ohio

ABSTRACT

The various meteorological parameters that influence millimeter wavelength satellite-to-ground space diversity links are summarized. Space diversity propagation statistics obtained using the 15.3 GHz down-link on ATS-5 are presented. These results include comparison of data obtained using site separations of 4 and 8 km. Propagation data were recorded at Columbus, Ohio, during 1970 using a site separation of 4 km and during 1971 using a site separation of 8 km. The radiometric temperature as well as attenuation of the satellite signal was recorded in both cases for correlation purposes. Both statistics of individual storm events and cumulative statistics have been analyzed yielding single site and joint fade distributions, correlation between attenuation experienced at the two receiving terminals, and correlation between path radiometric temperatures observed at the two receiving terminals. These data indicate that the use of space diversity is indeed effective in improving the reliability of millimeter wavelength satellite-to-ground communication links.

GENERAL

It has been well established that fade depths exceeding typical system margins may be encountered for significant periods of time on millimeter wavelength earth-satellite links. These deep fades are a result of intense rain rates associated with thunderstorm cells located along the propagation path. Unfortunately, the occurrence of thunderstorms is not uniformly distributed throughout the year. For example, in Ohio thunderstorms and intense rains are much more likely to occur during the months of May, June, and July. In addition, the occurrence of thunderstorms is not uniformly distributed throughout the day, their occurrence being more likely in the late afternoon and early evening hours. Thus we may conclude that fade distributions and reliability statistics expressed on an annual basis will be rather optimistic during the thunderstorm season and even during certain hours of the day.

In order to improve the reliability of these systems, the use of space diversity in the reception of the satellite signals has been proposed. This approach takes advantage of the fact that most of the deep fades are a result of high rain rates associated with intense thunderstorm cells. These thunderstorm cells are, in turn, quite limited in horizontal extent as compared with showers having lower rain rates, which may be rather widespread horizontally. Obviously, both types of rain are limited in vertical extent. An example of a single thunderstorm cell is shown in the PPI radar photograph in Figure 6-1. This cell was observed on June 14, 1971, using a 15 GHz radar system. The antenna elevation was 7°, the azimuth ranges from 240° to 330°, and the range marks are at two mile intervals. The finite extent of the cell and the irregular shape should be noted in particular. A second PPI photograph of this cell, taken a few minutes later, is shown in Figure 6-2. In this case the radar was being operated on a contour mode such that areas producing large reflected signals are blanked out. Here we note that the highly reflective area associated with intense rain is further concentrated within the cell itself. Thus, the space diversity technique takes advantage of the limited extent of intense rains by utilizing two receiving terminals, one of which is intended to "look" around or over the cell while the other is experiencing a fade. It is evident that the statistical properties of the cell shape, extent, orientation, and height, as well as the rain rate distribution within the cell, will ultimately determine the optimum separation distance and direction of the receiving terminals and the resulting improvement of system performance. Further complicating this problem is the fact that these controlling cell characteristics are dependent on the climatological region; and, thus, the optimum diversity configuration and resulting system improvement will vary throughout the United States.

Figures 6-3 and 6-4 show worst and best case examples, respectively, of three terminal space diversity data provided by Dr. D. C. Hogg, Bell Telephone Laboratories, Inc. The time delay between the occurrence of maximum attenuation at the different terminals varies from a few minutes to almost an hour. Nevertheless, some diversity improvement would result in each case.

Space diversity measurements were made by the Ohio State University, Columbus, Ohio, using the ATS-5 15.3 GHz down-link during 1970 and 1971. The terminal separation distance was approximately 4 km during the 1970 data period and 8 km during the 1971 data period. The initial spacing of 4 km was chosen because available rain distribution data[1] indicated that the cross-correlation between the fading observed at two terminals separated by this distance would be on the order of 0.5. Although this is not a desirable criterion for the establishment of a practical diversity system, it was felt that this approach would yield information concerning the dependence of correlation upon the site separation distance more rapidly than the choice of very large or small

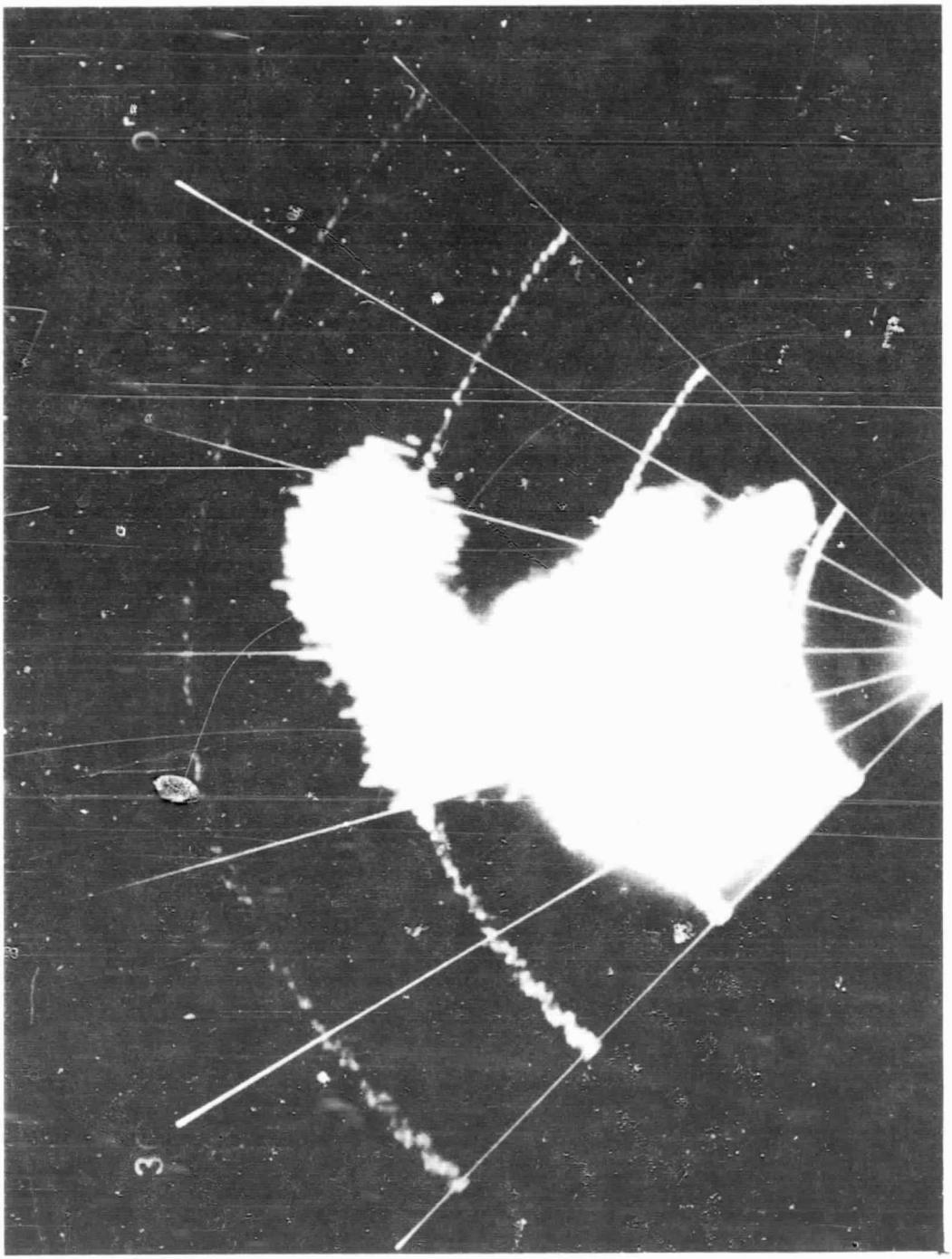

Figure 6-1. PPI Display of Thunderstorm Cell (Range Marks at 2 Mile Intervals)

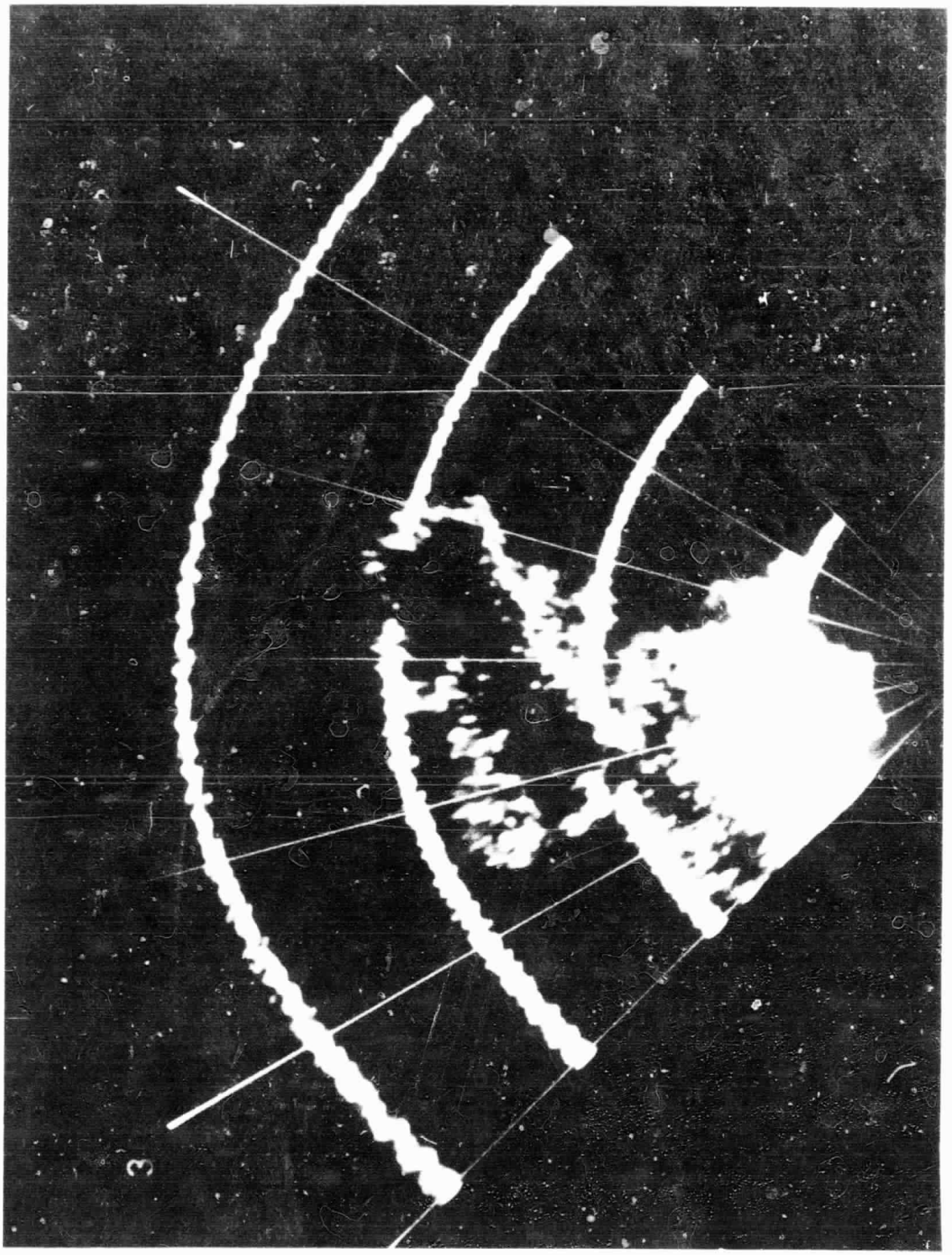

Figure 6-2. Contour Display of Cell Shown in Figure 6-1

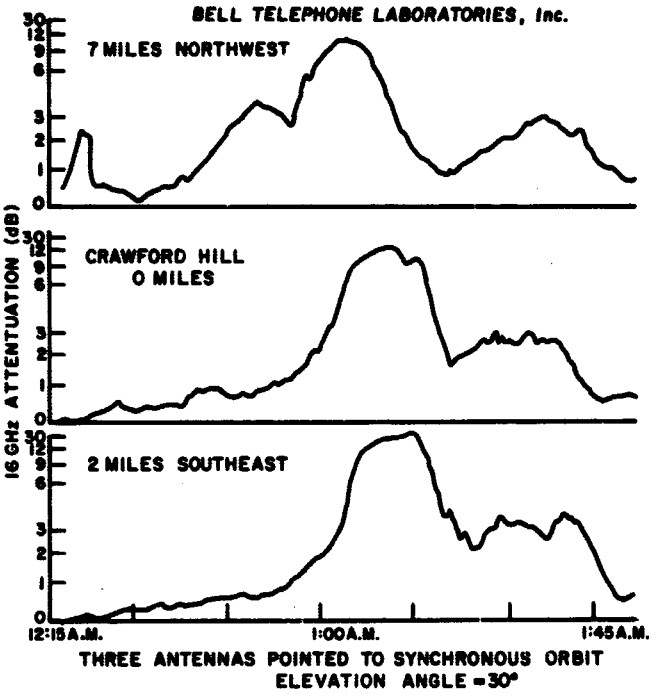

Figure 6-3. Three Terminal Diversity – Worst Case Example

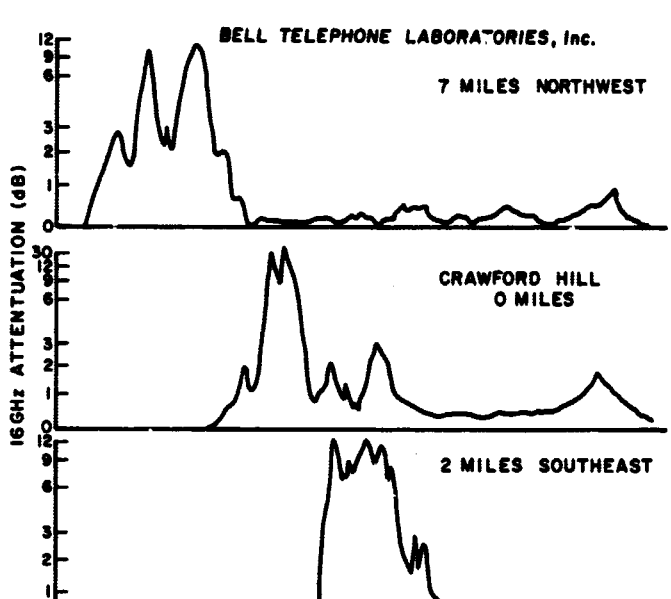

Figure 6-4. Three Terminal Diversity – Best Case Example

separation distances for the initial experiment. In addition, the direction of site separation was oblique with respect to the propagation paths rather than perpendicular to them in order to achieve vertical as well as horizontal separation between the two paths. The top and side views of the site locations are shown in Figures 6-5 and 6-6.

During the 1970 data period a 30 foot parabolic antenna was used at the fixed terminal and a 15 foot parabolic antenna was used at the transportable terminal, site 1. These antennas are shown in Figure 6-7 along with the transportable equipment van which may be seen to the right of the smaller antenna. Since the 30 foot antenna was not designed for operation in high wind speed environments, such as those encountered during the passage of severe thunderstorms, it was replaced by a new 15 foot antenna before the start of the 1971 data period. No significant reduction in system margin was incurred with this change since the gain of the original 30 foot antenna at this frequency was limited by surface roughness to approximately the same gain as the smaller, new antenna. Square, corrugated feed horns having equal E- and H-plane patterns were used to illuminate these antennas; the two orthogonal linearly polarized components were then fed, respectively to the PLL receiver and the radiometer. The remaining instrumentation has been described in References 2, 3, and 4.

A sample of the raw data obtained using the 4 km separation distance during 1970 is shown in Figure 6-8. The upper trace in each case gives the radiometric temperature measured along the propagation path and the lower trace is the pulse-by-pulse record of the received coherent signal. At approximately 1000 Z a small, rather intense thunderstorm cell passed through the propagation paths producing very rapid, deep fades. The fade depth at the fixed terminal was in excess of 12 dB, while the fade depth at the transportable terminal was approximately 6 dB. The maximum cross-correlation between the signals received at the two terminals was associated with a time delay of 8 minutes. The detailed analysis of the data obtained using a separation distance of 4 km is contained in Reference 5.

A sample of the raw data obtained using the 8 km separation distance during 1971 is shown in Figure 6-9. In this case a slowly moving cell produced a 13 dB fade at the fixed terminal while producing negligible attenuation at the transportable terminal. The increased signal level occurring at the fixed terminal at approximately 1715Z is a result of increasing the receiver gain by a factor of two.

For the purpose of studying the improvement resulting from space diversity operation, seven different storm events which produced significant fading were selected from the data obtained using the 4 km site separation for detailed

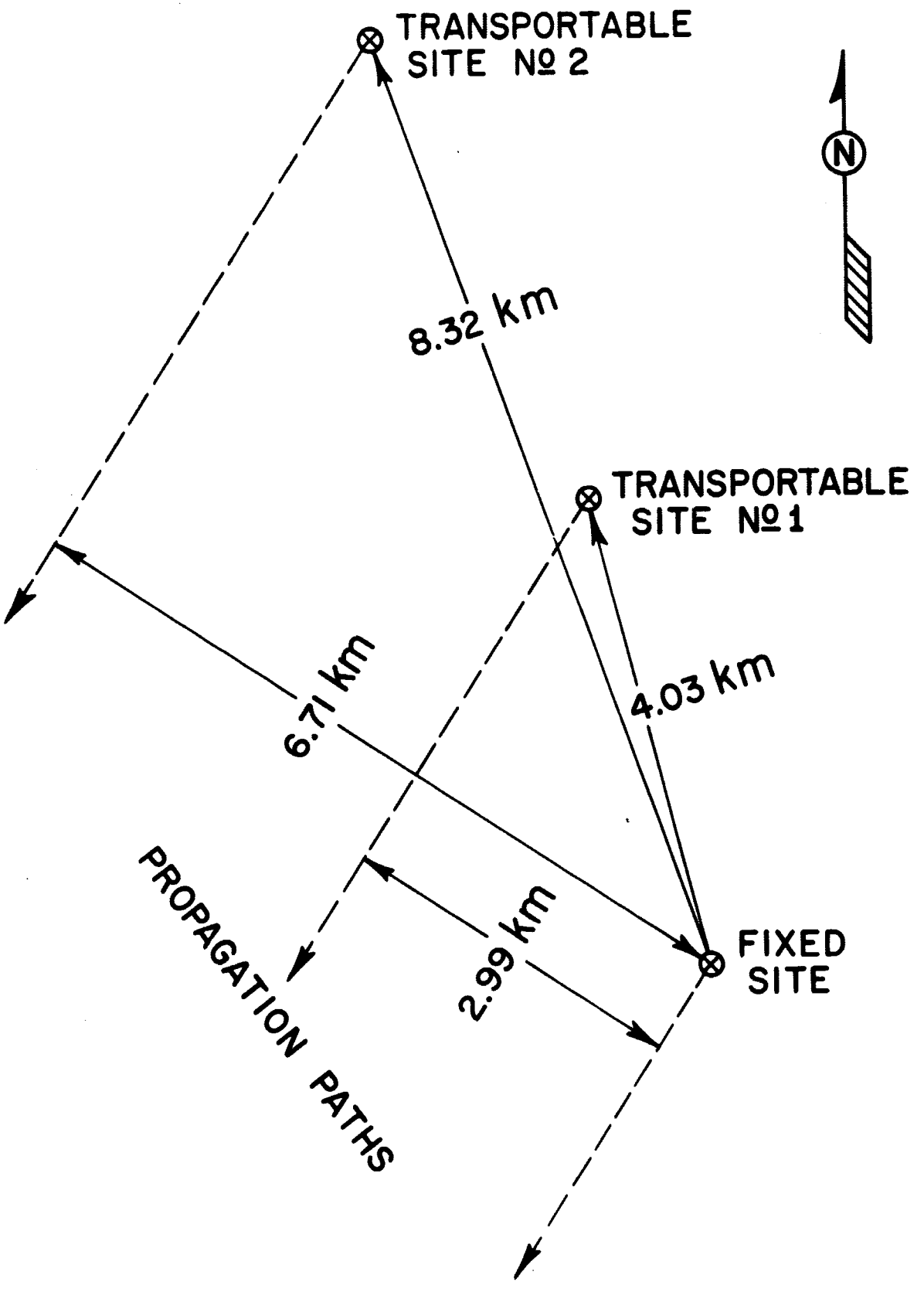

Figure 6-5. Top View of Site Locations

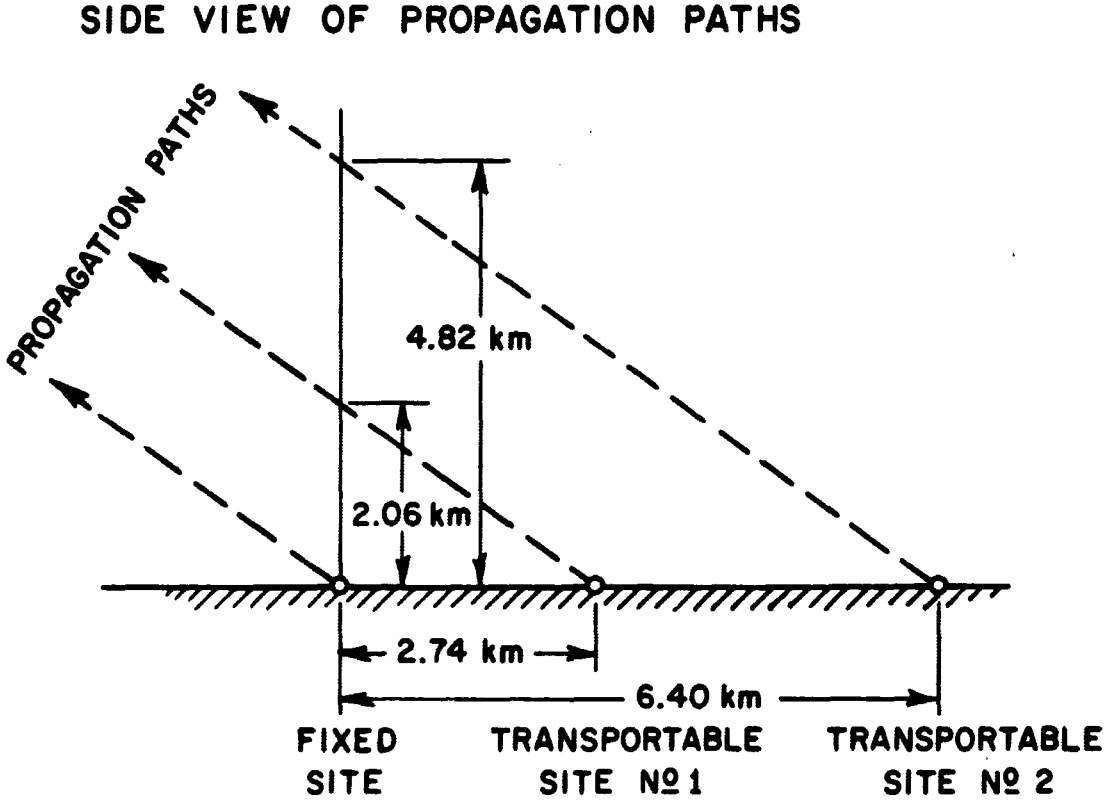

SITE	PATH SEPARATION		
	HORIZONTAL	VERTICAL	SPATIAL
Nº 1	2.99 km	2.06 km	3.41 km
Nº 2	6.71 km	4.82 km	7.73 km

Figure 6-6. Side View of Site Locations

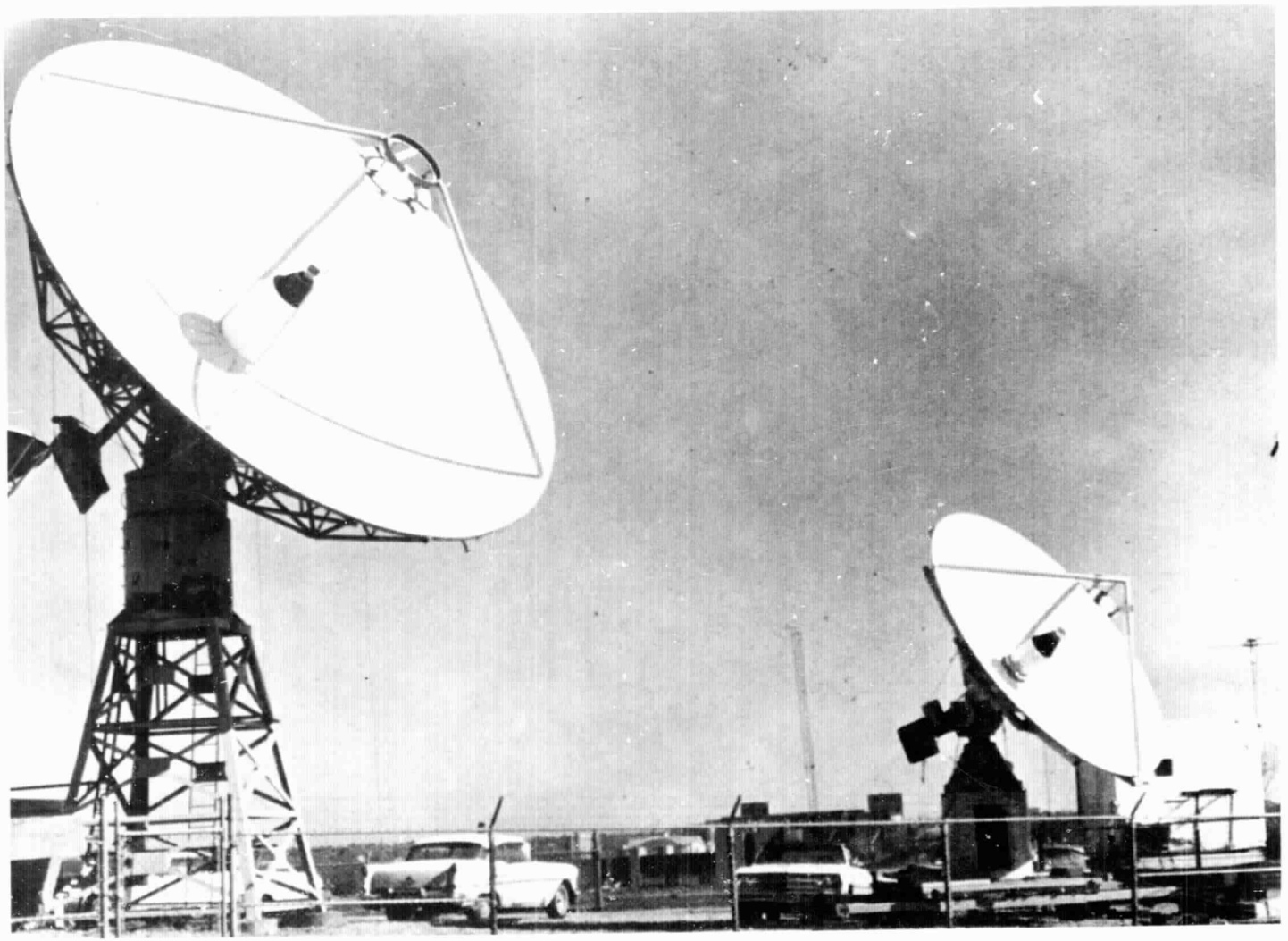

Figure 6-7. Fixed and Transportable Antennas (1970)

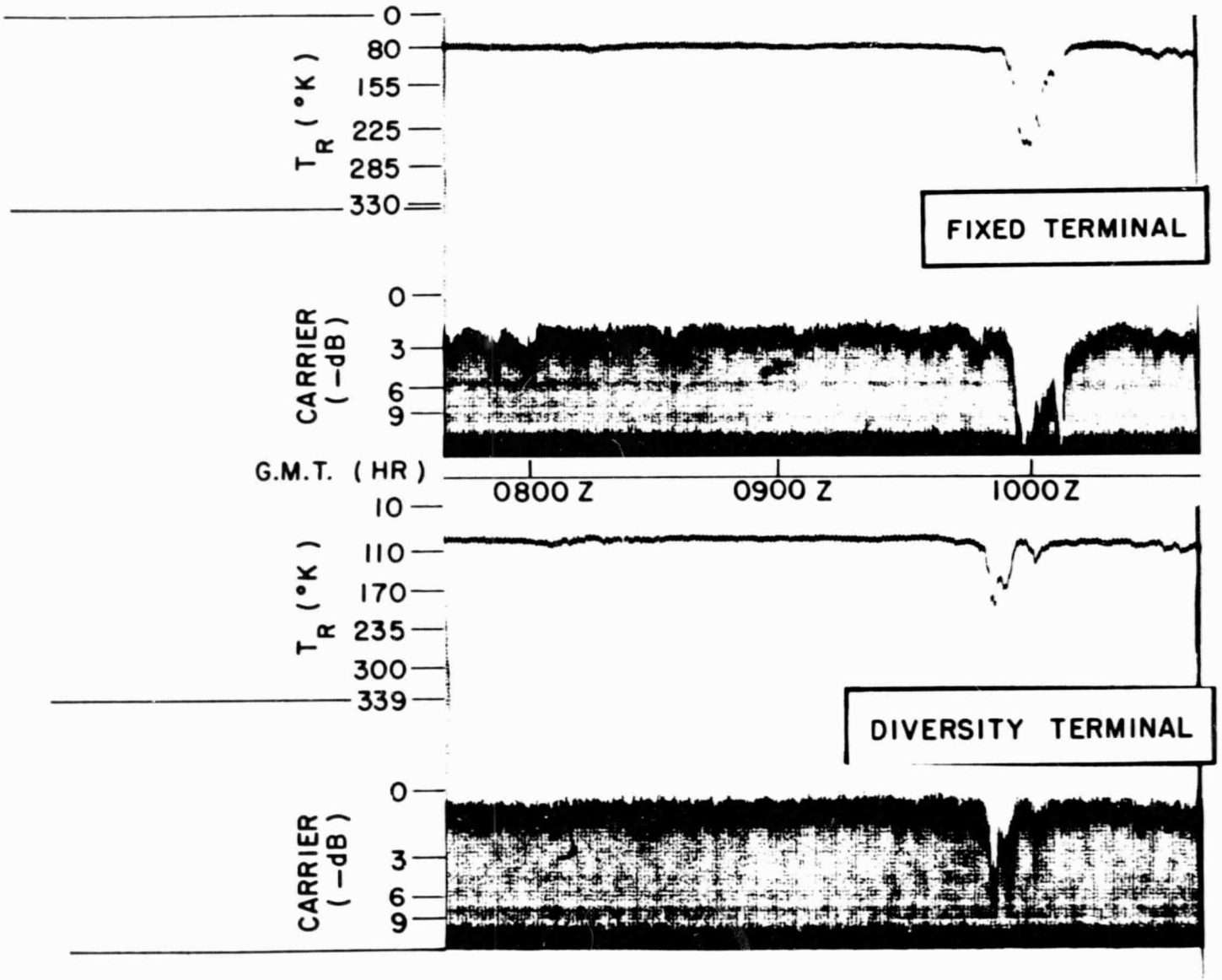

Figure 6-8. Sample Data at 4 km Site Separation, June 14, 1970

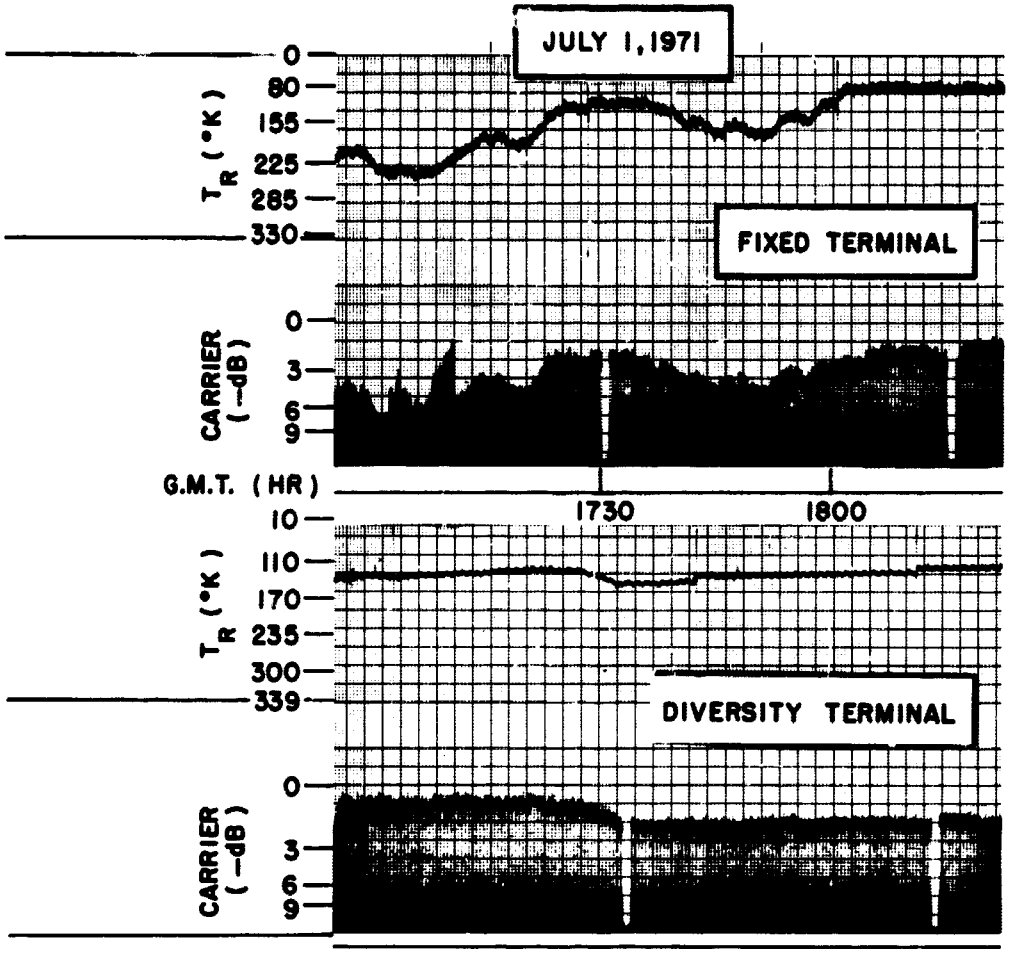

Figure 6-9. Sample Data at 8 km Site Separation

analysis; nine such events were also selected from the data obtained using the 8 km separation distance. Treating each storm event individually, the cross-correlation between the attenuations observed at the two sites was calculated. A sample cross-correlation function for one storm event is shown in Figure 6-10. Three characteristics of the storm event may be inferred qualitatively from this cross-correlation function. First, the time delay associated with the maximum of the cross-correlation function, in this case 8 minutes, is related to the speed with which the storm cell crosses the propagation paths. Second, the cross-correlation function evaluated for zero delay is an indicator of the effectiveness of a space diversity system operating in real time. And, third, the maximum value of the cross-correlation function is a measure of the change in the storm cell structure as it traverses through the two propagation paths, or, alternatively, the degree to which the propagation paths "slice" through different portions of the storm cell.

The cumulative cross-correlation functions for all the events analyzed in the two data periods were also calculated. The cumulative cross-correlation function at zero delay was 0.452 and the average delay time associated with the maximum cross-correlation function was 4.1 minutes for the data obtained using the 4 km terminal separation. Similarly, the cumulative cross-correlation function at zero delay was 0.268 and the average delay time of the maximum cross-correlation function was 10.2 minutes for the data using the 8 km terminal separation.

The fade distributions observed at the individual terminals as well as the fade distribution resulting from the space diversity mode of operation were also examined. These results for the 4 and 8 km separation distances are shown in Figures 6-11 and 6-12, respectively. As expected, the individual terminal fade distributions are quite similar for the 4 km separation and show less similarity for the 8 km separation. The diversity fade distributions, labeled "BOTH" in the figures were obtained by digitally comparing the individual terminal received signal records and selecting the larger signal on a second-by-second basis. This method of analysis corresponds to a simple switched diversity system operating in real time. Significant improvements in system performance would have resulted from the diversity mode of operation for both separation distances.

Diversity gain may be defined as the difference between the signal level resulting from the diversity mode of operation and the median of the individual terminal received signal levels, both evaluated at a given percentage of occurrence. The diversity gain then corresponds to the improvement derived from diversity operation as compared to single terminal operation over a long period of time. Diversity gain data for both the 4 and 8 km separation distances as a function of single terminal fade depth are shown in Figure 6-13. Note that the

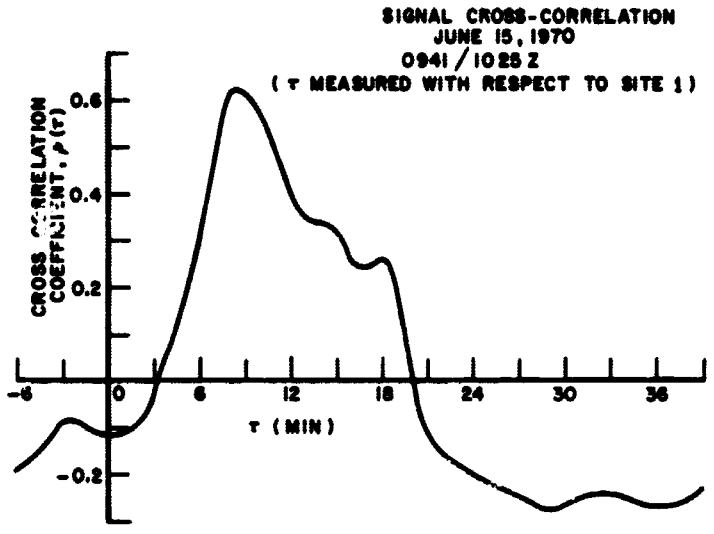

Figure 6-10. Cross-Correlation Between Receiver Signals at Two Terminals Separated by 4 km

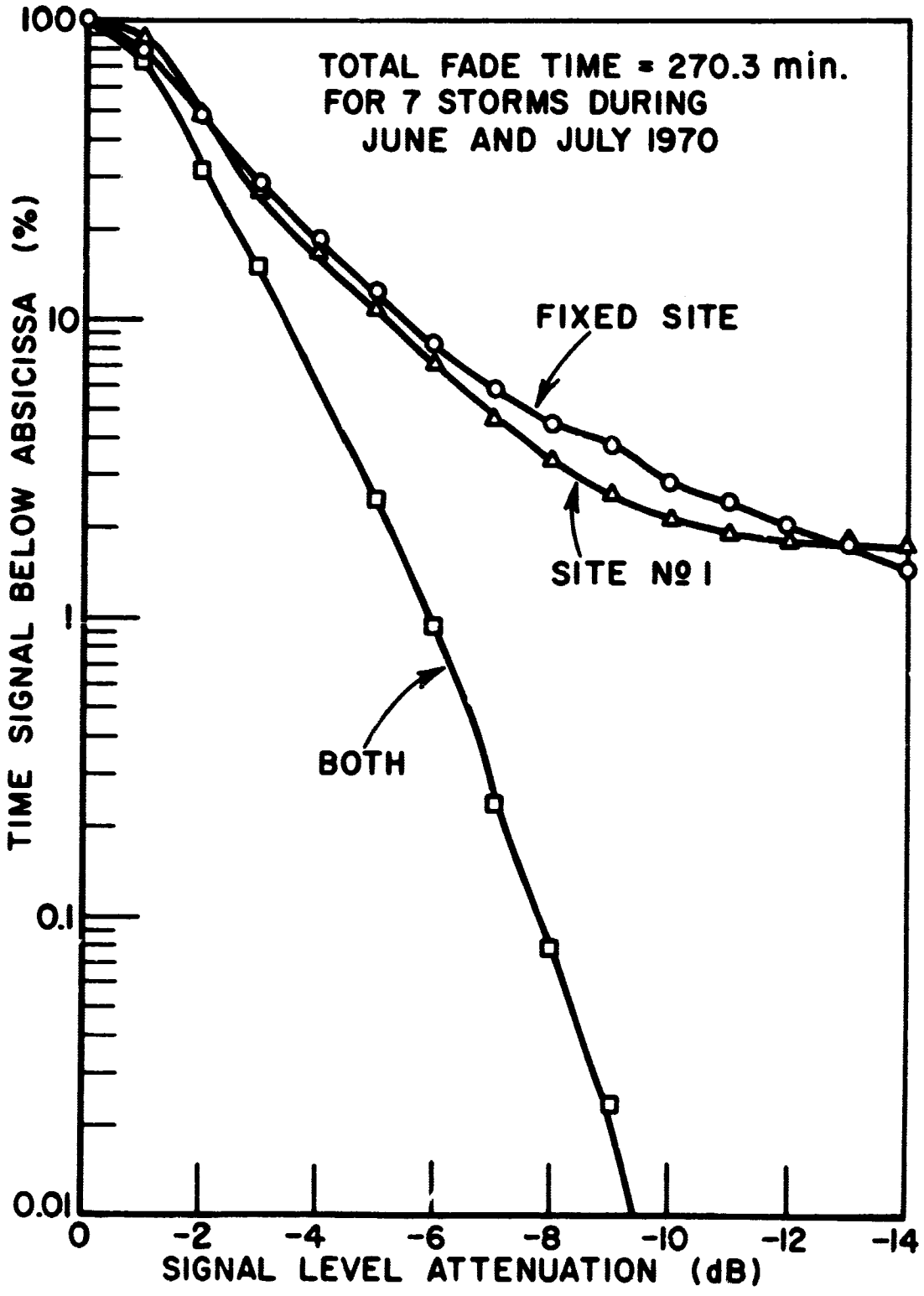

Figure 6-11. Fade Distributions for 4 km Data

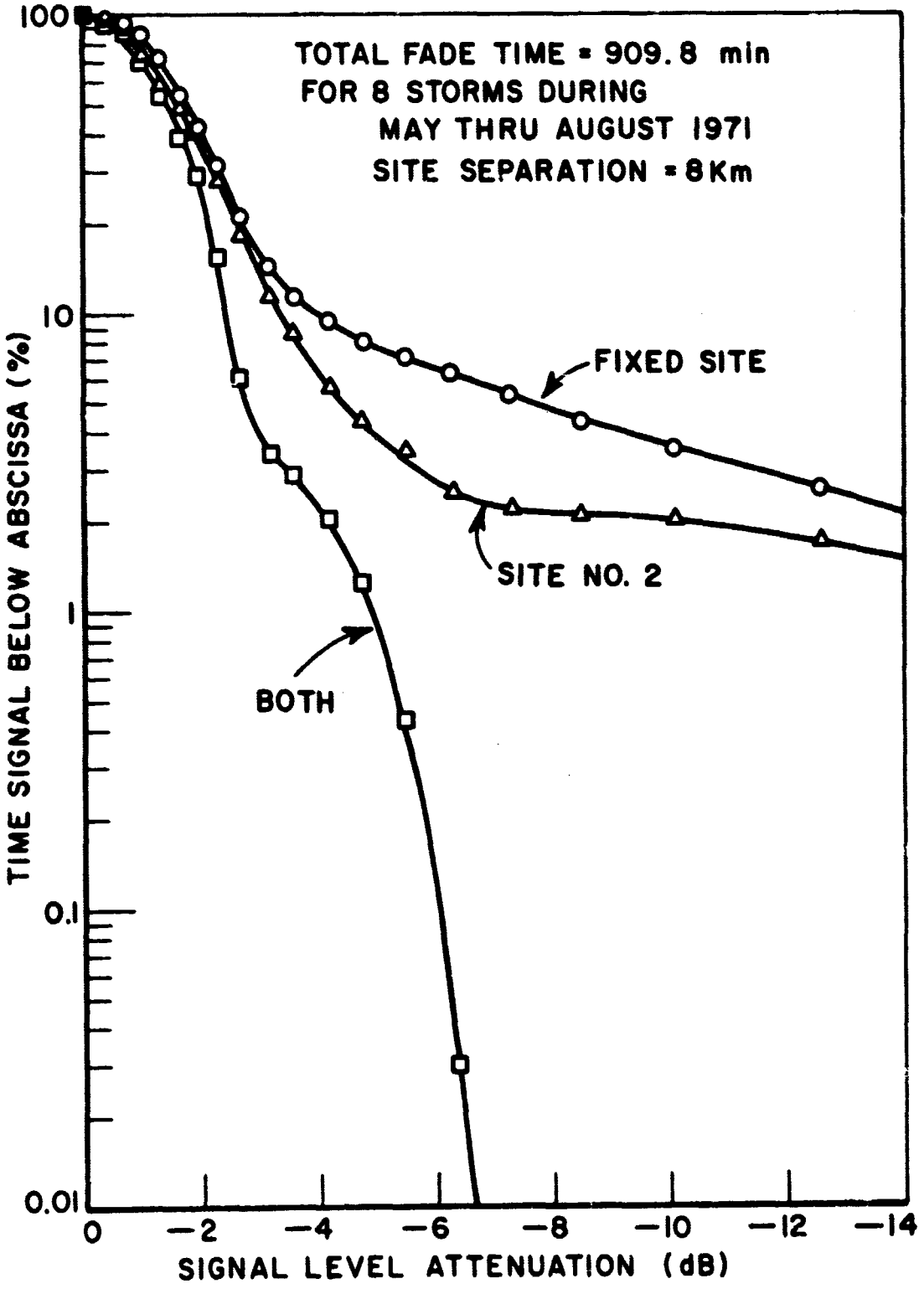

Figure 6-12. Fade Distributions for 8 km Data

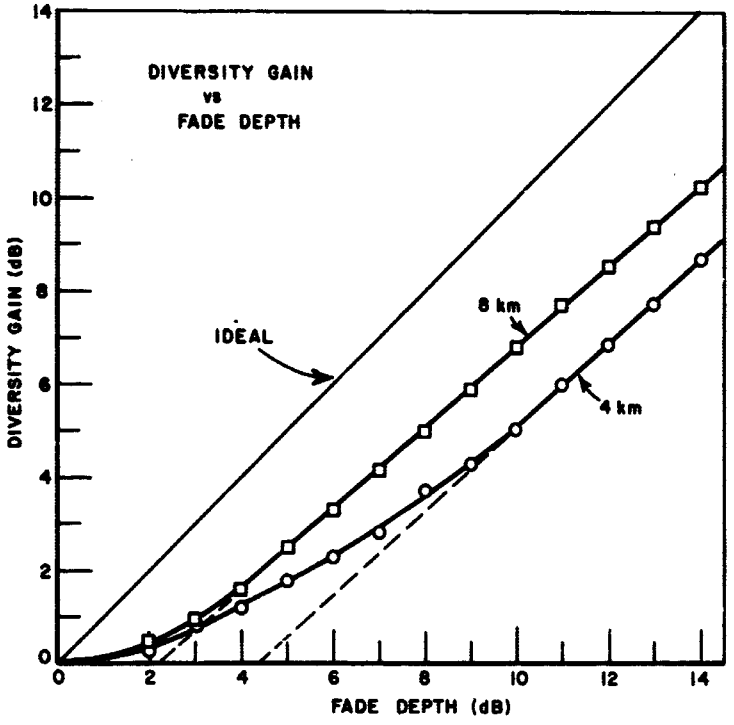

Figure 6-13. Diversity Gain Versus Single Terminal Fade Depth

abscissa itself corresponds to diversity operation with zero separation, and the straight line with unity slope through the origin corresponds to ideal case where diversity operation eliminates all fading. Obviously, then, the 4 and 8 km diversity data must lie between these two limiting cases. Note, also, that the experimental data fall very nearly on straight lines having approximately unity slopes for fade depths exceeding 10 dB for the 4 km separation and 4 dB for the 8 km separation. This characteristic indicates that the diversity system is operating very much like an ideal system for fade depths below these levels and is, indeed, quite effective in improving system performance during periods of deep fading. Further examination of the diversity gain data indicates that the use of larger terminal separation distances will provide proportionally less improvement in system performance. This reduced degree of improvement will also be purchased at the increased cost of the data link between the two ground terminals required for real time diversity operation. Another factor which will come into play as the separation distance is increased is fading due to the simultaneous intersection of the propagation paths by two different storm cells. PPI radar observations during the data gathering periods have indicated qualitatively that the events observed at the 4 and 8 km separation distances were completely dominated by single cells influencing both paths simultaneously.

In summary, data obtained using the ATS-5 15.3 GHz down-link have shown that significant system performance improvement results from the use of diversity receiving terminals spatially separated by 4 and 8 km. The durations of fades in excess of 10 and 6 dB, respectively, were reduced by at least two orders of magnitude in central Ohio. Further performance improvements to be gained by utilizing larger separation distances must be weighed against the increased costs of the data link between the ground terminals and the reduction in effectiveness resulting from the increased likelihood of fading produced by two different storm cells. Additional problems which remain to be examined include: the dependence of diversity gain upon a wider range of separation distances, the dependence of diversity gain upon the orientation of the separation baseline, and the dependence of both of these characteristics upon the meteorological environment encountered at various geographical locations.

REFERENCES

1. Freeny, A. E. and Gabbe, J. D., "A Statistical Description of Intense Rain," Bell System Technical Journal, V. 48, July 1969, p. 1789.

2. Semiannual Status Report, "Millimeter-Wavelengths Propagation Studies," Report 2374-3, 15 April 1969, ElectroScience Laboratory, The Ohio State University Department of Electrical Engineering, prepared under Grant

NGR 36-080-008 for National Aeronautics and Space Administration, Washington, D.C. (N69-27155)

3. Semiannual Status Report, "Millimeter-Wavelength Propagation Studies," Report 2374-4, 30 April 1970, ElectroScience Laboratory, The Ohio State University Department of Electrical Engineering, prepared under Grant NGR 36-080-008 for National Aeronautics and Space Administration, Washington, D.C.

4. Hodge, D. B., Semiannual Status Report, "Millimeter-Wavelengths Propagation Studies," Report 2374-8, January 1972, ElectroScience Laboratory, The Ohio State University Department of Electrical Engineering, prepared under Grant NGR 36-080-008 for National Aeronautics and Space Administration, Washington, D.C.

5. Grimm, K. R. and Hodge, D. B., "A 15.3 GHz Satellite-to-Ground Diversity Propagation Experiment Using a Terminal Separation of 4 Kilometers," Report 2374-7, December 1971, ElectroScience Laboratory, The Ohio State University Department of Electrical Engineering, prepared under Grant NGR 36-080-008 for National Aeronautics and Space Administration, Washington, D.C.

SECTION 7

THE ESTIMATION OF ATTENUATION STATISTICS FOR EARTH-SPACE MILLIMETER WAVELENGTH PROPAGATION

Logan R. Zintsmaster
Ohio State University
Columbus, Ohio

ABSTRACT

The attenuation probability distributions for a millimeter wavelength earth-space propagation path are estimated for a single site and for a diversity configuration. The precipitation attenuation phenomenon is modeled by a cylindrical storm cell having a homogeneous rain rate. The attenuation probability distributions are then calculated from this storm cell model in terms of the rain rate probability density function, the cell diameter as a function of rain rate, and a fixed cell height. A rain rate probability density function which can be related to National Weather Service rain rate measurements is used in the calculations. Data from ATS-5 measurements for single sites in Rosman, North Carolina, and Columbus, Ohio, are compared to results calculated using typical storm parameters. In addition diversity calculations are compared with ATS-5 diversity measurements in Columbus, Ohio.

GENERAL

Precipitation in the form of rain is one of the major factors influencing the propagation of millimeter wavelength signals. One means used to characterize this effect is the attenuation probability distribution function. The ATS-5 experiment has been used to empirically measure this function and a need exists for a method to predict this function. This paper presents such a technique using a storm cell model for calculating the attenuation probability distribution from tipping bucket rain rate data. This model may also use tipping bucket rain data published by the National Weather Service.

In calculating the attenuation probability distribution the assumption was made that the precipitation events affecting the propagation of millimeter wavelength signals could be represented by cylindrical storm cells as shown in Figure 7-1.

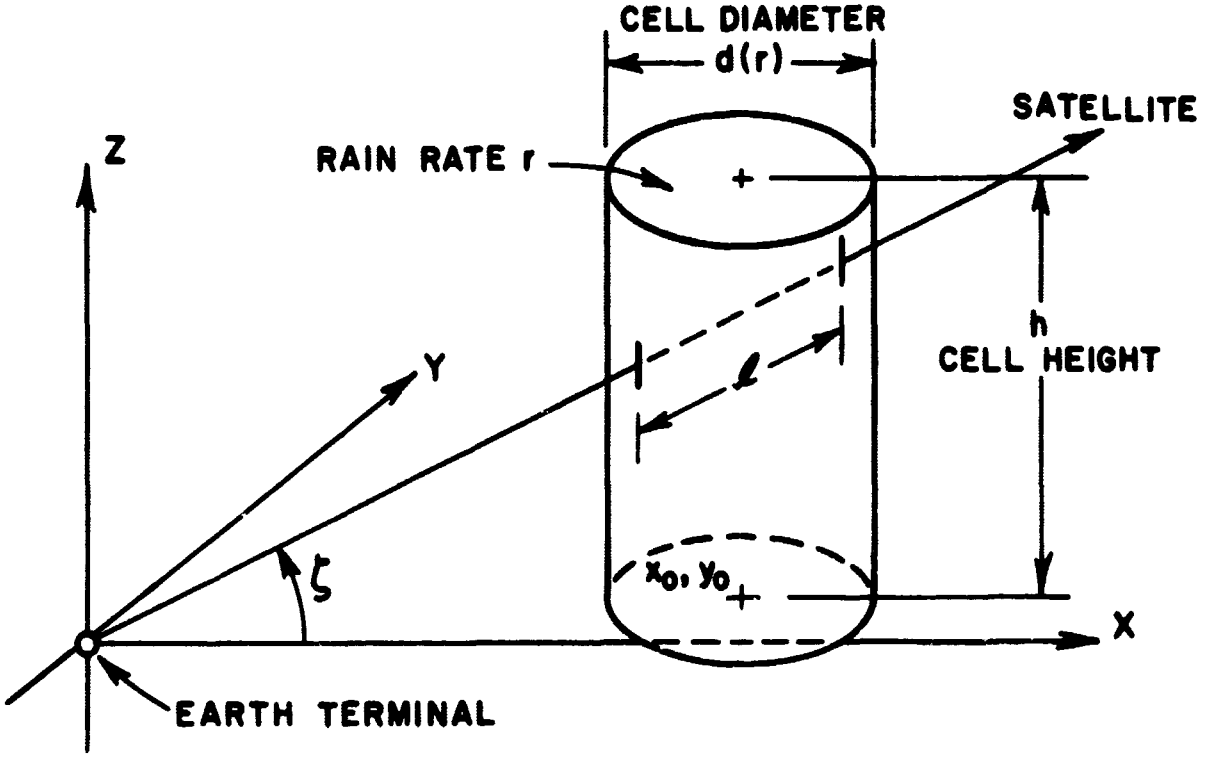

Figure 7-1. Model Storm Cell and Coordinate Axes

The storm cell is filled homogeneously with a rain rate r and has a fixed height, h. The diameter, a function of the rain rate r, represents an effective cell diameter. The location of the storm cell will be determined by the point where the vertical axis of the cell passes through the x,y plane. This point is identified as (x_0, y_0) and will be referred to as the center of the storm cell. The earth terminal, the propagation path and the coordinate axes are also shown. It is assumed that the terminal is located at the origin and that the propagation path lies in the x-z plane. The usual flat earth assumption has also been made.

There are four ways in which the storm cell may intersect the propagation path. In the first case, shown here, the propagation path enters the side of the cell and exits through the side. The length of the intersected path is shown as ℓ.

The other three types of intersections are:

1) The propagation path enters the side and exits through the top,

2) The path originates within the cell and exits through the top, and

3) The path originates within the cell and exits through the side.

In each of these four cases, the attenuation caused by the storm cell precipitation can be determined from the length of the intersected path, ℓ, and the storm cell rain rate, r, using the Gunn-East relation,

$$\alpha = .035\, \ell\, r^{1.10}. \tag{1}$$

The constants used here were interpolated from results calculated by Crane[1] from rain drop distribution measurements. In calculating the attenuation distribution the probability of a storm cell being centered at any point was assumed to be uniform over the universe of cell locations. Using the Gunn-East equation to relate the random variables α, r and ℓ, the attenuation probability distribution function was calculated and is

$$P_\alpha(\alpha_0) = N \int_{r_{min(\alpha)}}^{\infty} \left[p_B(r) + p_{B0}\,\delta(r)\right]\left[A\left(\ell_1(\alpha_0, r)\right)/A_B(r)\right] dr. \tag{2}$$

This equation relates the attenuation distribution function to the tipping bucket rain rate probability density function and two areas which are functions of the cell geometry and the propagation path geometry. The constant N is used to normalize the equation so that $P(0) = 1$.

The first term in the integrand, the tipping bucket rain rate probability density function, has two parts. The first, $p_B(r)$ is the probability density that a non-zero rain rate is measured by the tipping bucket. The second, p_{B0}, is the probability that a zero rain rate is measured. These functions account for the precipitation characteristics at the site being considered.

The functions which depend on the cell geometry are $A_B(r)$ and $A(\ell_1(\alpha_0, r))$. $A_B(r)$ is the area within which a storm center may be located and produce rainfall into the tipping bucket. The function $A(\ell_1(\alpha_0, r))$ is the area within which a storm center may be located and intersect the propagation path over a length greater than or equal to ℓ_1.

Since the storm cell has a finite maximum diameter, there is a maximum possible intersected path length for a given attenuation, α_0; this requires that a minimum rain rate be present in the cell for that attenuation to occur. This minimum rain rate is $r_{min}(\alpha)$, the lower limit of the integration.

For the model to be of maximum usefulness the rain rate density function should reflect the precipitation characteristics of each terminal location being considered. Data for stations all over the United States are published by the National Weather Service, however, the rain rates which are measured are averaged over a one hour time interval and are too coarse to use directly in the calculation.

It has been found by Rice and Holmberg[2] that the tipping bucket probability distribution function could be approximated by the sum of three exponential functions called modes. It was further found that the modes for different averaging times were related so that given the mode parameters for a particular averaging time the corresponding mode parameters for a different averaging time could be calculated.

From this distribution, the tipping bucket rain rate density function for non-zero rain rates was calculated and is shown in Eq. (3).

$$p_B(r) = \sum_{1}^{3} A_i / B_i \exp(-r/B_i). \qquad (3)$$

The mode coefficient, A_i, will be calculated from measured rain rate data. The mode rates, B_i, used are taken from the Rice-Holmberg calculations. The zero rain rate probability is determined from Eq. (3) and is given below.

$$P_{B0} = 1 - \sum_{1}^{3} A_i \qquad (4)$$

To include the precipitation characteristics of a particular site into the attenuation distribution the hourly precipitation data published by the National Weather Service is used to calculate a best fit Rice-Holmberg clock-hourly rain rate distribution function. From this function the clock one minute distribution function is calculated. Although it would be ideal to have the instantaneous statistic the clock one minute statistic is the best presently available.

The other terms in the integrand are functions of the storm cell and propagation path geometry. The area within which a storm cell can be located and rain in the tipping bucket rain gauge, $A_B(r)$, is a circular region, centered at the tipping bucket. This area is $\pi (d(r))^2/4$. The area within which a storm cell may be centered and intersect the propagation path is shown in Figure 7-2 for the single and two site calculations. For a single site the region is centered about the x-axis and represents the area where a storm cell may be centered and intersect the path over a length greater than or equal to $\ell_1(\alpha_0, r)$. To calculate the two site joint attenuation distribution, the storm cell must intersect both propagation paths simultaneously. Thus, the path intersection area $A(\ell_1(\alpha, r))$ is the area of overlap of the two single site intersection areas. The analytic forms of these areas is determined in a straight forward manner from the storm cell-propagation path geometry.

Having calculated the attenuation probability distribution function for the model storm cell, the storm cell dimensions, h and d(r), must now be related to the physical precipitation process so that calculations can be made. The cell height, h, represents the height of the precipitation cell. For most of the United States a value of 5 to 7 km is typical. It has been found that the results are not very sensitive to the exact choice so an average of 6 km was used in the calculations presented here.

Whereas the cell height corresponds to the physical height of a rain cell, the storm cell diameter represents an effective diameter and thus may not correspond well with the actual physical dimensions of rain cells. Several proposed diameter-rain rate functions are shown in Figure 7-3.

The first is a modified form of the CCIR function. The original function becomes negative for rain rates greater than about 50 mm/hr. Since this does not seem realistic, the function was modified so that the minimum cell diameter was clamped to 1.25 km. The choice of the minimum diameter was based on data from Bell Labs suntracker measurements presented by Hogg[3]. An exponential

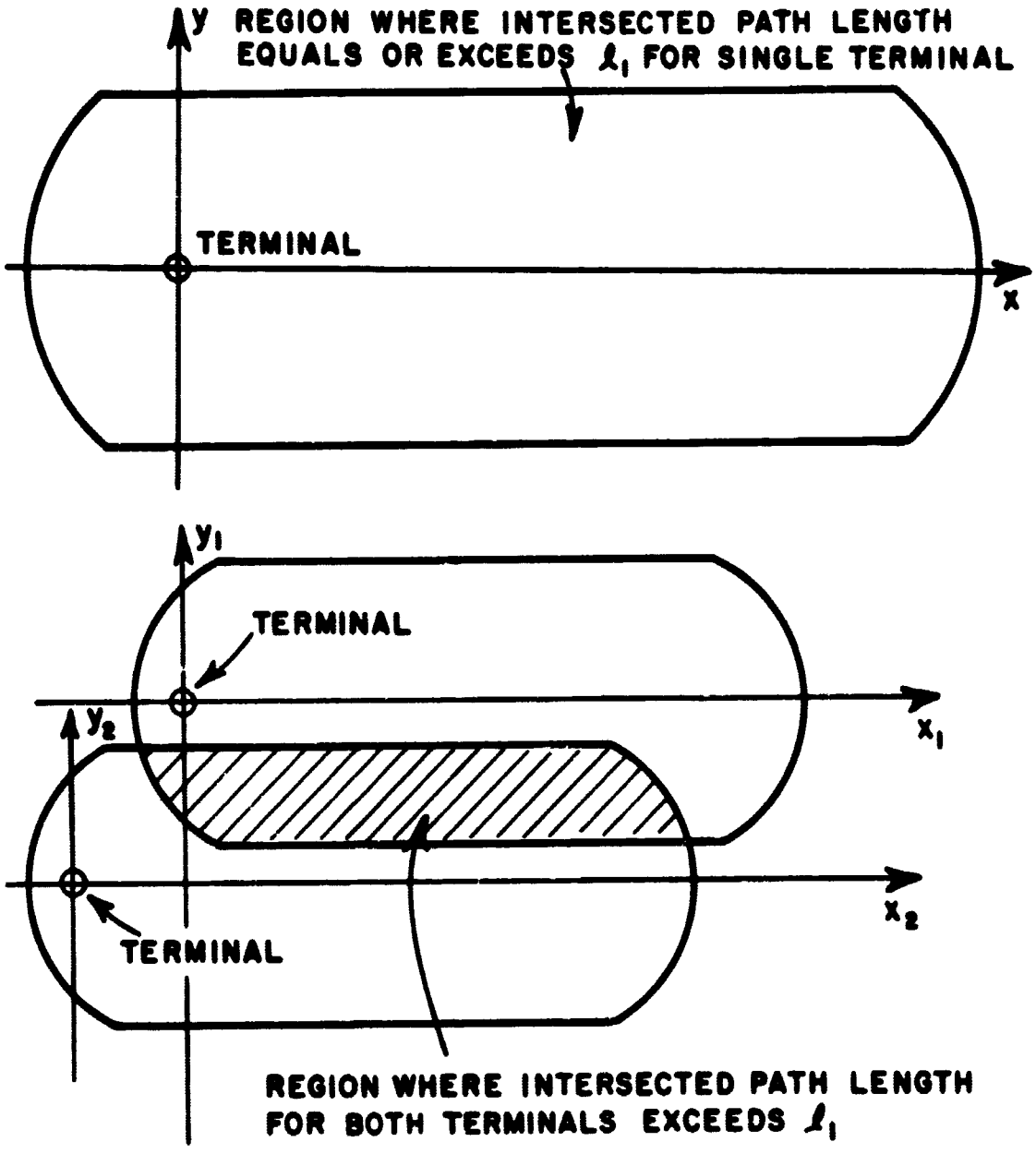

Figure 7-2. Areas of Storm Cell Center Locations for Propagation Path Intersections with One and Two Terminals

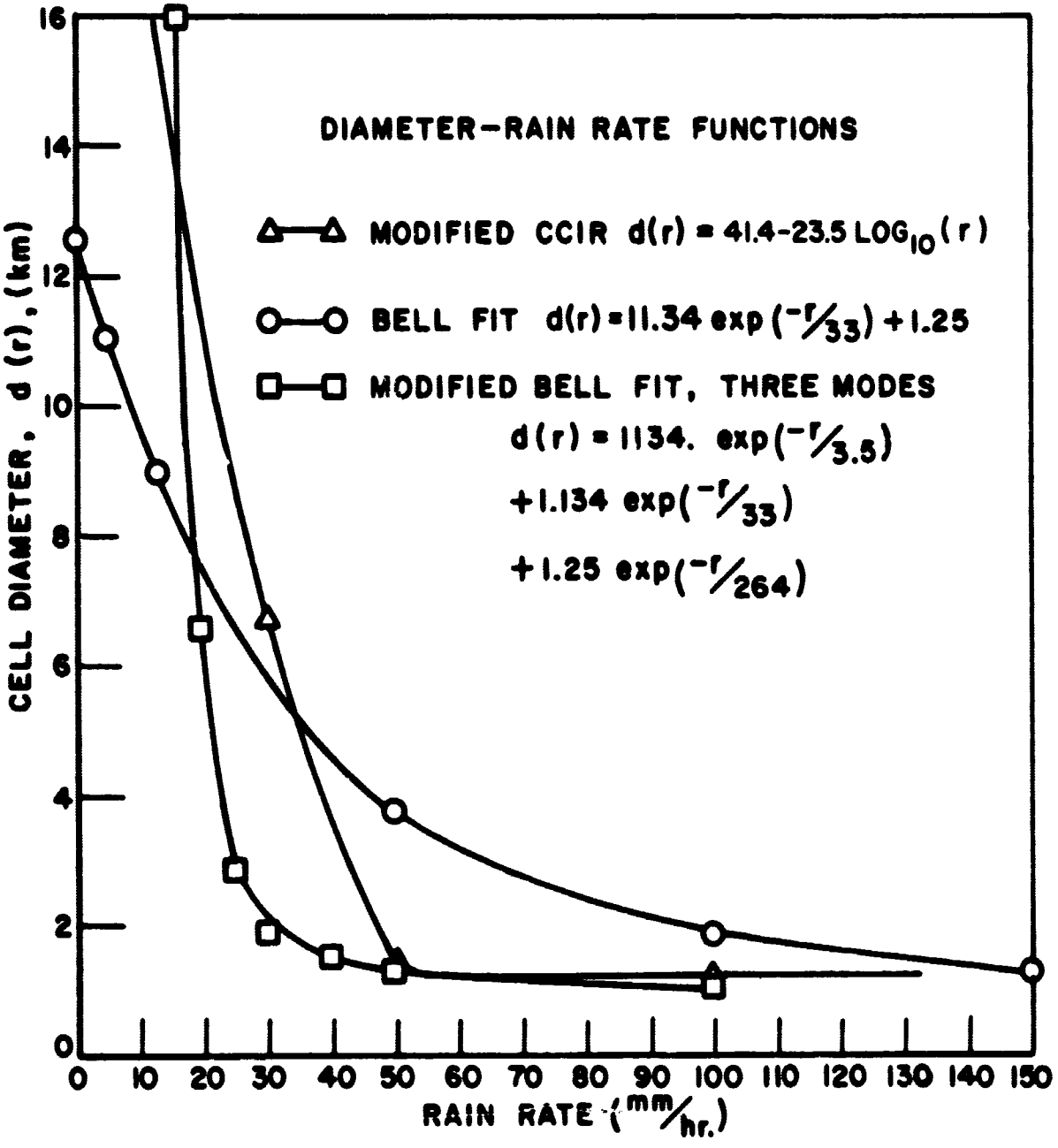

Figure 7-3. Diameter-Rain Rate Models

function was fitted to Hogg's data for use in numeric calculations and is also shown in this figure.

The third diameter function shown was determined empirically from the 1970 Ohio State University ATS-5 data using the mode concept presented by Rice and Holmberg. Since the Rice-Holmberg distribution characterizes different types of precipitation processes in terms of three modes, it seemed logical to characterize the size of these precipitation cells in a modal form also. For the calculations to be presented here, the Bell fit diameter function and the three mode diameter function were used.

In order to make a fair comparison between the calculated attenuation distribution and the measured attenuation distribution, the rain rates which occurred during the attenuation measurements were used to calculate the A_i's in the Rice-Holmberg distribution. A comparison of the best fit Rice-Holmberg distribution and the rain rates measured at NASA Rosman in 1970 are shown in Figure 7-4. It is seen here that the Rice-Holmberg distribution fits the data very well.

Using this rain rate distribution and the Bell fit diameter function the attenuation distribution for the NASA Rosman terminal was calculated and is shown in Figure 7-5. The error criterion which is used to evaluate the comparison of the measured and calculated results is the horizontal distance between the curves. This criterion gives the attenuation difference between the calculated and experimental attenuation for a constant probability. It can be seen that the calculated distribution brackets the measured distribution. For low attenuations the results are about 3 dB low. For high attenuations the calculated distribution is about 3 dB high.

Using the three mode diameter function the results were improved significantly as shown in Figure 7-6. The error at low attenuations has been reduced to 2 dB and at high attenuations the error is only .5 dB. It is seen that the calculated distribution agrees well with the measured distribution.

As mentioned earlier the three mode diameter function was found by fitting the calculated attenuation distribution to the single site distribution measured at Ohio State in 1970. This fit is shown in Figure 7-7. The flattening of the measured curve was ignored in the fit since it resulted from margin limitations in the measurements.

In Figure 7-8 the storm cell model was used to calculate the two terminal joint attenuation distribution for the 4 km spacing used in 1970 at Ohio State University. It is seen here that good agreement is also obtained.

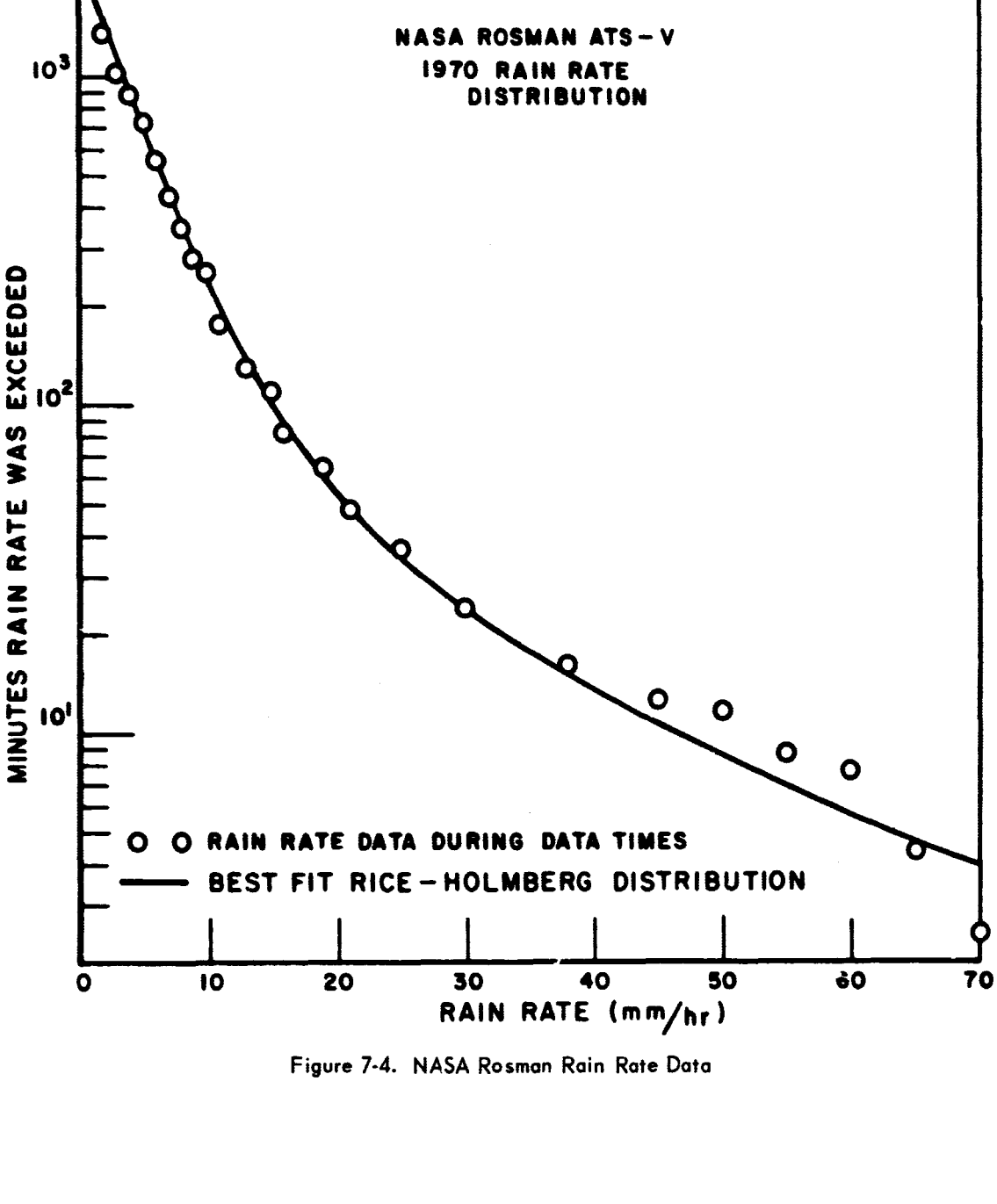

Figure 7-4. NASA Rosman Rain Rate Data

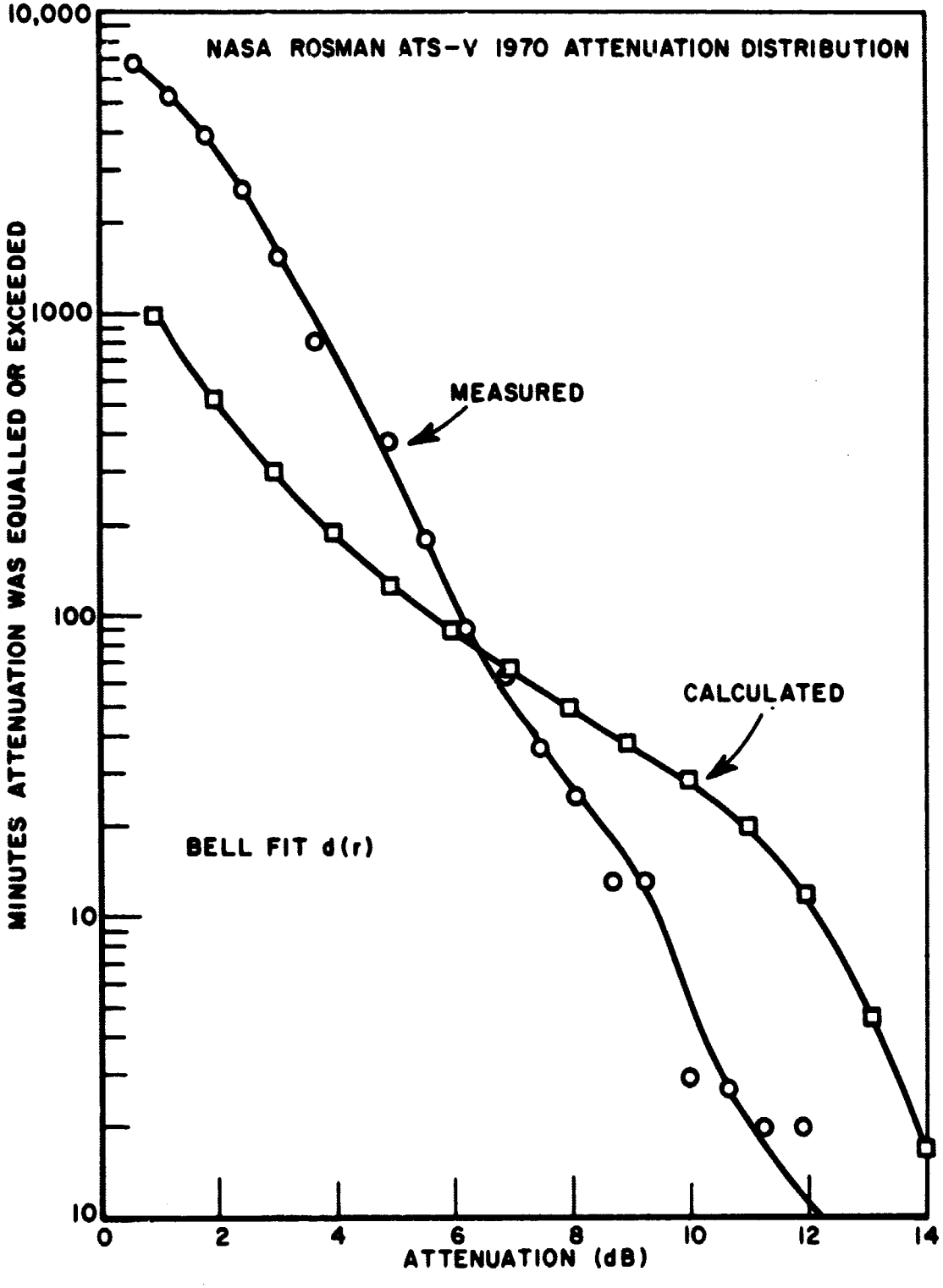

Figure 7-5. Calculated NASA Rosman Fade Distribution Using Exponential Diameter Model

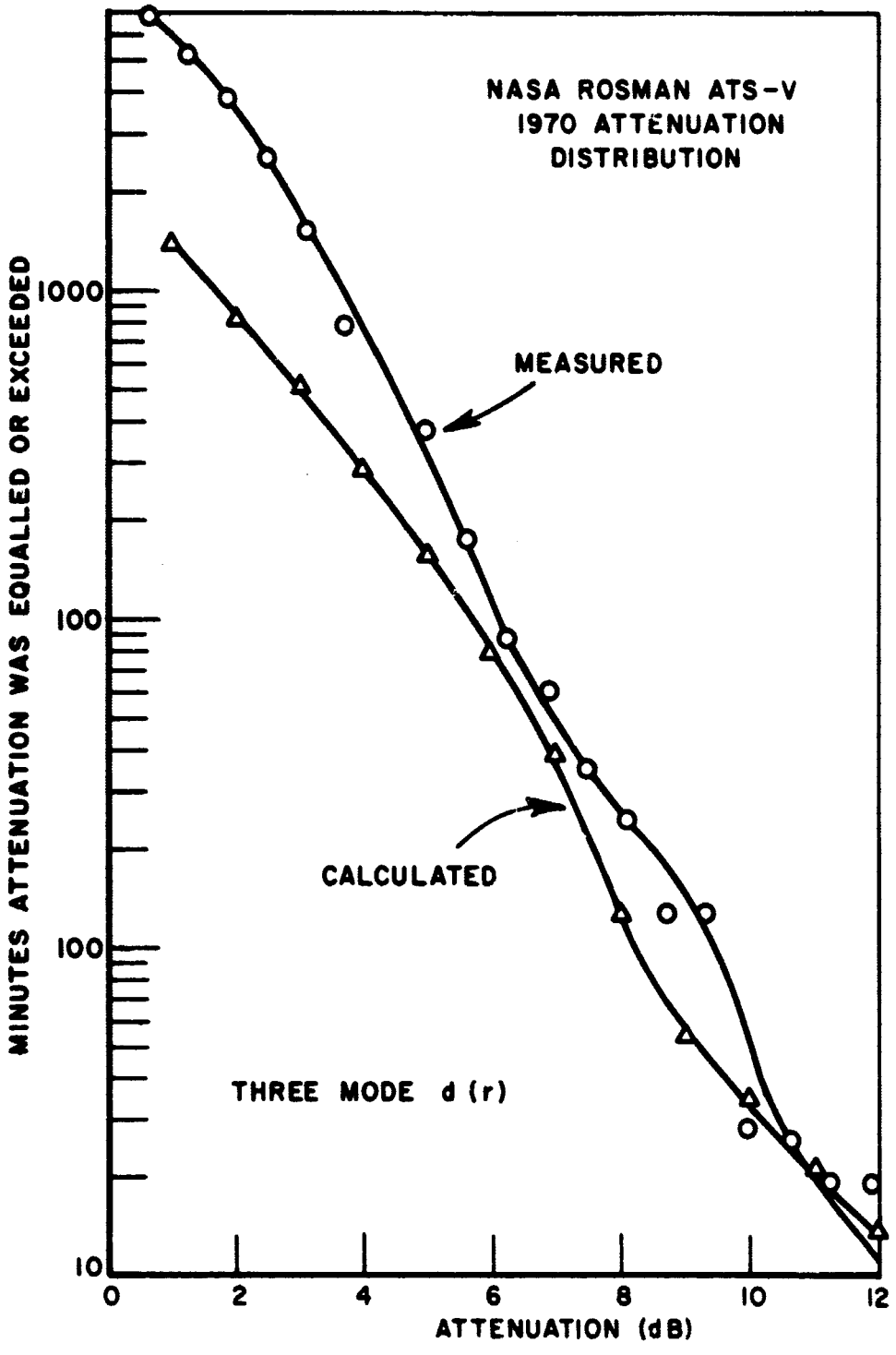

Figure 7-6. Calculated NASA Rosman Fade Distribution Using 3 Mode Diameter Model

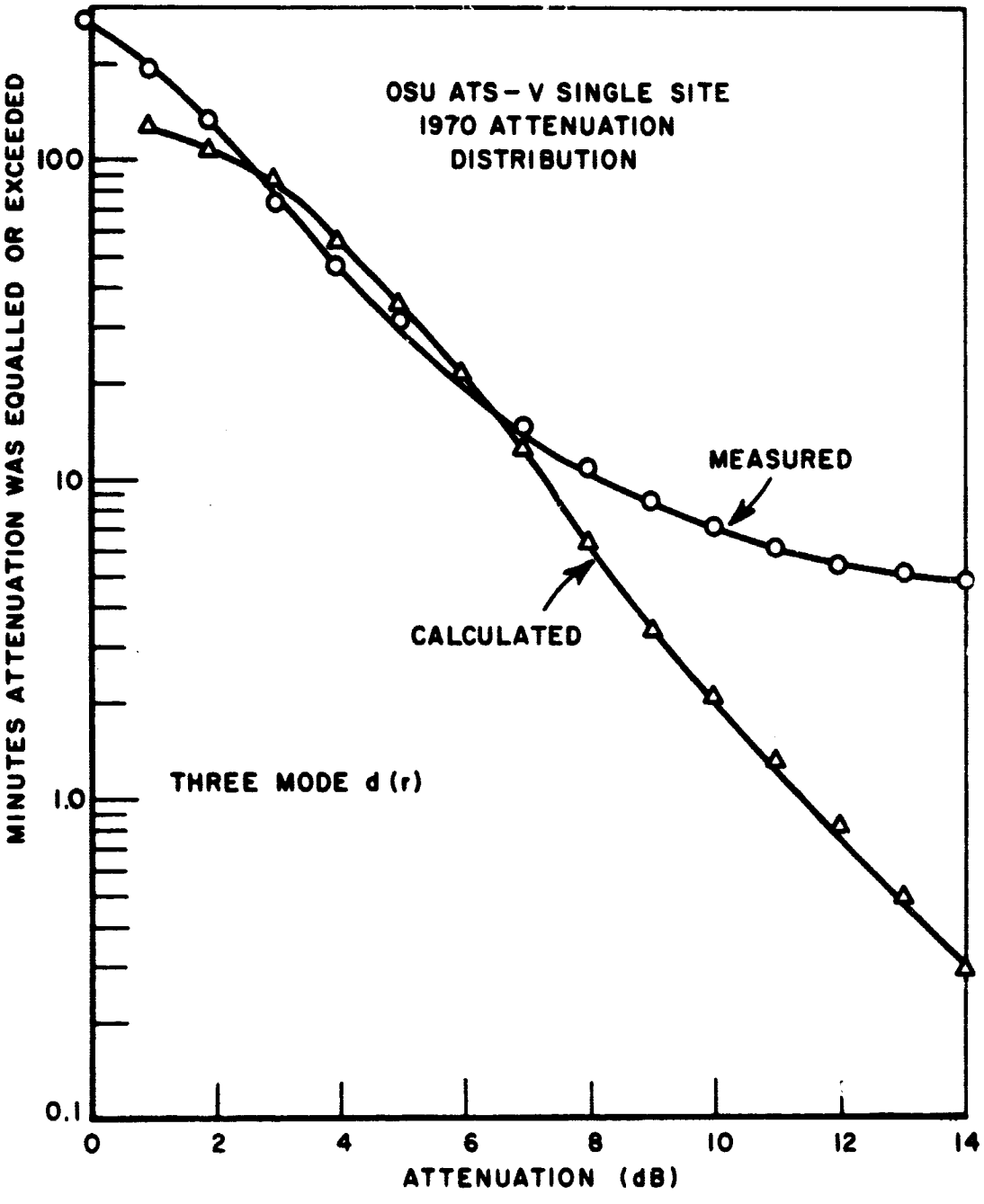

Figure 7-7. Calculated OSU Single Terminal Fade Distribution Using 3 Mode Diameter Model

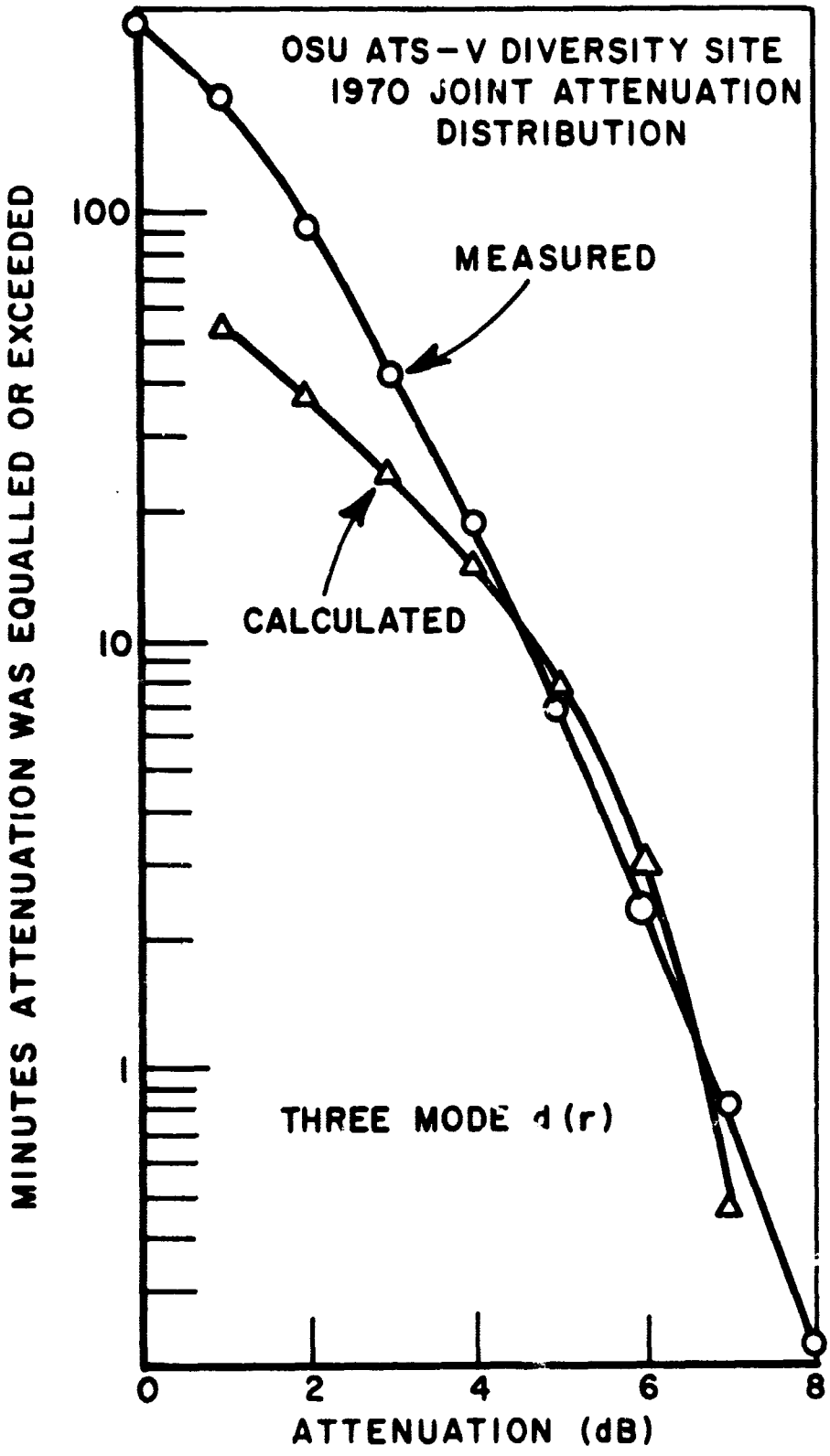

Figure 7-8. Calculated OSU Diversity Fade Distribution Using 3 Mode Diameter Model

To summarize the results using the three mode diameter function the error curves were calculated and are shown in Figure 7-9. It is seen that the three mode diameter function gives good agreement with the 1970 experimental data.

In conclusion, the single site attenuation distribution and the two site joint attenuation distribution were calculated using a cylindrical storm cell model. A technique was described for using National Weather Service precipitation data to calculate the attenuation distribution for a particular site location. Using a three mode diameter function it was shown that the model agreed within 2 dB for both the single site attenuation distribution and the two site joint attenuation distribution when compared with ATS-5 propagation measurements. Although this storm cell model represents a first attempt at making this type of calculation it appears to be a promising approach and provides a basis for future model development.

REFERENCES

1. Crane, R. K., "Propagation Phenomena Affecting Satellite Communication Systems Operating in the Centimeter and Millimeter Wavelength Bands," Proc. IEEE, 59, 1971, pp. 173-188.

2. Rice, P. L. and Holmberg, N. R., Private Communication, ITS Laboratories, Boulder, Colorado, 1971.

3. Hogg, D. C., "Rain on Earth-Space Paths," 1971 G-AP International Symposium.

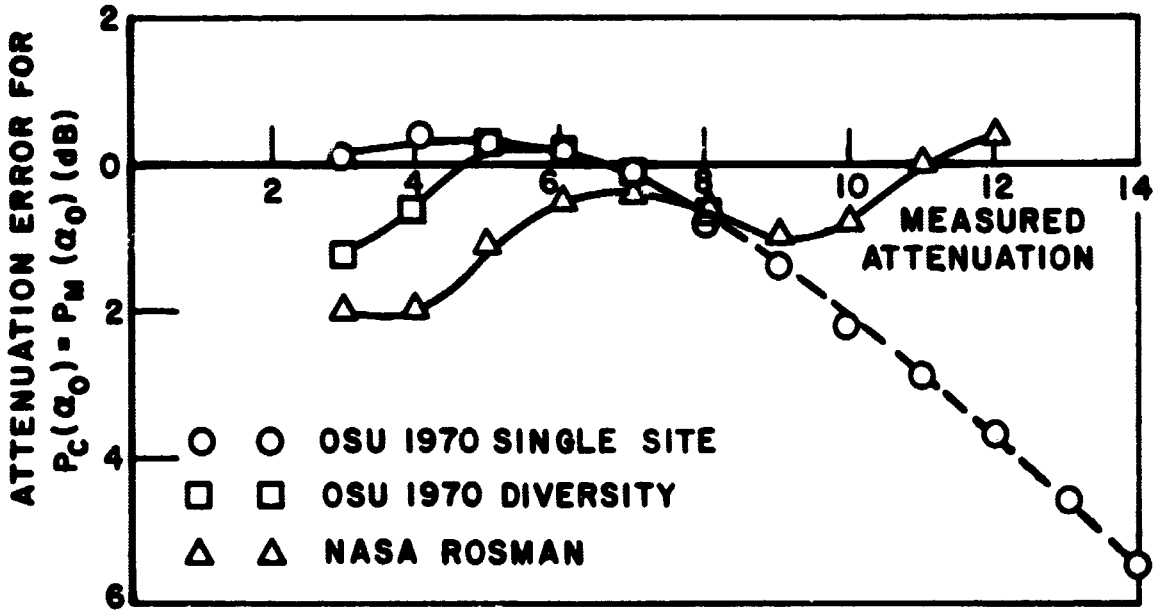

Figure 7-9. Attenuation Prediction Error for Storm Cell Model

SECTION 8

SUMMARY AND EVALUATION OF RESULTS FROM THE ATS MILLIMETER WAVE EXPERIMENT

Louis J. Ippolito
Principal Investigator
NASA/Goddard Space Flight Center
Greenbelt, Maryland

ABSTRACT

A summary of propagation measurements from eleven locations in the continental U.S. and Canada operating with the NASA ATS-5 Millimeter Wave Experiment's. 15.3 GHz earth-space link is presented, along with results of 31.65 GHz uplink measurements performed from Rosman, North Carolina, over a period of two years. Included are attenuation statistics comparisons at the various locations, and the correlation of attenuation measurements with rainfall rate, sky temperature, and radar observations. Attenuation ratio measurements of simultaneous 15.3 and 31.65 GHz transmissions are utilized to provide bounded cumulative distributions at the higher frequency. An overall accessment of the ATS-5 results and their impact on earth-space communications system performance are presented. In conclusion, future Millimeter Wave flight experiments planned for the ATS-F satellite are described, which will extend and improve upon the measurements obtained to date.

INTRODUCTION

This paper, the final presentation in this special session on millimeter wave propagation experiments with the ATS-5 Satellite, is intended to summarize and evaluate the results of the overall measurements obtained in the Experiment. The Experiment was initiated in October of 1969 and was terminated for most locations in September of 1971.

Part 2 of the paper reviews the results of the 31.65 GHz uplink which was operated from the single location at Rosman, North Carolina. Part 3 summarizes the 15.3 GHz downlink measurements, primarily from the Rosman station. Part 4 presents an evaluation of the overall results of the measurements obtained from all participating stations, and Part 5 briefly reviews the millimeter experiment presently under development for the ATS-F satellite.

REVIEW OF 31.65 GHz MEASUREMENTS

The operation of the 31.65 GHz uplink, particularly in the sideband mode, was severely limited because of the spacecraft spin and the downlink transmitter power degradations, as described in the first paper in this session. Several storm periods during the early portion of the measurement period were recorded, however, and some general comments on coherence bandwidth, attenuation ratios, and attenuation statistics for the Rosman location can be made.

Coherence Bandwidth

From the limited data available no quantitative information can be deduced from sideband measurements, however, the sideband amplitudes do tend to exhibit greater scintillations during periods of precipitation. An example of this effect is shown in Figure 8-1, where the 50 MHz upper and lower sideband differences are shown during an extended fade which reached 14 db, with a corresponding rainfall rate of 56 mm/hr. The sideband differences do exhibit increased variations during the fade period, however, they are not correlated with each other or with the magnitude of the carrier attenuation. A major part of the scintillations are under the measurement accuracy of the link (approximately ±1 db for high signal to noise ratio), and it is difficult to determine which scintillations, if any, were caused by the propagation path.

31.65 to 15.3 GHz Attenuation Ratio

The ratio of the uplink to downlink attenuation is a sensitive indicator of the distribution of the drop size diameters present in the propagation path and large variations were measured both for different storm events with similar attenuation intensities and during the duration of a single storm event. Figure 8-2 shows an example of an event with a nearly constant ratio of 3.33. The data covered a period of 155 minutes during a single continuous storm event.

Figure 8-3 shows an example of a storm of similar intensity but with a highly varying ratio during the storm. Most of the measured events were of this type, with most of the ratio values ranging from 2 to 3.5.

The expected range of attenuation ratio can be calculated utilizing the Gunn and East[1] emperical relationship between precipitation rate and attenuation of the form

$$A(db) = a R^b L$$

where R is the precipitation rate, in mm/hr over the path length L, in kilometers

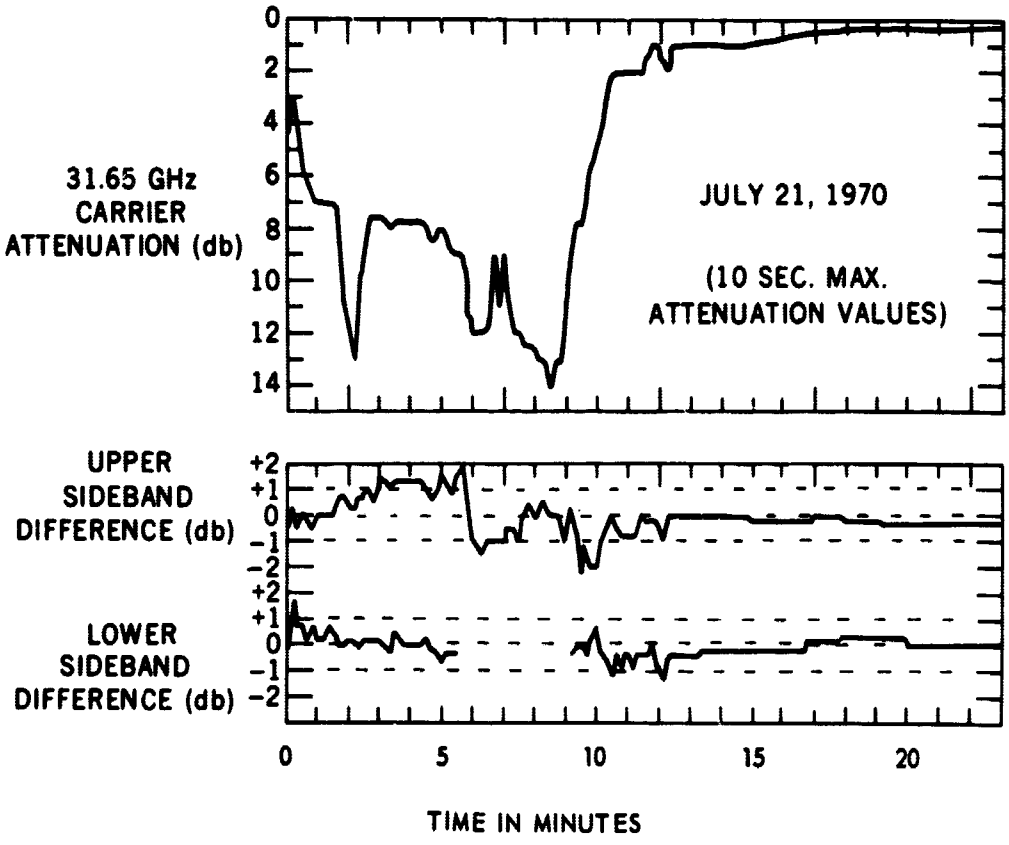

Figure 8-1. Uplink 50 MHz Sideband Variations During Rainstorm

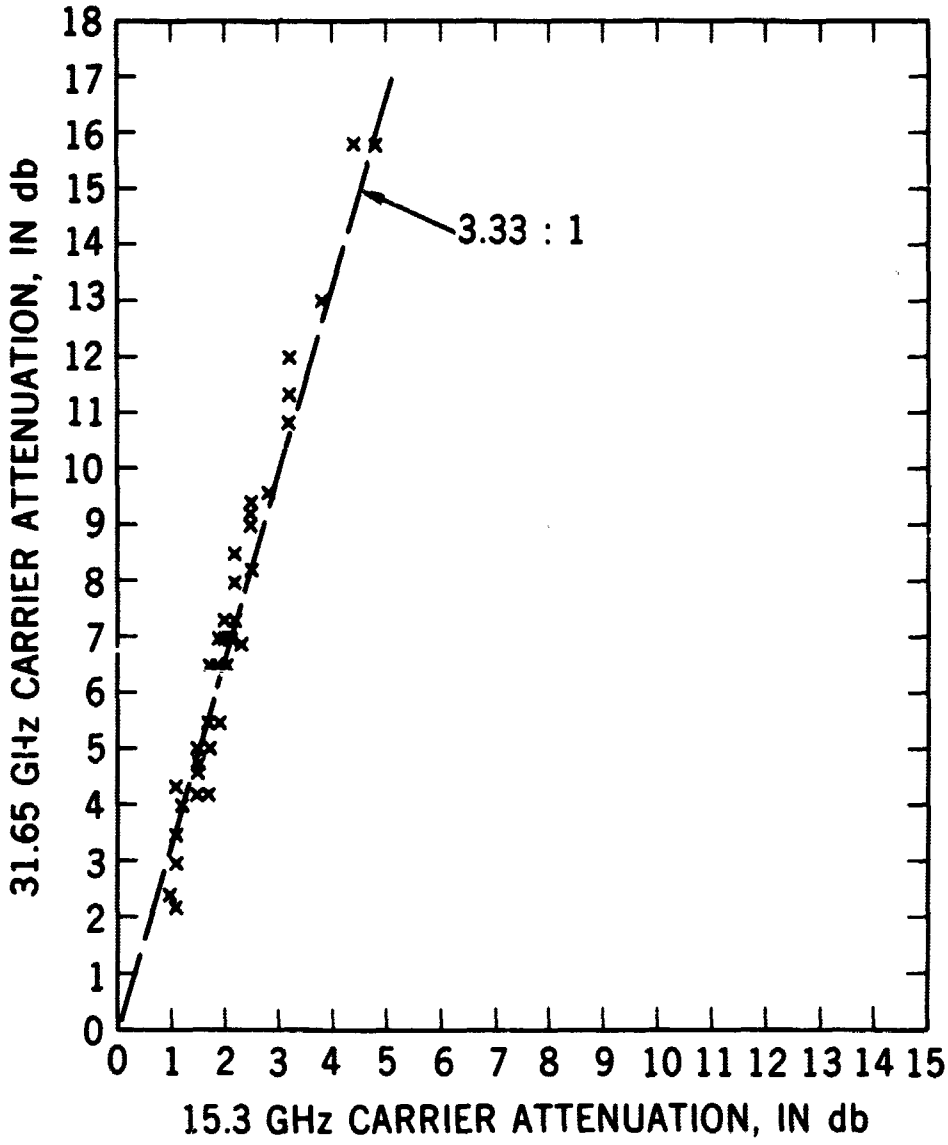

Figure 8-2. Uplink-Downlink Attenuation During Continuous Rain, Aug. 19, 1970

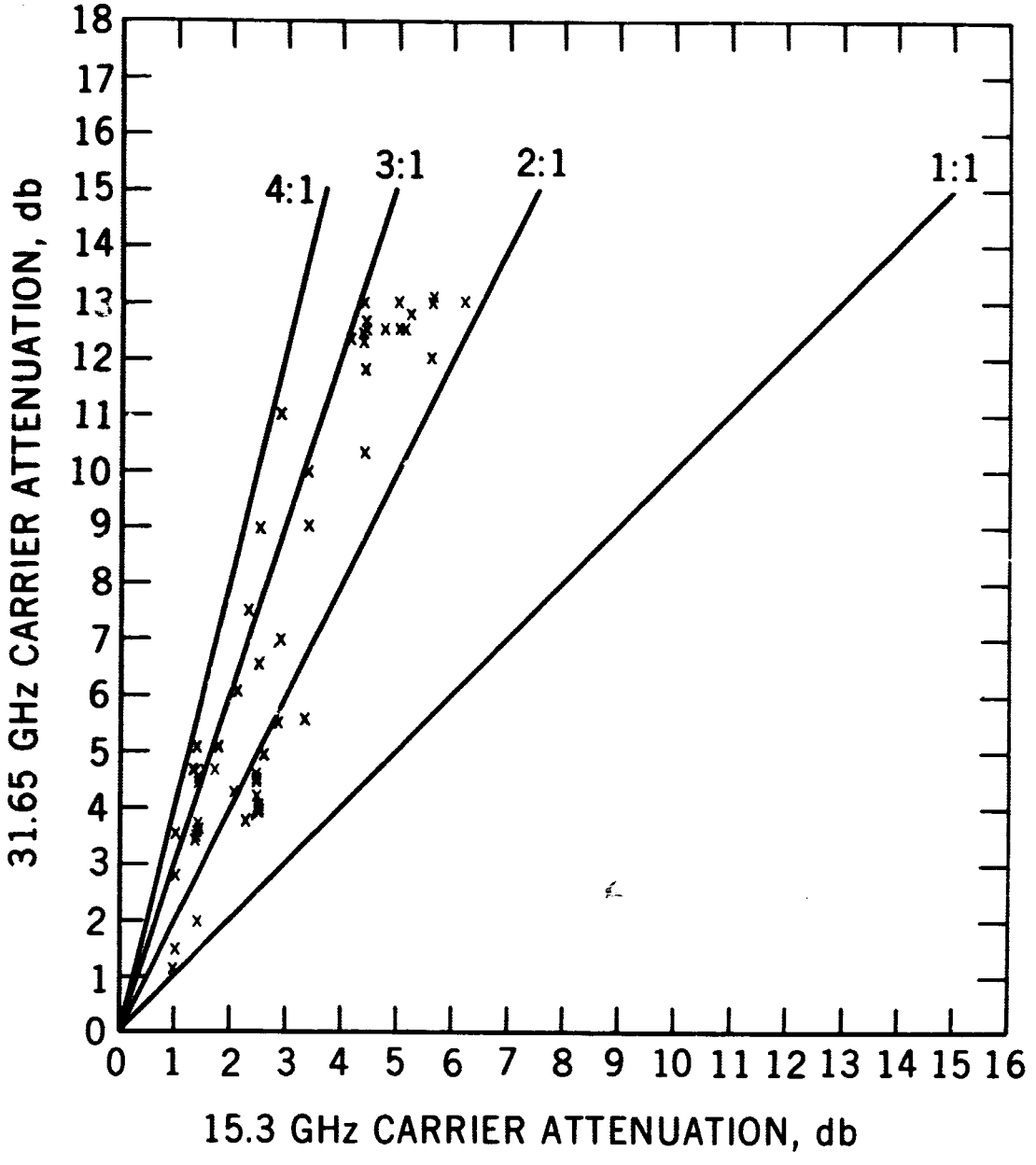

Figure 8-3. Uplink-Downlink Attenuation During Continuous Rain, July 21, 1970

and a and b are frequency dependent constants which also vary with the drop size distribution in the propagation path.

If we assume a Laws and Parsons drop size distribution[2], the constants for our frequencies of interest become:

$$A\,(db) = 0.2\,R\,L \qquad (@31.65\ GHz)$$

$$A\,(db) = 0.035\,R^{1.155} \qquad (@15.3\ GHz)$$

The 31.65 GHz to 15.3 GHz ratio as a function of the 15.3 GHz attenuation is shown in Figure 8-4 for three different assumed path lengths by the dashed curves. (The solid curve on the figure is developed from measured statistical data at Rosman and will be described in detail in Part 3.) Note that the expected ratio can vary over quite a large range, and the often used "rule" assuming that the attenuation ratio varies as the reciprocal of the wavelength squared (4.28 for the two wavelengths involved here) is not valid except for the unlikely case of low attenuations with long path lengths.

Figure 8-5 shows a comparison of the measured ratios with the predicted ratios for 4 storm events totaling 305 minutes for Rosman, North Carolina during 1970 and 1971. Very little data was available for high attenuation values and the large scatter of the lower attenuation values is due in part to the system inaccuracies of the uplink and downlink measurements, which can combine to produce large error ranges for low attenuation values. It is immediately apparent that a prediction of the 31.65 GHz attenuation from a measured value of the 15.3 GHz attenuation could not be accomplished and that, in general, to utilize attenuation measurements at one millimeter wavelength to infer results at another millimeter wavelength can be risky and rather unreliable.

An estimate of the range of annual attenuation statistics for the 31.65 GHz uplink can be accomplished by applying the measured range of attenuation ratios to the measured attenuation distribution at 15.3 GHz to produce a range of expected uplink attenuation. This result is shown in Figure 8-6. The 15.3 GHz curve, developed from 12,581 minutes of measurements during calendar year 1970, was extended to 31.65 GHz by utilizing the ratios of 2 to 1 and 3.5 to 1, resulting in the shaded area on the figure. (The dashed "best fit" curve will be discussed in Part 3 of this Section.)

This result shows that very high margins would be required to maintain a reliable link at the 31.65 GHz frequency; for example to maintain a 99.99% reliability (~1 hr. outage), a 41 db margin would have been required at Rosman during CY 1970.

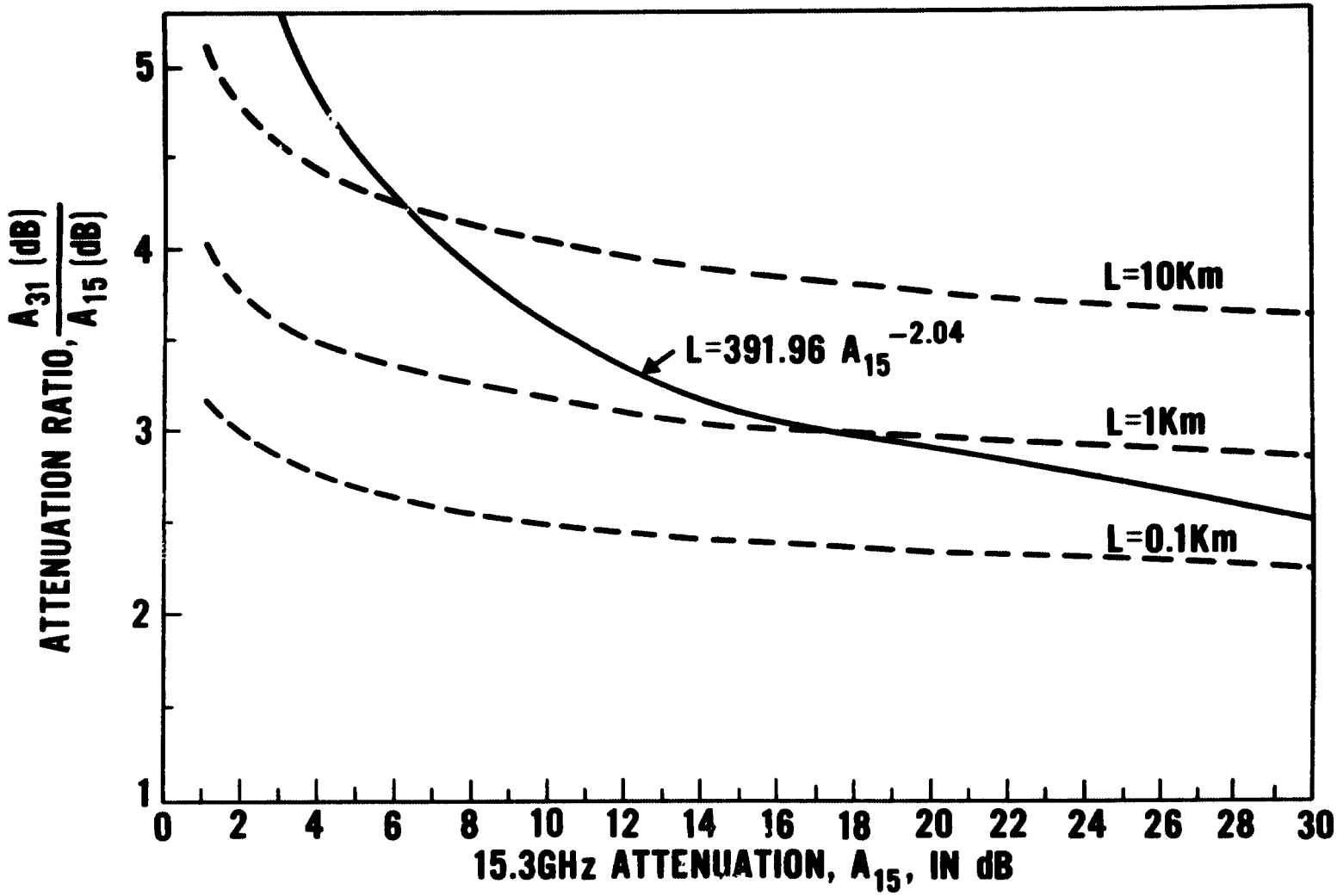

Figure 8-4. Attenuation Ratio as a Function of 15.3 GHz Attenuation Parametric in Path Length for Rosman, North Carolina

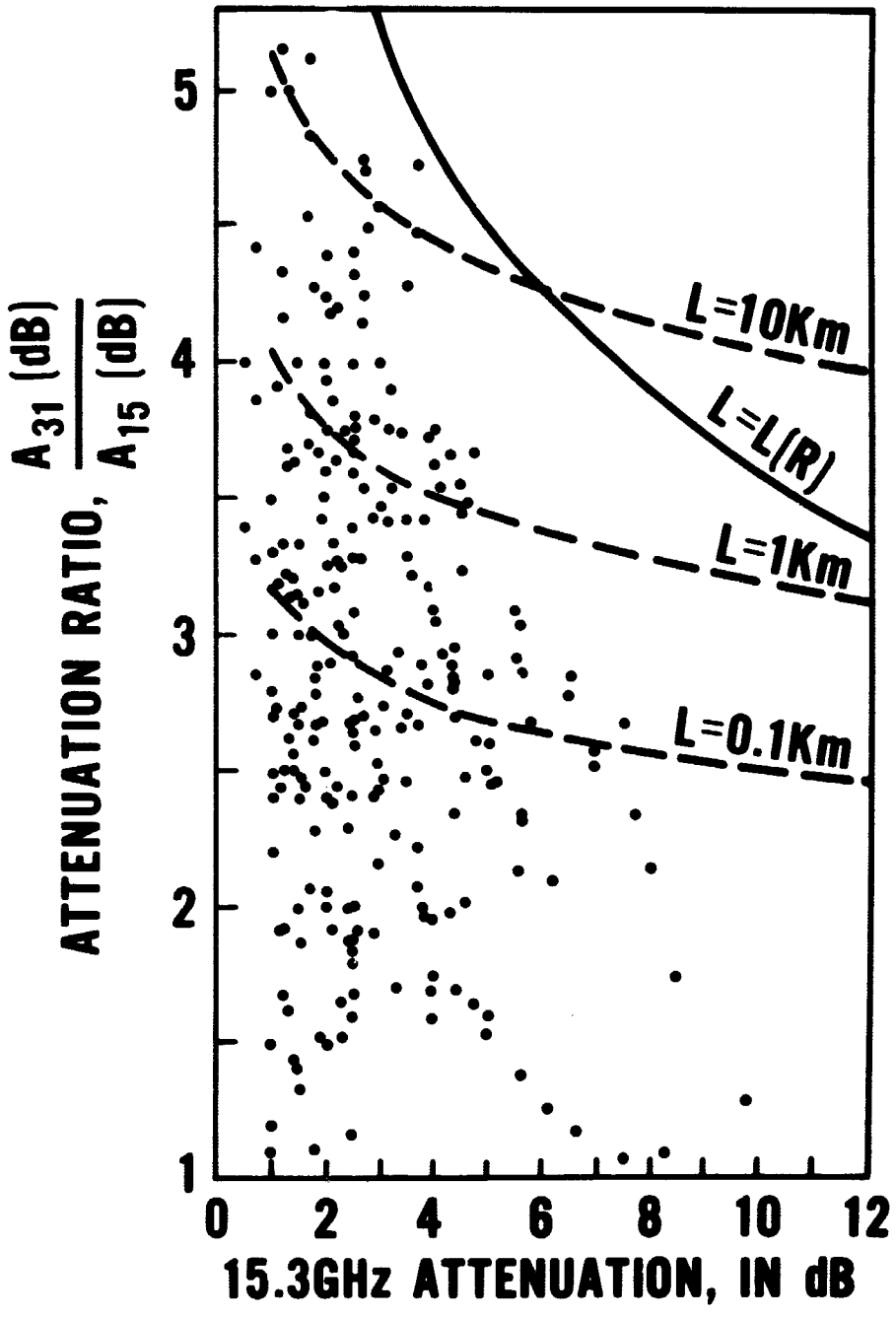

Figure 8-5. Measured Attenuation Ratio as a Function of 15.3 GHz Attenuation for 305 Minutes of Data, at Rosman, North Carolina

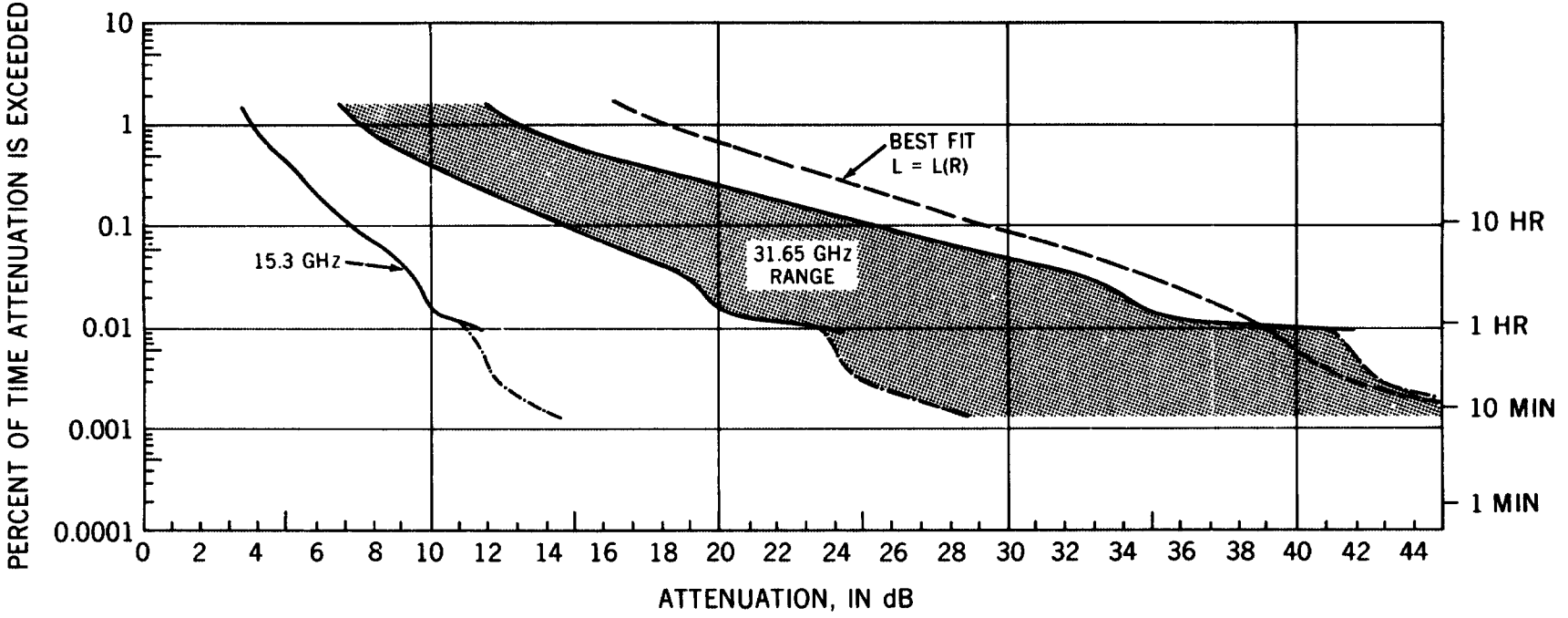

Figure 8-6. Attenuation Distributions for Calendar Year 1970 at Rosman, North Carolina

SUMMARY OF 15.3 GHz MEASUREMENTS

This section presents a summary of the major results of the 15.3 GHz downlink measurements taken at the NASA Rosman, North Carolina station. Detailed results can be found in References 3, 4, and 5.

All values of attenuation presented in this section, unless otherwise specified, are 10 second averages based on secondly samples of received signal level recorded on analog magnetic tape. An automated data processing program utilizing TBM OS 260/95 and OS 360/91 computers develops statistical plots and graphic presentations. An overall system accuracy of ±1 db in the attenuation measurements is maintained by daily receiver calibration and constant monitoring of spacecraft telemetry for transmitter power levels. The daily 4 db variations due to spacecraft motion are corrected in the automated program, since the orbital variations are measurable and predictable. The 0 db reference level for attenuation is based on the measured clear weather signal level received at Rosman for the data collecting period.

Sky Temperature — Attenuation Measurements

The sky temperature measured in the direction of the satellite beam has been found to be an excellent predictor of the attenuation simultaneously experienced by the satellite signal, up to values of 10 to 12 db.

A review of this result, which has been verified by all experimenters who have performed this measurement, is discussed in greater detail in another paper of this session (Section 4), and will not be dwelled upon here. Figure 8-7 summarizes the sky temperature-attenuation comparison for Rosman, where the cumulative distributions of measured 15.36 Hz attenuation with attenuation predicted from simultaneous 16 GHz sky temperature measurements are shown. The curves, which represent 939 total minutes of data taken during CY 1970, show very close agreement for the entire range of measurements, indicating that for statistical data of this type the radiometer is the best available tool for the prediction of atmospheric attenuation up to the 10-12 db range.

Correlation of Path Attenuation with Precipitation Rate

The instantaneous rainfall rate at the ground station antenna was measured by utilizing a "tipping bucket" type rain gauge which tips for each 0.254 mm of water accumulation. The instantaneous rainfall rate is computed by dividing the time between tips by the accumulation per tip. This technique provides increased resolution as the rainfall rate increases, since the time between tips is reduced with increasing rainfall rate.

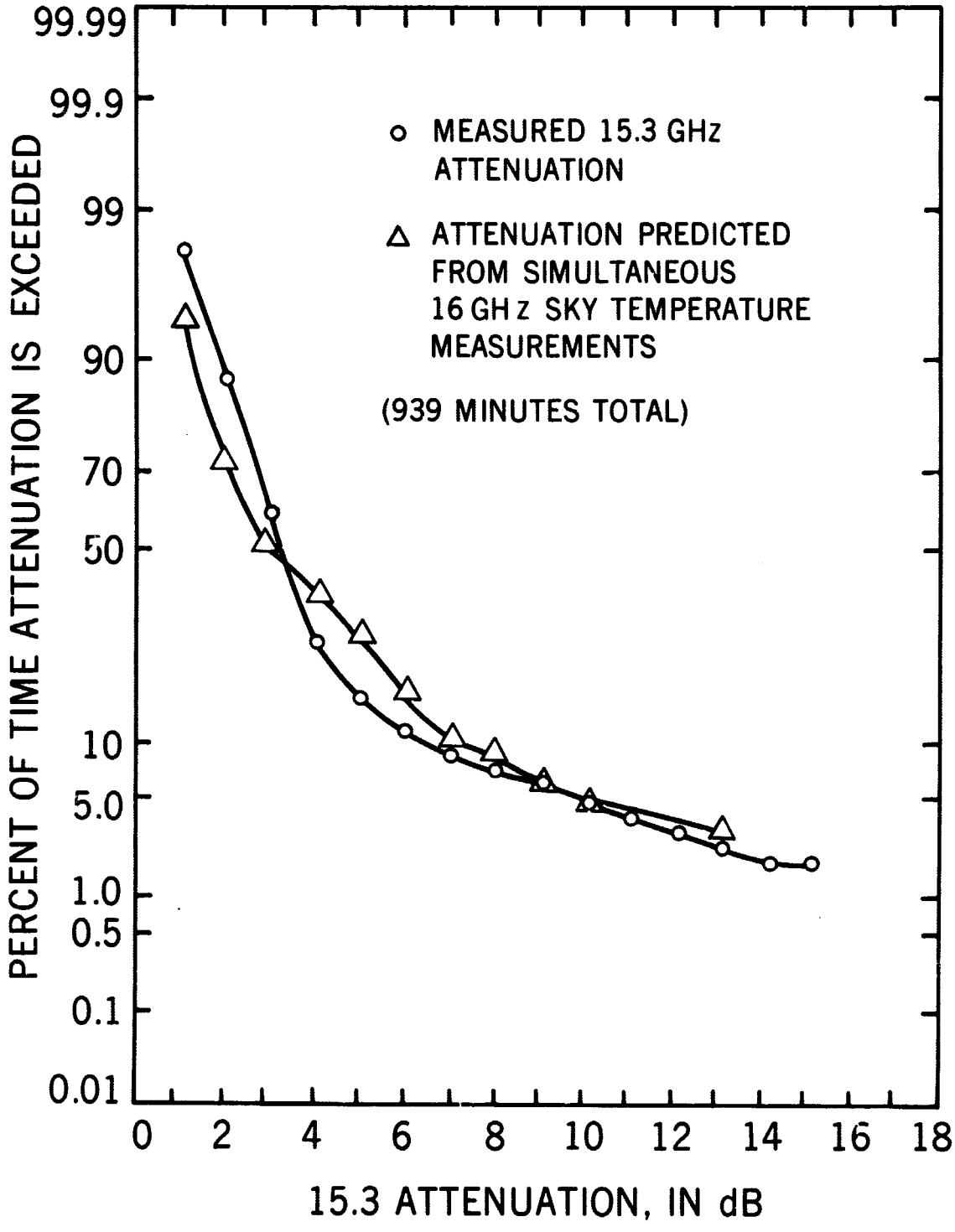

Figure 8-7. Comparison of Measured Attenuation and Attenuation Predicted from Sky Temperature – Rosman, North Carolina

Figure 8-8 shows the measured 15.3 GHz attenuation distributions parametric in four rain rate intervals. The curves were obtained from 422.3 minutes of measurements taken over several storm periods totaling over 19 hours at Rosman. Each distribution is with respect to the appropriate duration of the measurement, as given on the figure.

The distributions show the expected trend toward increasing attenuation with increasing rain rate, however, each distribution is quite wide, indicating that a wide range of path average rain rates can exist for each rate measured at the rain gauge. With distributions of this type, given the point rain rate distribution of any storm at Rosman or at a similar location, an equivalent attenuation distribution can be constructed reflecting a given percent confidence that the attenuation values will not be exceeded. For example, for a moderate rainfall (20 to 50 mm/hr) storm, a fade margin of some 15 db would be required to maintain a 90% reliability during the storm, while a 21 db fade margin would be required to maintain 99% reliability during that same storm.

A detailed study of the time correlation between measured 15.3 GHz attenuation and the ground rainfall rate as recorded on 10 rain gauges located along the axmuthal line of the satellite-earth satellite path was accomplished for several storms at Rosman during the February through June 1971 period (Ref. 5). The distance from the ground antenna to each rain gauge, and the height above the rain gauge to the earth-satellite beam intercept, are listed below:

Gauge No.	Distance From Antenna	Height of Beam Above Gauge
1	15 meters	14 meters
2	168	199
3	366	413
4	579	589
5	916	856
6	1144	1073
7	1524	1412
8	1891	1754
9	2377	2243
10	3172	2988

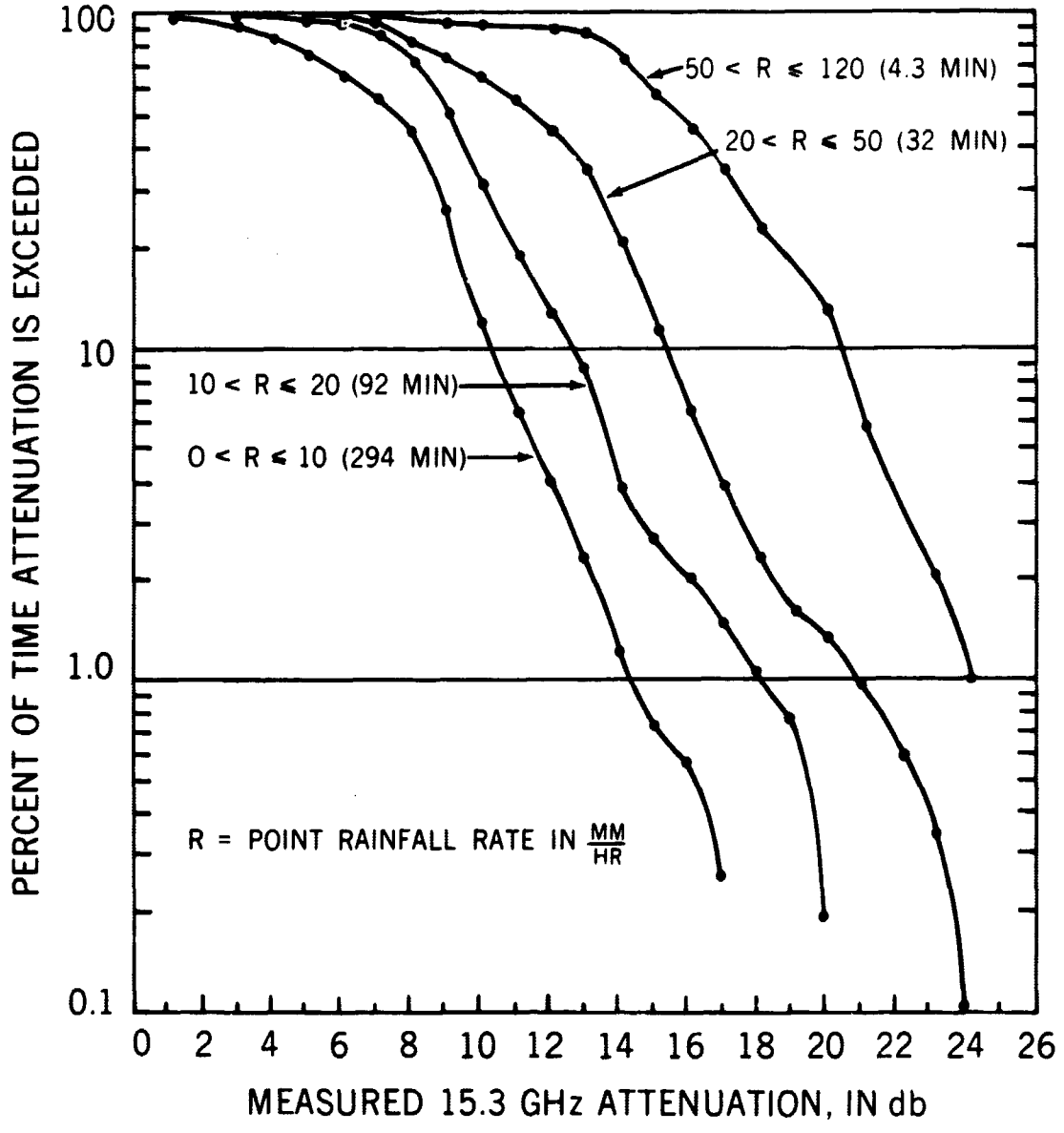

Figure 8-8. Distribution of 15.3 GHz Attenuation, for Various Rainfall Rate Intervals, Rosman, North Carolina, 1971

Figure 8-9 presents time displays and correlation plots for two typical storm events for the first five rain gauges. The correlation functions were computed from 10 second averages of the rainfall rate and path attenuation measurements.

Correlation studies of this type were accomplished for a number of events, and the results may be summarized as follows:

a. A comparison of 10 second average values of attenuation with ten second average values of rain rate for each bucket shows that maximum correlation (i.e., maximum cross-covariance) occurs when the attenuation is time shifted to lead the rainfall rate, in all cases.

b. The length of the time shift required for maximum correlation varied with each bucket and with each event, with values ranging from 10 to 320 seconds.

c. The correlation between rainfall rate and attenuation was not in general higher for the gauges closer to the antenna. (In only one event did the first rain gauge give the maximum time shifted covariance.)

d. The covariance coefficients showed large variations for different events which had similar rainfall characteristics, with values as high as .96 and as low as .45.

e. Covariance coefficients for the first five gauges were within 15% of each other for a given event, even though the maximum covariance for different events differed by as much as 30%.

The results of correlation measurements for the first five gauges for four events with similar rainfall ranges is shown in Figure 8-10. Note that in only one case did gauge #1 give the maximum correlation, while in another case it gave the lowest correlation.

Rain gauges 4 and 5 have a much greater foliage interference during the spring and summer months than the other gauges due to the difficult terrain surrounding their locations. Those two buckets do tend to show lower correlation than the other gauges for those periods when blockage would be present (see Figure 8-10) but the differences are quite small, usually less than 5%.

The results of this study are inconclusive in that the storm by storm correlation showed no repeatable trends in terms of time shift or rain gauge location. For long term statistics a non-time-shifted height-averaged rainfall rate

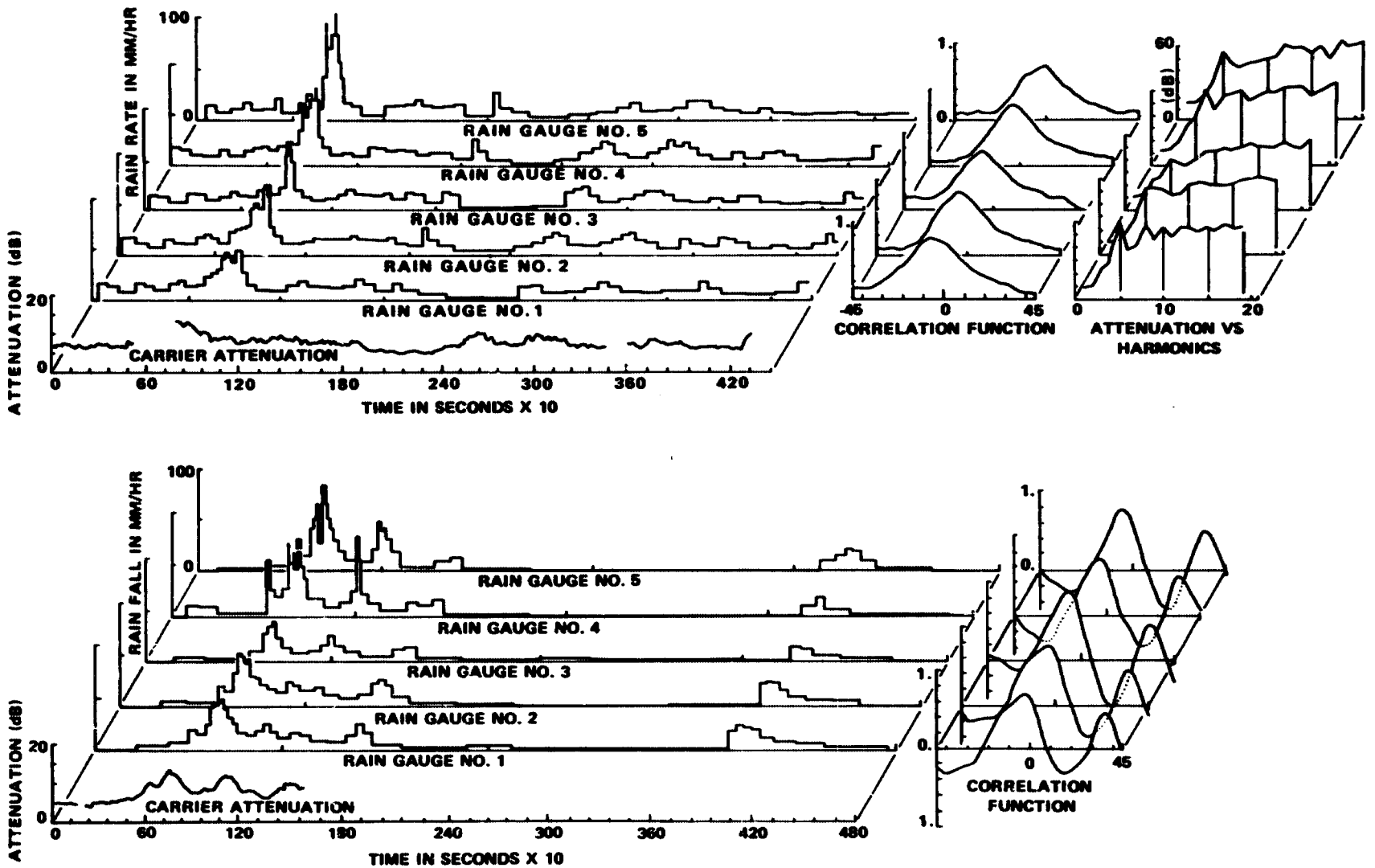

Figure 8-9. Attenuation – Rainfall Rate Correlation Diagrams Rosman, North Corolina

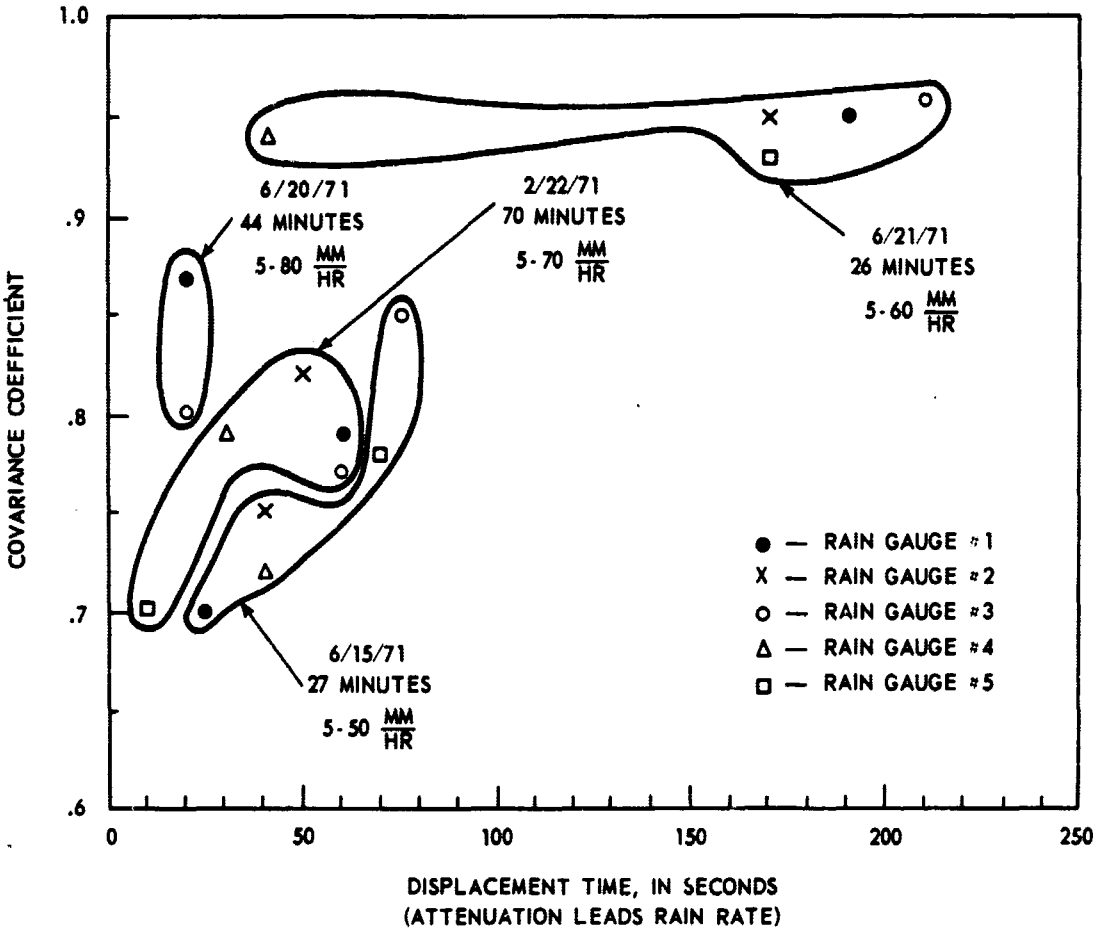

Figure 8-10. Correlation of Time Shifted Rainfall Rate with 15.3 GHz Attenuation for Rain Gauges 1 Through 5 for Four Similar Storms

utilizing all buckets where significant rain fall occurred will give a slightly better prediction than using just a single gauge, or a ground average of all the gauges (Ref. 4).

In order to utilize ground measured rainfall rate to predict earth-satellite attenuation, the effective path length (extent) of the rainfall must be available. This measurement is difficult to determine directly for high elevation angle satellite paths, but an estimate of the effective path length can be accomplished by comparing the measured attenuation-rainfall rate with the empirical relation (Ref. 1).

$$A\,(db) = 0.035\,R^{1.155}\,L \qquad \text{(for 15.3 GHz)}$$

where

A is the total path attenuation, in db

R is the rainfall rate, in mm/hr, over the path length L, in kilometers

The constraints in the equation above are developed from the Mie Theory for spherical particles with a Laws and Parsons drop-size distribution assumed (Ref. 2).

Figure 8-11 shows the function A (db) plotted for various path lengths from 1 km to 20 km. Also shown are plots of the least squares fits of four events with the aR^b relations as shown on the figure. The heavy portion of the curves cover the extent of measured values, i.e., event #1 contained measurements from 5 mm/hr to 70 mm/hr, event #2 from 5 mm/hr to 58 mm/hr, and so on. The least squares fit was accomplished after time shifting the rainfall rate data to obtain maximum cross-covariance, as described in the previous section. Also shown on Figure 8-11 is a plot of the least squares fit of all available calendar year 1970 measurements (12,581 minutes) using the non-shifted rainfall rate of the nearest rain gauge. The solid portion of the curve shows the portion where attenuation and rainfall measurements were available, the dashed portion is the extension to the maximum recorded rainfall rate for CY 1970 (136 mm/hr).

The effective path length for each storm as a function of R can be found by comparing the measured curves with the empirical curves for a given attenuation, and this is shown in Figure 8-12. The resulting curves are of the form

$$L(R) = \frac{a}{.035}\,R^{(b-1.155)} \qquad \text{(for 15.3 GHz)}$$

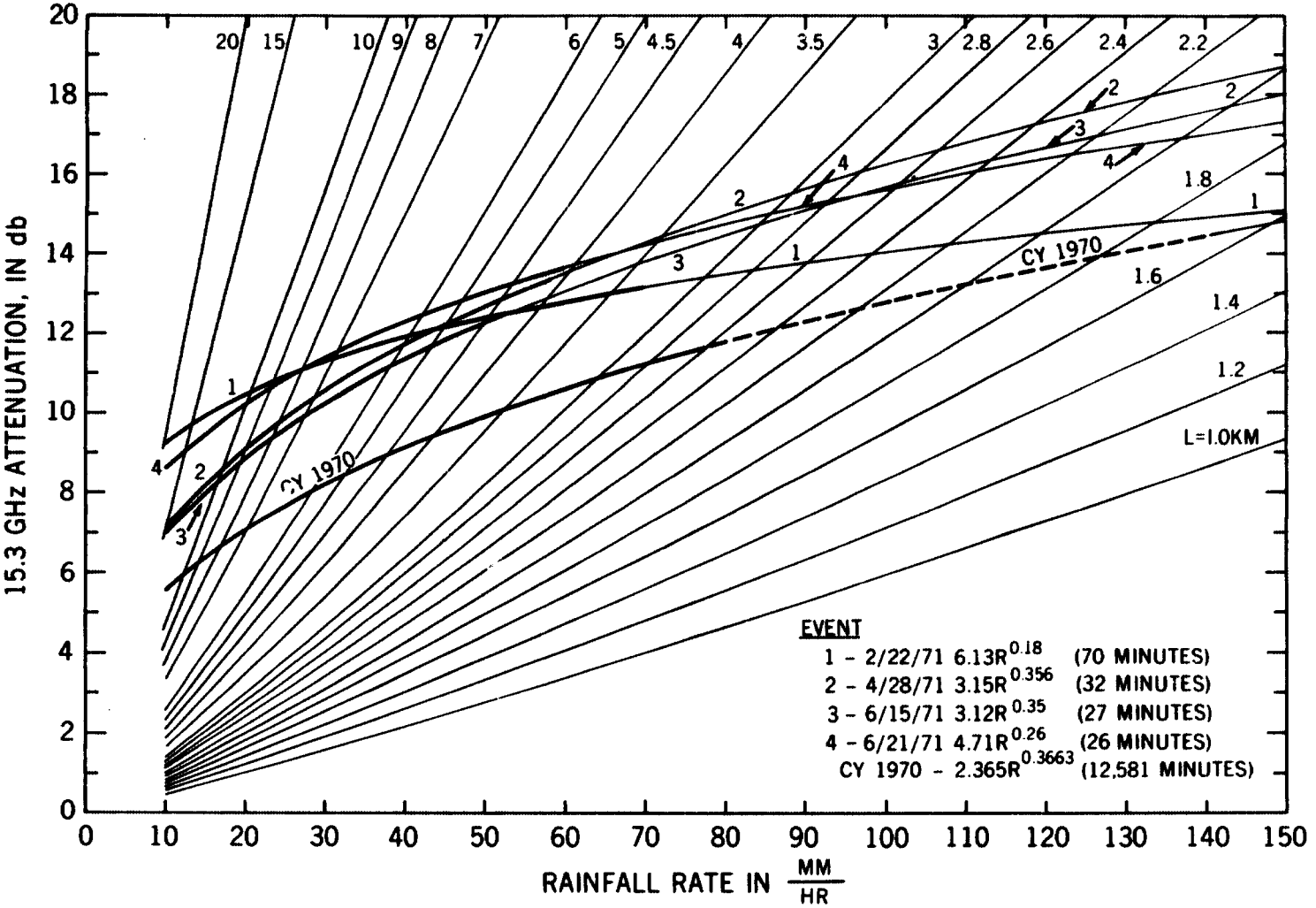

Figure 8-11. Measured 15.3 GHz Attenuation vs. Rainfall Rate Compared with Laws and Parsons Prediction

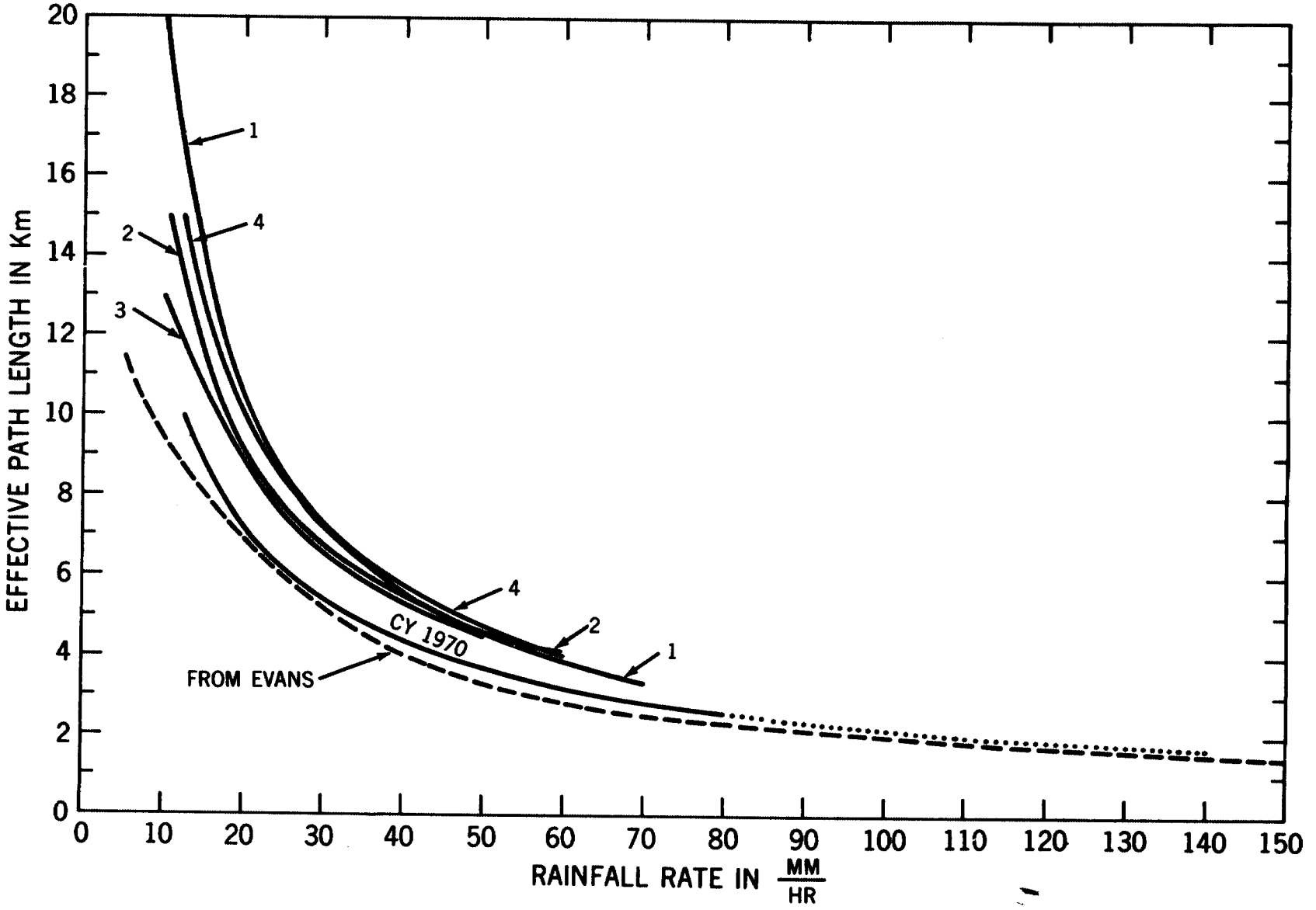

Figure 8-12. Effective Path Length Required for a Given Rainfall Rate from 15.3 GHz Measurements at Rosman, North Carolina

where a and b are the constants of the least squares fit of each event. All of the curves show a very similar trend, and the CY 1970 curve compares to within .5 km to the results given by Evans (Ref. 6) for sun tracker measurements taken at 15 and 30 GHz. As expected, the higher the rainfall rate, the shorter the effective distance. The effective path length appears to be asymptotic to 1 km for high rainfall rates, and is quite large for the lower rates. It would be interesting to see data of this type from other locations and weather conditions to determine if a "universal" relationship does exist for long term statistical measurements of this type.

Attenuation Statistics

The comparison of attenuation statistics from various locations has been thoroughly covered in a previous paper (Section 2), and this section will briefly review the determination of the annual statistics for the Rosman location.

Figure 8-13 presents a summary of calendar year 1970 attenuation statistics for the 15.3 GHz downlink at Rosman. Shown on the figure is the cumulative distribution of 11,756 minutes of satellite attenuation measurements. The data periods covered in this curve were generally randomly distributed throughout the year, except for the January 1 thru February 13 period when the link was down for repairs. Cumulative distributions of rainfall rate at the ground antenna for the total year and for the total period of data acquisition are also shown in Figure 8-13. The two rainfall rate curves are in excellent agreement up to the 70 mm/hr rate, with the upward offset of the acquisition period curve due to the proportionately greater rain accumulation during spacecraft measurements than throughout the year as a whole. The superimposibility of the two rain rate distributions indicates that the acquisition period was a reasonable sampling of the rain statistics for the total year (up to 70 mm/hr rate), thereby permitting us to construct an estimate of the attenuation distribution for the total year.

The yearly estimate of satellite attenuation, shown as the dashed curve of Figure 8-13, was developed from ordered pairs of measured attenuation and rainfall rate for a given percent of time on the distribution curves. For example, from Figure 8-13, it is seen that from 0.1% of the time during satellite attenuation measurements the rainfall rate exceeded 50 mm/hr, and, for the same percent of time, the attenuation exceeded 9.5 db. During the year as a whole the rainfall rate exceeded 50 mm/hr for 0.03% of the time. Had we measured satellite attenuation continuously during the total year, we would therefore expect to have measured attenuations in excess of 9.5 db for 0.03% of the time also, because of the similarity of the rainfall distributions. This process was repeated for all measured attenuation and rainfall rate pairs for the dashed curve of Figure 8-13, up to the 11.5 db (70 mm/hr) point.

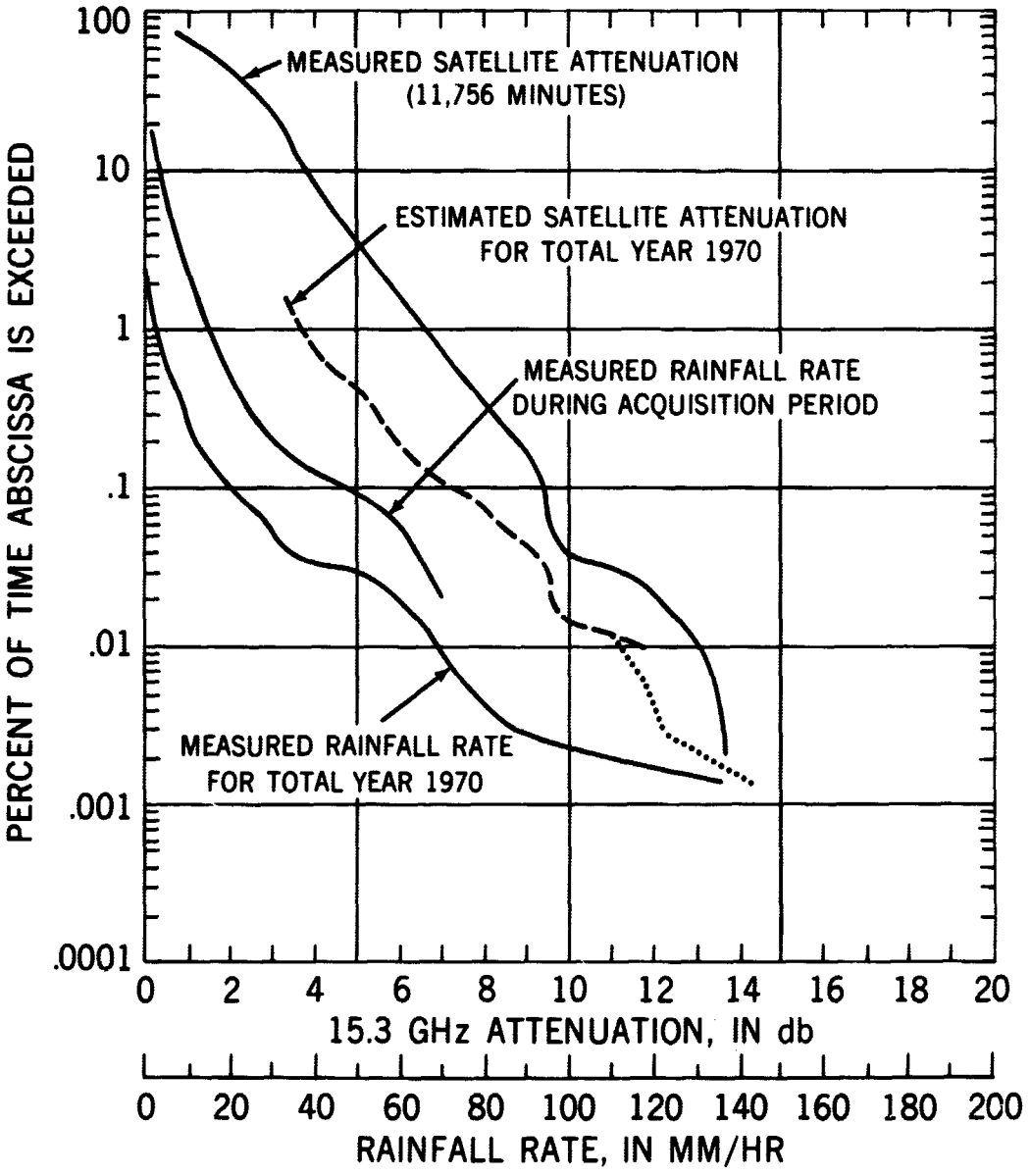

Figure 8-13. Cumulative Distributions for Calendar Year 1970 Rosman, North Carolina

For rainfall rates above 70 mm/hr, the attenuation was estimated from the relationship

$$A = aR^b$$

where A is the path attenuation, in db, and R is the rainfall rate in mm/hr. The constants a and b were found from a least squares fit of all of the measured attenuation and rainfall rate data for the year, and were found to be a = 2.365 and b = .3663, with a correlation coefficient of 0.97. The results are shown as the dotted curve on Figure 8-13. This curve shows that a maximum attenuation of 14.3 db would have been experienced at Rosman for 7.88 minutes (0.0015%) during the total year, corresponding to the maximum measured rainfall rate of 136 mm/hr for the year.

A similar set of distributions were developed for data accumulated during 1971, and they are shown in Figure 8-14. A total of 825 minutes of data, taken during the April through August rain season, was compared with the January through August eight month period and the resulting curve is shown as the dashed line. (Only eight months of rainfall rate-satellite data were available in 1971 at Rosman.) The two rainfall rate distributions are not as similar as for the previous year, but the general slope of the curves is the same. The attenuation for rainfall rates above 112 mm/hr was again estimated from a least squares fit of all available data for 1971. The constants were found to be a = 2.149 and b = .4879 with a correlation coefficient of 0.95. The maximum recorded rainfall rate during the 1971 period was 190 mm/hr, and the attenuation would have been 27.8 db for 14 seconds (0.000045%) at Rosman during the first eight months of 1971.

A comparison of the two yearly distributions indicate that power margins of 3 to 4 db larger would have been required in 1971 over 1970 to maintain the same annual link reliability percent.

The best fit Rosman equation for CY1970 was then applied to a number of other locations where instantaneous precipitation rate data was available, and the resulting distributions are shown in Figure 8-15. The Columbus Ohio curve was developed from rain gauge data supplied by L. R. Zintsmaster, OSU, and the remaining curves were developed from rain gauge data published by D. C. Hogg, BTL (Refs. 7 and 8).

Except for the Miami, Florida location, all other sites could be considered as fairly similar to Rosman in their general weather profile, and the results indicate the wide range of attenuation values that result for a given percent of time. If the effective path length, L(R), were available for each site, the curves could be modified to reflect a better estimate of the expected attenuation. Until

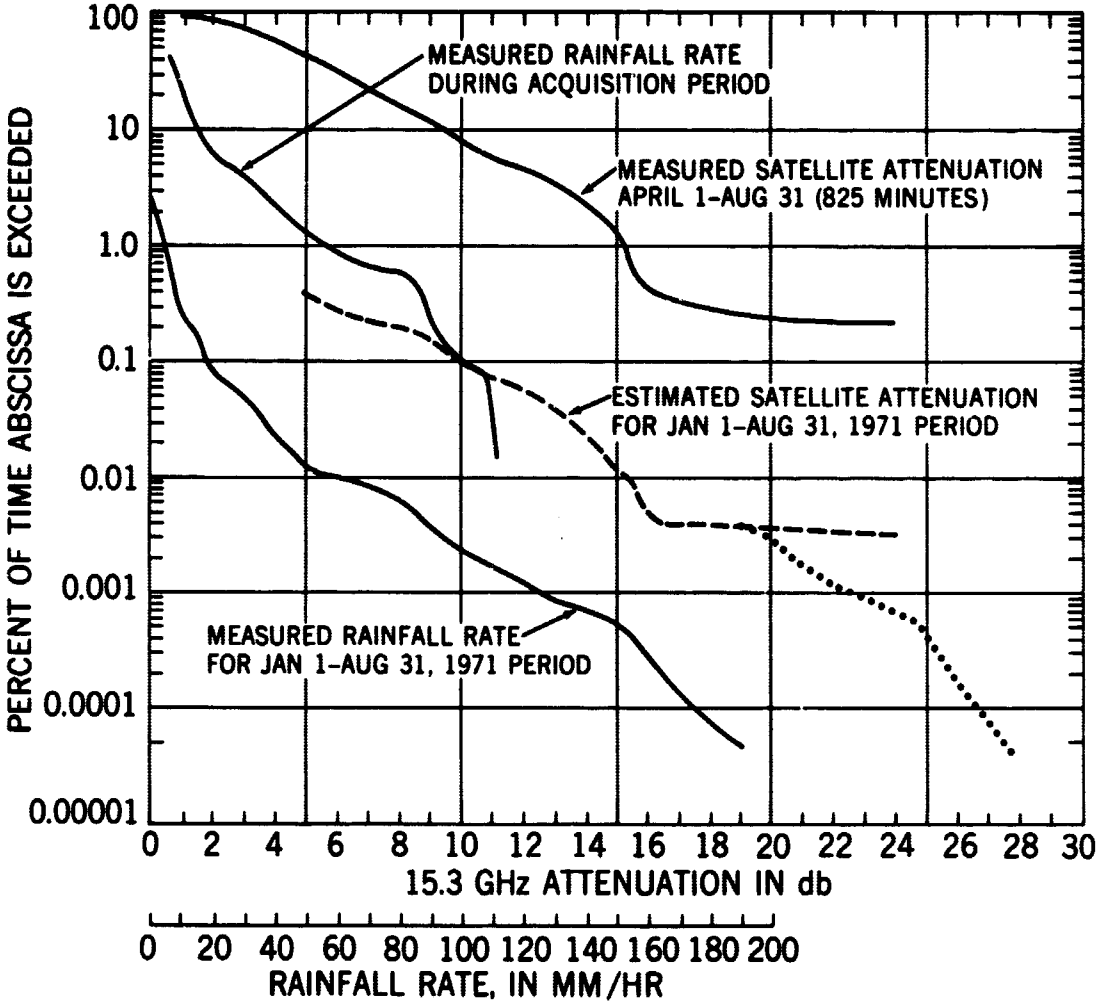

Figure 8-14. Cumulative Distributions for 1971 Rosman, North Carolina

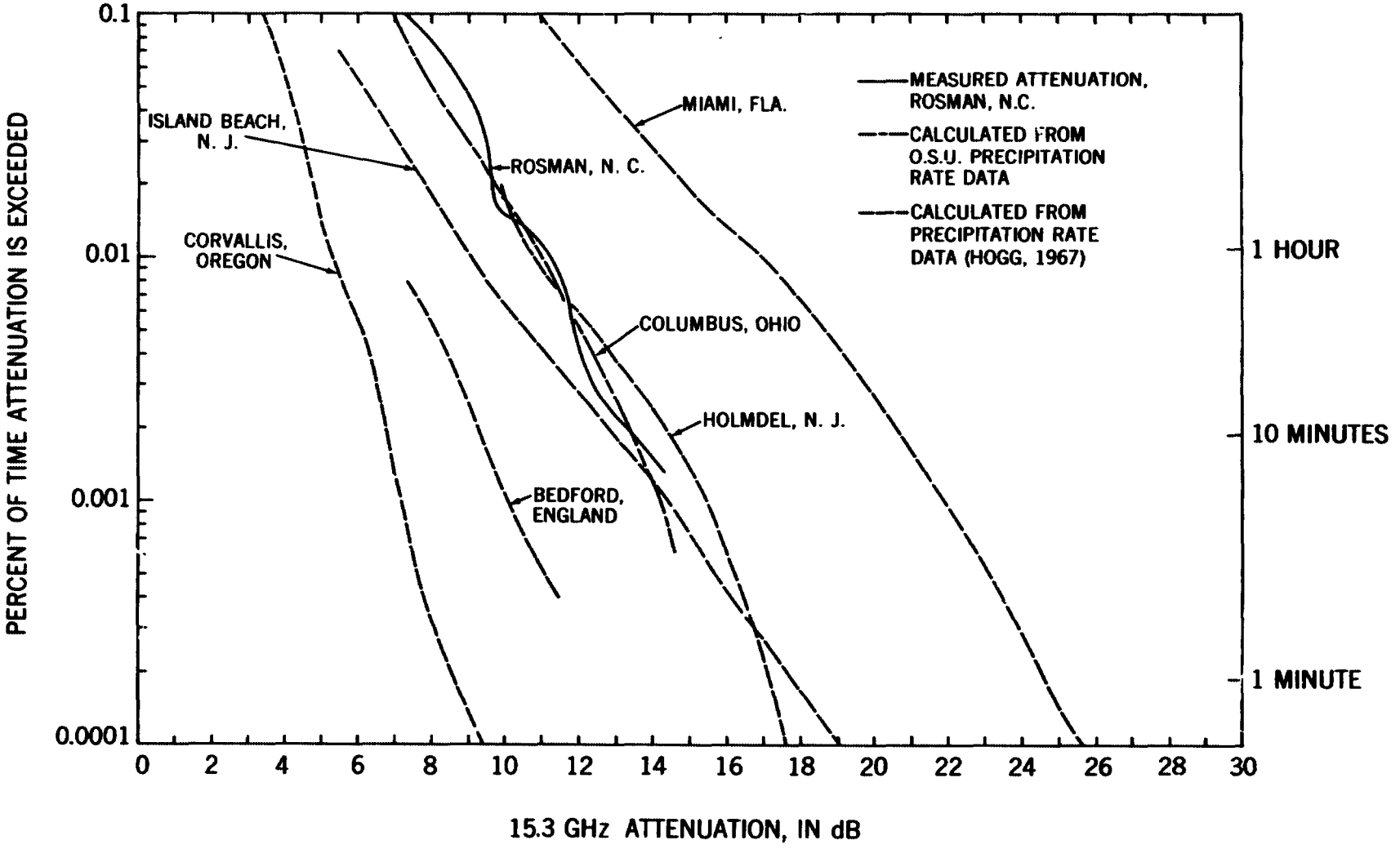

Figure 8-15. Predicted Attenuation Distributions from Precipitation Rate Data for Various Locations

further satellite data and effective path length data are available, however, curves developed from least fit data such as those on Figure 8-15 must serve as a general guide to the annual statistics expected at sites where only precipitation rate data is available.

EVALUATION OF OVERALL RESULTS OF THE ATS-5 MILLIMETER WAVE EXPERIMENT

In reviewing the vast amount of data presented here and elsewhere from the many participants and from nearly two years of operations with the ATS-5 Experiment, a number of factors emerge which appear often enough to be classified as "conclusions", in the general sense. Some are obvious and were expected, others were new in that they differed with previous results or produced an unexpected result. The list below highlights the major results of the ATS-5 Experiment, and is presented in no particular order of importance or priority.

a. Outage time statistics are not repeatable for different locations with similar general weather profiles, and can differ greatly year to year at the same location.

b. Rainfall rate measurements, even if "instantaneous", are of limited use in the prediction of earth-satellite path attenuation. The prediction can be improved slightly by utilizing effective path length measurements, by time-shifting techniques and by multiple gauge averaging.

c. Radiometric sky temperature measurements provide the best available technique for the prediction of 15 and 31 GHz attenuation up to 10-12 db and 8-10 db, respectively. For site diversity studies, this limited margin of measurement may be sufficient.

d. The extension of attenuation results from one frequency to another frequency, namely 15 to 31 GHz or a similar set of frequencies, is severely limited because of the unpredictable drop size variations which can occur during a weather event. Bounds on the expected attenuation can be determined for the higher frequency based on a statistical sampling of the range of attenuation ratios experienced at a given location.

e. Site diversity is a necessity at 31 GHz and may be required at 15 GHz in many regions of the U.S. in order to meet the reliability requirements of most proposed operational systems. The separation distance required to achieve reasonable diversity enhancement does not appear

to be as large as expected; 4 to 8 km may suffice in areas similar to the Columbus, Ohio environment.

f. Backscatter measurements at an attenuating wavelength, while qualitatively useful for observing cell structure and movement, are not quantitatively useful for the prediction of path attenuation.

g. Longer wavelength radar measurements appear to show good potential for the prediction of path attenuation, but the extension of the results to prediction at the millimeter wavelengths requires further study and more measurements to determine if a consistent and reliable prediction technique can be developed.

h. Initial results in the development of a storm modeling technique which is consistent with the measured data is encouraging, but further work needs to be done to define the model for more general application and to verify the results at other locations.

THE ATS-F MILLIMETER WAVE EXPERIMENT

The first space communications system to operate at millimeter wavelengths is presently under development for launch in 1974 on the sixth Applications Technology Satellite (ATS-F). The ATS-F Experiment is designed to provide engineering data on wideband space-to-earth transmissions at 20 GHz and 30 GHz as a function of meteorological conditions and modulation techniques (Ref. 9). The experiment consists of wideband 1440 MHz bandwidth propagation measurements and 40 megabit communications links centered at 20 GHz and 30 GHz. Parameters under investigation include amplitude and phase statistics, coherence bandwidth, site diversity improvement, and prediction techniques from meteorological measurements.

The basic objective of the communications mode testing is to observe and evaluate the propagation effects of the earth's atmosphere, primarily caused by heavy fog and precipitation, on modulated signals transmitted during the weather occurrence. To accomplish this, the experiment will be operated on a call basis, 24 hours a day, 7 days per week. That is, when precipitation is expected or observed, the communications links will be energized and monitored through the extent of the storm or until the required data has been obtained. Test runs for a number of modulation techniques, data rates, and durations are planned for as many weather events as possible during the 9 to 12 month period of satellite availability.

Both analog and digital modulation techniques will be utilized, and engineering data on carrier-to-noise, modulation index, error rate, and information rate will be developed as a function of meteorological conditions and modulation techniques.

The propagation measurements obtained from the ATS-5 Millimeter Wave Experiment, together with the extended communications measurements to be obtained from the ATS-F Experiment, will provide the engineering data necessary to characterize and optimize millimeter wave communications, which will form the basis for the next generation of operational space communications systems.

REFERENCES

1. Gunn, L. S. and East, T. W. R., "The Microwave Properties of Precipitation Particles, Journal of the Royal Meteorological Society, Vol. 80, 1954.

2. Laws, J. O. and Parsons, T. A., "The Relation of Raindrop Size to Intensity," Transactions, American Geophysical Union, Hydrology, 1943.

3. Ippolito, L. J., "Millimeter Wave Propagation Measurements from the Applications Technology Satellite (ATS-V)", IEEE Trans. on Antennas and Propagation, Vol. AP-18, No. 4, July 1970.

4. Ippolito, L. J., "Effects of Precipitation on 15.3 GHz and 31.65 GHz Earth-Space Transmissions with the ATS-V Satellite," IEEE Proceedings, Vol. 59, No. 2, February 1971.

5. ATS-5 Millimeter Wave Experiment Final Report, January 1972, prepared for NASA/GSFC by Westinghouse Electric Corporation under contract NAS 5-21598.

6. Evans, H. W., "Attenuation on Earth-Space Paths at Frequencies up to 30 GHz," International Conference on Communication, June 1971, Montreal, Canada, pp. 27-1 to 27-5.

7. Hogg, D. C., "Statistics on Attenuation of Microwaves by Intense Rain," Bell System Technical Journal, November 1969.

8. Hogg, D. C., "Millimeter Wave Communication Through the Atmosphere," Science, January 5, 1968.

9. Ippolito, L. J., "The ATS-F Millimeter Wave Propagation Experiment," NASA/GSFC Report No. X-731-71-460, October 1971.

APPENDIX 1

REPORTS AND PRESENTATIONS ON THE ATS-5 MILLIMETER WAVE EXPERIMENT

Binkley, W. O., Ippolito, L. J., King, J. L., Ratliff, R. B., The ATS-E Millimeter Wave Propagation Experiment, NASA/GSFC, X-733-68-196, April, 1968.

Biuge, A., Levatich, J., and Robertson, E., Propagation Experiment above 10 GHz for Application to Communications Satellite System, presented at the AIAA 3rd Communications Satellite Conference, April 8, 1970, Los Angeles, Calif.

Buige, A., Craft, H., Jr., Levatich, J., Robertson, E., Millimeter Wave Propagation Measurements with ATS-5 at COMSAT Labs., presented at the Fall 1970 USNC/URSI Meeting, Columbus, Ohio, September 15, 1970.

Bohley, P., Hodge, D. B., A Millimeter Wave Diversity Propagation Experiment, presented at the Fall 1970 USNC/URSI Meeting, Columbus, Ohio, September 15, 1970.

Day, J. W. B., Strickland, J. I., "Microwave Attenuation Measurements Using the ATS-5 Satellite," AGARD Tropospheric Radio Wave Propagation, Pt. 1, Feb. 1971.

Dees, J. W., Kefalas, G. P., Wiltse, J. C., "Millimeter Wave Communications Experiments for Satellite Applications", Int. Conf. on Communications, San Francisco, Calif., Vol. 1, June 8-10, 1970 Proceedings.

Dees, J. W., King, J. L., Wiltse, J. C., A Millimeter Wave Propagation Experiment from the ATS-E Spacecraft, NASA/GSFC, TM-X-60763, 1968.

Fannin, B. M., Straiton, A. W., Pate, D. N., Effects of Rain on Earth-Satellite Path at 15 GHz, presented at the Fall 1970 USNC/URSI Meeting, Columbus, Ohio, September 15, 1970.

Fannin, B. M. and A. H. Kwesah, "Calculation of Rain Scattering Effects in Radiometric Measurements," Abstracts of 1971 Fall URSI Meeting and International G-AP Symposium, Sept. 21-24, 1971, pp. 319-321.

Final Report, ATS-5 Millimeter Wave Propagation Experiment, prepared by Westinghouse Corporation for NASA-GSFC, Contract NAS 5-21598, January 1972.

Ippolito, Louis J., ATS-V Millimeter Wave Experiment Data Report, October-December 1969, March 20, 1970, NASA/GSFC Report X-733-70-123.

Ippolito, Louis J., Millimeter Waves for Domestic Satellite Systems, presented at AIAA 3rd Communications Satellite Systems Conference, Los Angeles, Calif., April 7, 1970.

Ippolito, Louis J., Millimeter Waves for Space Communications, presented at the IEEE 1970 International Conference on Communications, San Francisco, Calif., June 9, 1970.

Ippolito, Louis J., Millimeter Wave Propagation Measurements from the Applications Technology Satellite (ATS-V), IEEE Trans. on Antennas and Propagation, July 1970, pg. 525-552.

Ippolito, L. J., Propagation Statistics for 15 and 32 GHz Earth-Space Transmissions from the Applications Technology Satellite (ATS-V), presented at the Fall 1970 USNC/URSI Meeting, Columbus, Ohio, Sept. 15, 1970.

Ippolito, L. J., Effects of Precipitation on 15.3 and 31.65 GHz Earth-Space Transmissions with the ATS-V Satellite, Proceedings of the IEEE, Special Issue on Space Communications, February, 1971.

Ippolito, L. J., Millimeter Wave Space Communications — Recent Experimental Results and Present Development Programs, National Telecommunications Conference, Houston, Texas, December 1972.

Millimeter-Wave Propagation Experiments Utilizing the ATS-5 Satellite — Papers from the Fall 1970 URSI Meeting, Columbus, Ohio, NASA-GSFC Report X-751-70-428, November 1970.

Mondre, E., Correlation Analysis and Scintillation for 15 GHz Line of Sight Propagation Channels, NASA/GSFC, (NASA-TN-D-5613), Washington, April 1970.

Nichols, G. B., The Millimeter Wave Propagation Experiment for the ATS-E Spacecraft, NASA/GSFC, NASA-TM-X-63026; X-733-66-532, Nov. 1966.

Otsu, Y., Experimental Report on 16 GHz and 35 GHz Radiometers Associated with the ATS-V Millimeter Wave Experiment, NASA/GSFC, X-733-69-554, NASA-TM-X-63834, November, 1969.

Penzias, A. A., First Result from 15.3 GHz Earth-Space Propagation Study, The Bell System Technical Journal, July-August 1970, pg. 1242-1245.

Penzias, A. A., Propagation Data from Crowford Hill, presented at the Fall 1970 USNC/URSI Meeting, Columbus, Ohio, September 15, 1970.

Straiton, A. W., and Fannin, B. M., Comparison of 15 GHz Propagation Data from the ATS-V Satellite with Ground Based Radio and Meteorological Data, XVI Symposium on EEP/AGARD, Dusseldorf, Germany, Sept. 1970.

Straiton, A. W., Lai-iun Lo, and David N. Pate, "Propagation of 15.3 and 35 GHz over a 15.5 km Path," Proceedings of the 1971 Fall URSI Meeting and International G-AP Symposium, Sept. 21-24, 1971, pp. 333-335.

Straiton, A. W., "Statistics on Attenuation at 15 GHz and 31.2 GHz," Abstracts of 1972 Spring URSI Meeting and International G-AP Symposium, April 13-15, 1972, pp. 21-22.

Straiton, A. W., D. N. Pate, and B. M. Fannin, "Statistics on Earth-Satellite Attenuation at Two Texas Locations," XVIIIth Meeting of the Electromagnetic Wave Propagation Panel, NATO-AGARD, 18-22 September 1972, Gausdal Hotel, Norway.

Strickland, J. I., Attenuation, Emission and Backscatter by Precipitation, presented at the Fall 1970 USNC/URSI Meeting, Columbus, Ohio, Sept. 15, 1970.

Strickland, J. I., "Simultaneous Measurement of Attenuation, Emission and Backscatter by Precipitation Along a Satellite to Earth Path", American Meteorological Society, Radar Meteorology Conference, 14th Proceedings, Tuscon, Ariz., Nov. 17-20, 1970. American Meteorological Society, Boston, 1970, pp. 215-219.

Vammen, C. M., McCormick, F. L., "ATS-5 Millimeter Wave Propagation Experiment," IEEE Transactions on Aerospace and Electronic Systems, Vol. AES-6, Nov. 1970, pp. 825-831.